

**Acoustic Emission Monitoring of Reinforced Concrete Beams
Repaired with Engineered Cementitious Composites**

by

© Yara A. Zaki

A Thesis submitted to the School of Graduate Studies in partial fulfillment of the
requirements for the degree of

Master of Engineering

Faculty of Engineering and Applied Science – Civil Engineering

Memorial University of Newfoundland

October 2023

St. John's, Newfoundland, Canada

Abstract

In this thesis, acoustic emission (AE) monitoring was employed to analyze, characterize, and quantify the cracking behavior of a total of thirteen large-scale reinforced concrete (RC) multi-layered beams under flexural testing. The experimental work performed in this thesis was divided into two studies. In the first study, four RC beams were repaired with engineering cementitious composites (ECC) in either the tension zone or the compression zone of the beam. Two types of fibers were used in the ECC repair material: polyvinyl alcohol fiber (PVA) and steel fiber (SF). Three control beams (reference beams used for comparison) were tested for comparison including one normal concrete beam and two fully cast ECC beams with PVA and SF. AE parameters such as number of hits, cumulative signal strength (CSS), signal amplitude, peak frequency, absolute energy, and b -value (defined as the log-linear slope of AE's frequency-magnitude distributions) were considered and used to evaluate the cracking behavior of both the repaired and unrepaired beams. Furthermore, rise time/maximum amplitude (RA) vs. average frequency (AF) analysis was implemented to categorize different failure modes (flexural, shear, or debonding). Varying the fiber type as well as sensor location/repair location seemed to have a significant effect on the signal amplitude and number of hits. With the aid of analyzing AE parameters (number of hits, CSS, and b -value), the first crack for all tested beams was successfully determined in the seven tested beams.

In the second study, the flexural testing of four ECC multi-layered beams incorporated either crumb rubber (CRECC) or powder rubber (PRECC). Four beams were repaired in either the tension zone or the compression zone of the beam. Three beams were fully cast

in normal concrete, CRECC, and PRECC, and were used as control beams (reference beams used for comparison). A variety of AE parameters such as number of hits and CSS as well as b -value were used to analyze the crack propagation of the tested beams. Damage quantification charts pertaining to different cracking stages (first crack and ultimate load), based on historic index $[H(t)]$ and severity $[S_r]$, were created in this study to categorize and quantify damage severity in terms of crack growth in composite beams. Alternating the rubber particle size, repair location or sensor location resulted in noticeable variations in the AE parameters (signal amplitude, CSS, and number of hits).

For both studies, the addition of a new concrete layer (ECC incorporating fiber and/or rubber particles) seemed to result in a noticeable effect on AE parameters such as signal amplitude. In addition, varying the strengthening location, sensor location, and fiber type/rubber particle size showed an impact on several AE parameters including number of hits, CSS, and b -value. By carrying out the AE analyses mentioned, the first crack identification for both the repaired and unrepaired beams was possible. Damage quantification and failure mode classification charts were successfully obtained by intensity analysis and rise time/amplitude analysis.

Acknowledgments

I would like to express my sincere appreciation to my esteemed supervisors Prof. Assem A. Hassan and Dr. Ahmed A. Abouhussien. I am grateful for their support and guidance throughout my master's degree. Without their dedication and expertise, I would not have been able to complete this journey successfully.

I would like to thank my mom, my dad, and my brother for their endless support, for their unconditional love, and for always being there for me.

I owe the deepest gratitude to my close friends who were always by my side, encouraging and motivating me in every possible way, even when we're continents apart.

And most importantly, I am grateful to the almighty God, Allah, for without his will, none of this would have been possible.

The completion of this Journey wouldn't have been possible without the generous financial contributions through the NSERC Discovery Grant. My Team and I are grateful for your support and belief in our work.

Yara A. Zaki

Disclaimer

It should be noted that the published versions of each paper presented in chapters 2 and 3 have been slightly modified to fit the required thesis format.

Co-Authorship Statement

I, Yara A. Zaki, hold the principal author status for all the manuscript chapters (Chapters 2 and 3) in this thesis. However, each manuscript is co-authored by my main supervisors Prof. Assem A. A. Hassan and Dr. Ahmed A. Abouhussien whose contributions have significantly facilitated the development of this work. Dr. Assem A. A. Hassan presented the idea for this project to me, and it was my task to carry out the work necessary to complete this thesis as part of the master's degree requirements.

In the papers presented in Chapters 2, and 3, Dr. Mohamed K Ismail and Dr. Basem H AbdelAleem (Co-researchers) assisted in the experimental work, including the preparation and testing of the thirteen beams. Dr. Ahmed A. Abouhussien guided with the setup of the AE system, collection, filtering, and analysis of the AE data from all tests and formulating the results and conclusions presented in this thesis. Prof. Assem A. A. Hassan supervised all the stages of this research including the experimental work, data analysis, and manuscripts' preparation.

My supervisors, Prof. Assem A. A. Hassan and Dr. Ahmed A. Abouhussien assisted in the experimental phase, data analysis, and helped me in finalizing the manuscripts for each chapter presented in the thesis.

Described below is a detailed breakdown of the work facilitated by my team and me.

- Paper 1 in Chapter 2: Yara A. Zaki, Ahmed A. Abouhussien, Assem A. A. Hassan, Mohamed K. Ismail, and Basem H. AbdelAleem (2023) “*Crack Detection and Classification of Repaired Concrete Beams by Acoustic Emission Monitoring*”, **Published in Ultrasonics Journal, Volume 134, 107068.**

I was the primary author, with second, third, fourth, and fifth authors contributing to the idea, its formulation, development, and refinement of the format in which the final version of the paper was prepared.

- Paper 2 in Chapter 3: Yara A. Zaki, Ahmed A. Abouhussien, and Assem A. A. Hassan (2023) “*Damage Characterization in Large-Scale Multi-Layered Reinforced Concrete Beams by Acoustic Emission Analysis*”, **Submitted for Publication in the Materials and Structures Journal.**

I was the primary author with the second, and third authors contributing to the idea, its formulation, development, and refinement of the format in which the final version of the paper was prepared.

Yara A. Zaki

October 23, 2023

Yara A. Zaki

Date

Table of Contents

Abstract	ii
Acknowledgments	iv
Disclaimer	v
Co-Authorship Statement	vi
Table of Contents	viii
List of Tables	xii
List of Figures	xiii
List of Symbols, Nomenclature, or Abbreviations	xv
1. Introduction	1
1.1. Background	1
1.2. Structural Health Monitoring and Acoustic Emission Analysis Overview	3
1.3. Research Objectives.....	6
1.4. Thesis outline	7
1.5. Chapter References	8
2. Crack Detection and Classification of Repaired Concrete Beams by Acoustic Emission	14

2.1. Abstract	14
2.2. Introduction.....	15
2.3. Research Significance	18
2.4. Overview of AE Analysis in Composite Concrete Structures	19
2.5. Experimental Program	20
2.5.1. Material Properties	20
2.6. Details of Tested Beams	21
2.7. Test Setup, Instrumentation, Loading Procedures, and AE Setup.....	23
2.8. Processing and Analysis of AE data	26
2.8.1. AE Filtering	26
2.8.2. b-value Analysis.....	27
2.8.3. RA Analysis	28
2.9. Results and Discussion	29
2.9.1. Structural Performance and Cracking Behavior of the Tested Beams	29
2.9.2. Evaluation of Damage Progression by AE analysis	31
2.9.3. Comparison of the First Crack Time between the Tested Beams.....	35
2.9.4. Classification of Damage Using AF and RA Analysis.....	37
2.9.5. Effect of Sensor Location on Damage Detection	41
2.9.6. Effect of Fibers on AE Activity and Failure Mode of Beams	44

2.9.7. Effect of Strengthening Location/Failure Mode of Repaired Beams on AE Parameters.....	48
2.10. Conclusions.....	48
2.11. Chapter References	50
3. Damage Characterization in Large-Scale Multi-Layered Reinforced Concrete Beams by Acoustic Emission Analysis	58
3.1. Abstract.....	58
3.2. Introduction.....	59
3.3. Research Significance	62
3.4. Experimental program	62
3.4.1. Material properties	62
3.4.2. Selection of beam specimens	64
3.4.3. Four-point loading test setup and loading procedure.....	65
3.5. AE monitoring procedure	67
3.5.1. AE setup.....	67
3.5.2. Post-testing AE Data filtering.....	68
3.6. AE Analysis and Processing	69
3.6.1. b-value analysis.....	69
3.5.2. Intensity analysis.....	70

3.7. Results and discussion	71
3.7.1. Crack detection using AE analysis.....	74
3.7.2. Time to first crack detection comparison among the tested beams.....	76
3.7.3. Impact of rubber particle size on the AE parameters.....	78
3.7.4. Impact of layer/sensor location on AE parameters.....	80
3.7.5. Damage classification by AE intensity analysis	83
3.8. Conclusions.....	85
3.9. Chapter References	87
4. Summary and recommendations	96
4.1. Summary	96
4.2. Recommendations for Future Research and Potential Applications/Limitations of the Current Study	98
Bibliography.....	101

List of Tables

Table 2- 1 Mix Design (Ismail and Hassan 2021).....	21
Table 2- 2 Properties of Fibers (Ismail and Hassan 2021).....	21
Table 2- 3 Test Results of all Beams (Ismail and Hassan 2021)	25
Table 2- 4 AE System Configuration.....	25
Table 2- 5 Rejection Limits for AE Data Filter	27
Table 2- 6 AE Parameters for all Beams at Failure	35
Table 2- 7 AE Parameters for all Beams at the First Crack.....	44
Table 3- 1 Mix design for all tested beams.....	63
Table 3- 2 Flexural test results for all tested beams.....	66
Table 3- 3 Pre-testing AE data built-in filter ranges.....	68
Table 3- 4 Post-testing AE data amplitude-duration filter ranges	69
Table 3- 5 AE parameters obtained at the first crack and ultimate load.....	78
Table 3- 6 Severity analysis parameters obtained at two different cracking stages	84

List of Figures

Figure 1- 1 Basic AE signal parameters (Behnia et al. 2014).....	5
Figure 2- 1 Test Setup.....	22
Figure 2- 2 Load vs. Displacement Curves for all Tested Beams	30
Figure 2- 3 Typical Variations in AE Parameters for SFRCC-C Beam (Sensor 3).....	34
Figure 2- 4 Time for the First Crack for all Tested Beams.....	36
Figure 2- 5 Failure Mode Classification Based on AF vs RA for all Beams: (a) NC, (b) ECC, (c) SFRCC, (d) SFRCC-C, (e) SFRCC-T, (f) ECC-C, and (g) ECC-T	39
Figure 2- 6 Cracking pattern of the tested beams at failure: (a) NC, (b) ECC, (c) SFRCC, (d) ECC- C, (e) SFRCC-C. (f) ECC-T, and (g) SFRCC-T (Ismail and Hassan 2021)....	40
Figure 2- 7 Signal Amplitude at the First Crack for NC and SFRCC-T Beams.....	43
Figure 2- 8 Comparison of Amplitude vs Time between NC Beam and ECC-T Beam: (a)	47
Figure 3- 1 (a) Powder rubber; (b) Crumbrubber; (c) PVA fibers.....	64
Figure 3- 2 Test setup for all tested beams	66
Figure 3- 3 Cracking behavior for all tested beams: (a) NC; (b) CRECC; (c) PRECC; (d) NC-CRECC-C; (e) NC-PRECC-C; (f) NC-CRECC-T; (g) NC-PRECC-T; (h) Debonding of NC-PRECC-T (AbdelAleem and Hassan 2022)	73
Figure 3- 4 AE parameters and load vs time curves for PRECC beam sensor 2: a) CSS; b) number of hits; c) b -value; d) $H(t)$; e) S_r	75
Figure 3- 5 Time of the first crack load for all beams	77

Figure 3- 6 Variations in the Amplitude (ultimate load) of the three sensors	82
Figure 3- 7 Crack classification chart for all tested beams	85

List of Symbols, Nomenclature, or Abbreviations

AE	refers to “acoustic emission.”
ASTM	refers to “the American Society for Testing and Materials.”
B	refers to “binder content”
C	refers to “cement”
C.A.	refers to “the coarse aggregate.”
C/B	refers to the “cement to binder content”
CR	refers to “crumb rubber”
CSS	refers to “the cumulative signal strength.”
dB	refers to “the decibel unit.”
ECC	refers to “Engineering cementitious composites”
F.A.	refers to “the fine aggregate.”
FA	refers to “the fly ash.”
$H(t)$	refers to “the historic index.”
N	refers to “number of hits.”
NC	refers to “normal concrete.”
NDT	refers to “non-destructive testing.”
PR	refers to “powder rubber”
PVA	refers to “polyvinyl alcohol fiber”
SCC	refers to “self-consolidating concrete.”
SCM	refers to “supplementary cementing material.”
SHM	refers to “structural health monitoring.”

STS	refers to “splitting tensile strength”
SF	refers to “steel fiber”
S_r	refers to “the severity index.”
SS	refers to “silica sand”
W/B	refers to “water to binder ratio.”

1. Introduction

1.1. Background

In recent years, there has been a notable increase in the construction of concrete structures, including bridges, parking garages, offshore structures, and marine structures. (AbdelAleem and Hassan 2022; Mechtcherine 2013). Such structures are often vulnerable to external factors such as harsh environmental conditions, aging, increased mechanical loading, and impact stresses (Ramachandra Murthy et al. 2018). Consequently, those factors result in the degradation of those concrete structures, which leads to concrete spalling, cracks, reinforcement corrosion, and large deflections (Ramachandra Murthy et al. 2018). Consequently, there is a need for strengthening and repair of such structures in certain situations. Typically, the process of repairing/strengthening of any reinforced concrete structure is usually carried out by removing the old damaged concrete layer and replacing it with a new concrete layer (Engindeniz et al. 2005).

In the past few decades, research was mainly focused on repairing concrete structures using mortar, concrete, steel, and plastic composites (Kim et al. 2007). However, recently, there has been a switch on focus to fiber reinforced polymers (FRP) as repair materials. Due to its corrosion resistance, lightweight properties, and high strength, FRP has been viewed as an effective strengthening material (Sui et al. 2018). However, recent studies showed that the utilization of FRP as a strengthening material results in a weak bond between the concrete and the FRP, resulting in debonding and shear cracks (Sui et al. 2018 & Pan et al. 2022). As a result, there is a need to develop repair/strengthening materials with exceptional qualities such as high durability, strength, better bonding characteristics, ductility, cost-effectiveness, and structural performance. Such superior qualities can be

achieved by using engineering cementitious composites (ECC). ECC were originally formed by the micromechanics theory and offer very high tensile and compressive strengths (Li 1993; Li 2012). ECC are characterized by metal-like ductile, multi-cracking behavior (Li 1998). The maximum crack width accompanied by ECC are about 100 μm (Şahmaran and Li 2010). Furthermore, ECC exhibit ultimate tensile strengths ranging from 4 to 6 MPa with a strain capacity that can reach up to 5% (Li et al. 2002; Said and Razak 2015). Compressive strength of ECC falls within the range of 30 to 80 MPa with a strain capacity ranging from 0.45-0.65% (Said and Razak 2015). In comparison to normal concrete, ECC were found to exhibit a tensile ductility 600 times than that of normal concrete. (Kong et al. 2003; Li 1998). The incorporation of polyvinyl fibers (PVA) and steel fiber (SF) with a percentage of 2% has been found to have a favorable effect on the overall cracking behavior of ECC. PVA fibers were proven to show better performance (when compared to SF) at the pre-cracking stage due to their miniature size and low density, which allows for more fibers to exist at the same paste when placed in comparison with SF at the same fiber percentage. On the other hand, SF proved to show better performance at the ultimate stage due to their hooked ends that enhance the pullout strength, resulting in high compressive strength (Batra et al. 2021).

Waste rubber has recently been viewed as an economically friendly recyclable material for the use of production in the ECC (Rashad 2016). Rubber particles are characterized by low stiffness and high ductility and can further enhance the ductility, energy absorption and impact resistance of ECC (Ismail and Hassan 2016; Parveen and Sharma 2013; Thomas et al. 2016; Wang et al. 2013). Earlier studies have shown that augmenting the amount of rubber particles in concrete leads to a decrease in the compressive and tensile strength

(Ismail and Hassan 2016; Siad et al. 2019). However, this negative effect is counteracted in the ECC mixtures via the incorporation of fibers (AbdelAleem and Hassan 2022).

1.2. Structural Health Monitoring and Acoustic Emission Analysis Overview

The costs associated with the inspection and maintenance of several reinforced concrete structures constitute a big portion of any structure's life-cycle cost. According to the American society of Civil Engineers (ASCE), a C+ grade was attributed to the structural integrity of bridges: 25% of the US bridges are referred to as deficient (ASCE 2009). About \$20.5 billion is needed to be spent annually to eliminate deficient bridges (Volovski 2015). A cost-effective method, therefore, is needed to ensure scheduled maintenance and repair of any damage exhibited by such structures.

In recent years, the term "Structural Health Monitoring" (SHM) has been used to refer to a variety of systems installed in civil engineering structures to monitor and alert the owners on the structural state that might have gone through any gradual/sudden changes (Farrar and Worden 2007). The changes any reinforced concrete structure can go through include cracking, corrosion, and large deformations. SHM has a promising potential since it not only has economic and practicality benefits, but also it has the ability to provide periodic and scheduled updates/maintenance regarding a structure's integrity. This will ensure that all structures serve their intended function in the face of unavoidable factors such as aging and environmental changes (Di Benedetti 2012).

Acoustic emission (AE) monitoring is a SHM non-destructive evaluation (NDE) method usually carried out in situ. It is also referred to as NDE because it is can be applied during the loading period of the structure. AE monitoring is a unique method used to detect and monitor damage in structures over a long period of time. It is a useful method because it

has the ability to detect damage at a very early stage which results in a maintenance process that is cost-effective and efficient. AE works by releasing elastic waves as a result of any strain occurring in a structure. The strain energy detected by the AE sensors are generated from any source of damage (cracking, spalling, or corrosion) (Guo and Li 2020).

Generally, there are two types of AE analysis: parameter-based analysis and signal-based analysis. In the signal-based analysis, as many complete signals of AE events as possible are collected and saved together which is considered to be a more thorough and time-consuming approach. (Grosse et al. 2003). In addition, in the parameter-based analysis, signal characteristic parameters are used to assess damage severity and determine the type of damage (Behnia et al. 2014). Figure 1-1 illustrates the basic parameters of an AE signal (Behnia et al. 2014). Definition of all parameters can be found in ASTM E1316. The resulting parameter-based analyses include *b*-value analysis which is a very essential tool in evaluating the cracking propagation behavior over time until failure in several concrete structures (Colombo et al. 2003; Farhidzadeh et al. 2013; Schumacher et al. 2011). Intensity analysis is also a very effective method in creating a damage quantification chart relating to different damage levels (Abouhussien and Hassan 2017; Abouhussien and Hassan 2019; Abouhussien and Hassan 2019; Abouhussien and Hassan 2020). Moreover, RA (risetime/max amplitude) analysis is a successful approach in classifying different failure modes (flexural, shear, or debonding) (Ohno and Ohtsu 2010; Shahidan et al. 2013).

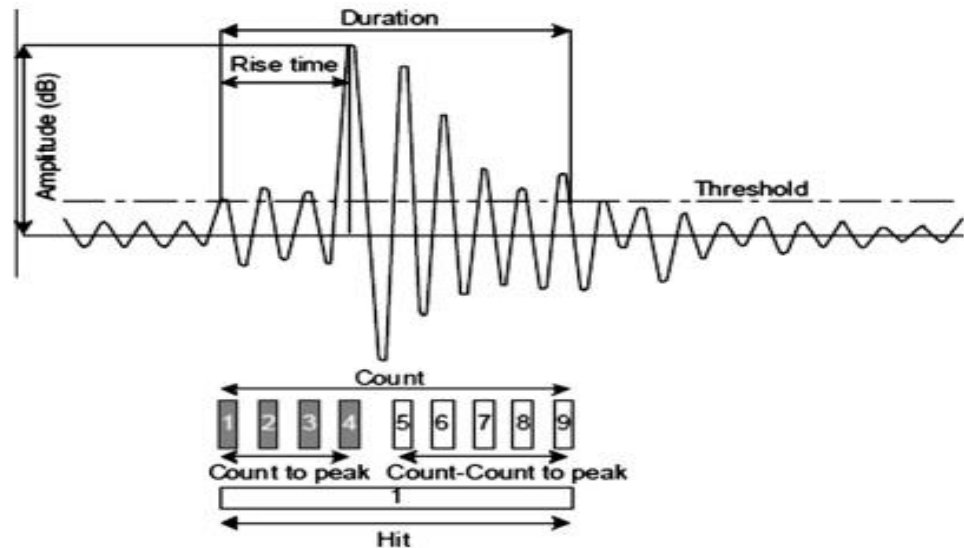


Figure 1- 1 Basic AE signal parameters (Behnia et al. 2014).

In the available literature, AE has proven to be effective in analyzing the cracking behavior in several hybrid composite structures. For instance, RA analysis has been used to characterize different failure modes (flexural, shear, or debonding) in composite multi-layered beams (Ranjbar et al. 2016); *b*-value has been used to monitor cracking propagation in FRP strengthened reinforced concrete beams (Selman et al. 2015); AE events vs time was utilized to represent the crack growth in hybrid composite concrete beams (Verbruggen et al. 2016). Furthermore, AE has proven efficacy in crack propagation and structural integrity monitoring in a variety of composite structures including polymer concrete slabs (Qin et al. 2020), carbon fiber reinforced polymer slabs (Degala et al. 2009), ECC beam-column connections (Abouhussien et al. 2019), hybrid fiber reinforced polymer columns (Mirmiran et al. 1999), ECC beams (Abouhussien and Hassan 2019), and many others.

Even though the AE technique is a very promising, non-destructive method with several practical advantages, it still comes with challenges/limitations to be considered. One of the

main challenges/limitations in the application of AE is the wave attenuation which can be a result of the non-homogeneous nature of multi-layered concrete. Properties of the materials investigated such as mechanical strengths, densities, and geometries need to be carefully studied prior to AE analyses to understand the source of the wave attenuation. Additionally, the location of the sensors within the area of interest is crucial for achieving a high level of accuracy. Consequently, AE sensors must be carefully placed closest to the area with the highest cracking activity (damaged zone). Finally, to remove any unwanted noise/signals that could impair the accuracy of the AE results, filtering the raw AE data is a very crucial step (Grosse et al. 2021).

The addition of new concrete to an old concrete layer (NC-ECC, for instance) is expected to have some effect on the AE parameters. The existence of two different materials with different microstructural properties is expected to result in signal attenuation (variation in signal amplitudes) (Ervin et al. 2007; Schumacher et al. 2011). Another concern is studying the effect of the repair location in terms of sensor location. AE waveforms collected by AE sensors are anticipated to be significantly impacted by changing the repair locations in repaired beams. Furthermore, the effect of repair using ECC, including different fibers or different rubber sizes, is expected to have some effect on the AE parameters.

1.3. Research Objectives

This thesis aimed to investigate the changes in the AE waveforms traveling through different concrete repaired beams under flexural loading. The experimental program of this study included eight reinforced normal concrete beams repaired in either the tension side or the compression side of the beams, four fully cast beams, and one normal concrete beam used for reference. The repaired beams included ECC as a repair material with different

types of fibers and different rubber particle sizes while the fully cast beams were fully cast in ECC containing different types of fibers and different rubber particle sizes. The purpose of this study was to analyze the effect of adding a new concrete layer (ECC with either fibers or rubber) to an existing layer with the aid of the variations in the AE parameters and to investigate the effect of varying the repair material and location through the changes in AE parameters and analyses. Furthermore, this research's objective was also to create damage quantification charts pertaining to different cracking stages as well as failure characterization charts related to different failure modes (flexural, or shear/debonding).

1.4. Thesis outline

As previously mentioned, this study aimed to evaluate the changes accompanied by the AE waves in thirteen ECC repaired beams and were titled as follows:

Chapter 2 titled "*Crack Detection and Classification of Repaired Concrete Beams by Acoustic Emission Monitoring*" studies the effect of the sensor/strengthening location and the fiber type (PVA or SF) on the AE parameters of ECC multi-layered beams.

Chapter 3 titled "*Damage Characterization in Large-Scale Multi-Layered Reinforced Concrete Beams by Acoustic Emission Analysis*" investigates the behavior of AE wave propagations emitted in ECC multi-layered rubberized concrete mixtures as a result of using different rubber particle size as well as alternating strengthening/sensor location.

Chapter 4 includes a summary of the results presented in Chapters 2 and 3, and recommendations for future studies.

1.5. Chapter References

- AbdelAleem, B. H., and Hassan, A. A. (2022). "Use of rubberized engineered cementitious composite in strengthening flexural concrete beams." *Engineering Structures*, 262, 114304.
- Abouhussien, A. A., and Hassan, A. A. (2017). "Application of acoustic emission monitoring for assessment of bond performance of corroded reinforced concrete beams." *Structural Health Monitoring*, 16(6), 732-744.
- Abouhussien, A. A., and Hassan, A. A. (2019). "Crack Growth Monitoring in Fiber-Reinforced Self-Consolidating Concrete via Acoustic Emission." *ACI Materials Journal*, 116(5), 181-191.
- Abouhussien, A. A., and Hassan, A. A. A. (2019). "Assessment of Crack Development in Engineered Cementitious Composites Based on Analysis of Acoustic Emissions." *Journal of materials in civil engineering*, 31(6).
- Abouhussien, A. A., Hassan, A. A., Ismail, M. K., & AbdelAleem, B. H. (2019). Evaluating the cracking behavior of ECC beam-column connections under cyclic loading by acoustic emission analysis. *Construction and Building Materials*, 215, 958-968.
- Abouhussien, A. A., and Hassan, A. A. A. (2020). "Classification of damage in self-consolidating rubberized concrete using acoustic emission intensity analysis." *Ultrasonics*, 100, 105999-105999.
- Batran, T. Z., Ismail, M. K., and Hassan, A. A. (2021). "Flexural behavior of lightweight self-consolidating concrete beams strengthened with engineered cementitious composite." *ACI Materials Journal*, 118(4), 39-50.

- Behnia, A., Chai, H. K., and Shiotani, T. (2014). "Advanced structural health monitoring of concrete structures with the aid of acoustic emission." *Construction and Building Materials*, 65, 282-302.
- Colombo, I. S., Main, I., and Forde, M. (2003). "Assessing damage of reinforced concrete beam using" b-value" analysis of acoustic emission signals." *Journal of materials in civil engineering*, 15(3), 280-286.
- Degala, S., Rizzo, P., Ramanathan, K., & Harries, K. A. (2009). Acoustic emission monitoring of CFRP reinforced concrete slabs. *Construction and Building Materials*, 23(5), 2016-2026.
- Di Benedetti, M. (2012). *Acoustic emission in structural health monitoring of reinforced concrete structures*, University of Miami.
- Ervin, B. L., Bernhard, J. T., Kuchma, D. A., and Reis, H. "Monitoring general corrosion of rebar embedded in mortar using high-frequency guided mechanical waves." *Proc., Sensors and Smart Structures Technologies for Civil, Mechanical, and Aerospace Systems 2007*, SPIE, 447-458.
- Farhidzadeh, A., Salamone, S., Luna, B., and Whittaker, A. (2013). "Acoustic emission monitoring of a reinforced concrete shear wall by b-value-based outlier analysis." *Structural health monitoring*, 12(1), 3-13.
- Farrar, C. R., and Worden, K. (2007). "An introduction to structural health monitoring." *Philosophical Transactions of the Royal Society A: Mathematical, Physical and Engineering Sciences*, 365(1851), 303-31.

- Grosse, C. U., Ohtsu, M., Aggelis, D. G., & Shiotani, T. (Eds.). (2021). "Acoustic emission testing: Basics for research–applications in engineering". *Springer Nature*.
- Grosse, C. U., Reinhardt, H. W., and Finck, F. (2003). "Signal-based acoustic emission techniques in civil engineering." *Journal of materials in civil engineering*, 15(3), 274-279.
- Guo, B., and Li, Y. "Review of Research on Damage Identification of Reinforced Concrete Structures Based on Acoustic Emission Technology." *Proc., IOP Conference Series: Earth and Environmental Science*, IOP Publishing, 012039.
- Ismail, M. K., and Hassan, A. A. A. (2016). "Impact resistance and acoustic absorption capacity of self-consolidating rubberized concrete." *ACI materials journal*, 113(6), 725-736.
- Kim, J.-H. J., Lim, Y. M., Won, J.-P., Park, H.-G., and Lee, K.-M. (2007). "Shear capacity and failure behavior of DFRCC repaired RC beams at tensile region." *Engineering structures*, 29(1), 121-131.
- Kong, H.-J., Bike, S. G., and Li, V. C. (2003). "Development of a self-consolidating engineered cementitious composite employing electrosteric dispersion/stabilization." *Cement and Concrete Composites*, 25(3), 301-309.
- Li, V. C. (1993). "From micromechanics to structural engineering the design of cementitious composites for civil engineering applications." *Doboku Gakkai Ronbunshu*, 1993(471), 1-12.
- Li, V. C. (1998). "Engineered cementitious composites (ECC)-tailored composites through micromechanical modeling."

- Li, V. C., Wu, C., Wang, S., Ogawa, A., and Saito, T. (2002). "Interface tailoring for strain-hardening polyvinyl alcohol-engineered cementitious composite (PVA-ECC)." *Materials Journal*, 99(5), 463-472.
- Li, V. C. (2012). "Tailoring ECC for special attributes: A review." *International Journal of Concrete Structures and Materials*, 6, 135-144.
- Mechtcherine, V. (2013). "Novel cement-based composites for the strengthening and repair of concrete structures." *Construction & building materials*, 41, 365-373.
- Masuelli, M. A. (2013). "Introduction of fibre-reinforced polymers– polymers and composites: concepts, properties and processes." *Fiber reinforced polymers-the technology applied for concrete repair*, IntechOpen.
- Mirmiran, A., Shahawy, M., & Echary, H. E. (1999). Acoustic emission monitoring of hybrid FRP-concrete columns. *Journal of Engineering Mechanics*, 125(8), 899-905.
- Ohno, K., and Ohtsu, M. (2010). "Crack classification in concrete based on acoustic emission." *Construction and Building Materials*, 24(12), 2339-2346
- Pan, B., Liu, F., Zhuge, Y., Zeng, J. J., & Liao, J. (2022). ECCs/UHPFRCCs with and without FRP reinforcement for structural strengthening/repairing: A state-of-the-art review. *Construction and Building Materials*, 316, 125824.
- Qin, L., Guo, C., Sun, W., Chu, X., Ji, T., & Guan, H. (2022). Identification of damage mechanisms of polymer-concrete in direct shearing tests by acoustic emission. *Construction and Building Materials*, 351, 128813.

Ramachandra Murthy, A., Karihaloo, B. L., Vindhya Rani, P., and Shanmuga Priya, D.

(2018). "Fatigue behaviour of damaged RC beams strengthened with ultra high performance fibre reinforced concrete." *International journal of fatigue*, 116, 659-668.

Rashad, A. M. (2016). "A comprehensive overview about recycling rubber as fine aggregate replacement in traditional cementitious materials." *International Journal of Sustainable Built Environment*, 5(1), 46-82.

Şahmaran, M., and Li, V. C. (2010). "Engineered cementitious composites: Can composites be accepted as crack-free concrete?" *Transportation Research Record*, 2164(1), 1-8.

Said, S. H., and Razak, H. A. (2015). "The effect of synthetic polyethylene fiber on the strain hardening behavior of engineered cementitious composite (ECC)." *Materials & Design*, 86, 447-457.

Siad, H., Lachemi, M., Ismail, M. K., Sherir, M. A., Sahmaran, M., and Hassan, A. A. (2019). "Effect of rubber aggregate and binary mineral admixtures on long-term properties of structural engineered cementitious composites." *Journal of Materials in Civil Engineering*, 31(11), 04019253.

Schumacher, T., Higgins, C. C., and Lovejoy, S. C. (2011). "Estimating operating load conditions on reinforced concrete highway bridges with b-value analysis from acoustic emission monitoring." *Structural Health Monitoring*, 10(1), 17-32.

- Shahidan, S., Pulin, R., Bunnori, N. M., and Holford, K. M. (2013). "Damage classification in reinforced concrete beam by acoustic emission signal analysis." *Construction and Building Materials*, 45, 78-86.
- Sui, L., Luo, M., Yu, K., Xing, F., Li, P., Zhou, Y., & Chen, C. (2018). Effect of engineered cementitious composite on the bond behavior between fiber-reinforced polymer and concrete. *Composite Structures*, 184, 775-788.
- Verbruggen, S., De Sutter, S., Iliopoulos, S., Aggelis, D., and Tysmans, T. (2016). "Experimental structural analysis of hybrid composite-concrete beams by digital image correlation (DIC) and acoustic emission (AE)." *Journal of Nondestructive Evaluation*, 35, 1-1.

2. Crack Detection and Classification of Repaired Concrete Beams by Acoustic Emission

2.1. Abstract

In this study, acoustic emission (AE) monitoring was used to investigate the cracking behavior of normal reinforced concrete beams repaired with fiber-reinforced cementitious composites (FRCC). The investigated beams were strengthened at two locations: tension side and compression side of the beam. Two different fibers were used in FRCC strengthening material: steel fibers and polyvinyl alcohol fibers. One normal concrete beam and two fully cast FRCC beams were also tested for comparison. All beams were tested under four-point loading until failure. The investigation considered the variations in several AE parameters such as number of hits, cumulative signal strength, signal amplitude, peak frequency, absolute energy, and *b*-value analysis. In addition, rise time/amplitude analysis was successfully utilized in this study to classify the failure modes (flexural or shear/debonding failure between the repair layer and existing beam) for all beams. The impact of the fiber type, strengthening location, and sensor location on the aforementioned parameters was clearly highlighted. Varying the fiber type of the FRCC or changing the repair location of the beam seemed to have a significant impact on the resulting AE parameters. A good correlation was found in repaired and unrepaired beams between AE parameters and the progression of cracks beyond the first crack until failure. The results also indicated that the AE analysis carried out in this study led to the identification of the first crack in repaired and unrepaired beams.

Keywords: Fiber-reinforced cementitious composites; acoustic emission analysis; reinforced concrete beams; crack detection; failure mode.

2.2. Introduction

Many existing concrete structures are undergoing low to high levels of damage because of concrete aging, environmental conditions, and/or lack of maintenance, (Ismail and Hassan 2021; Kenai and Bahar 2003; Mukherjeel and Joshi). This damage includes cracks, concrete spalling, excessive deflections, and rebar corrosion (Ramachandra Murthy et al. 2018). In the past decade, several research efforts were focused on the topic of repairing/strengthening concrete using repair materials such as mortar, concrete, steel, and plastic composites (Kim et al. 2007). Recently, various types of repairing materials have been receiving attention (Jumaat et al. 2006). These include hybrid fiber reinforced concrete, steel fiber reinforced concrete, and engineered cementitious composites (ECC).

ECC were originally developed from the micromechanics theory which connects between material structures and composite properties (Li 1993). ECC typically consist of cement, fine silica sand, fly ash, fibers (polymeric fibers, carbon fibers, and/or steel fibers (SFs)), and high range water reducer admixtures (Ismail et al. 2018; Ismail et al. 2018; Li 1998; Singh et al. 2019). The volume of fibers present in ECC is typically 2% of the total volume (Ismail et al. 2018; Li et al. 2002). ECC possess very high ductility characteristics when provided with discontinuous fibers (Singh et al. 2019). One of the significant properties of ECC is the tensile strain-hardening after the first crack and multiple microcracks with a very small crack width. Other properties include high ductility under uniaxial tensile loading and the improved ductility due to the appearance of the multiple microcracks with tight widths (Şahmaran and Li 2010).

Acoustic Emission is a unique, non-destructive method used to detect and continuously monitor cracks in structures. AE works by the release of elastic waves whenever any defects occur in a concrete structure (Guo and Li 2020). Many experimental and real-life applications of AE monitoring have been performed in the past few years. These applications include: maintenance of bridges by detection of damage (Golaski et al. 2002), early corrosion detection of concrete pre-stressed girders (ElBatanouny et al. 2014), mechanical analysis of multi-layered reinforced concrete composite beams (Ranjbar et al. 2016), classification of alkali–silica reaction damage in concrete (Abdelrahman et al. 2015), monitoring of crack propagation in reinforced concrete walls (Farhidzadeh et al. 2013), analysis of crack evolution in plain concrete (Saliba et al. 2016), and investigation of fatigue damage of both rubberized and plain concrete (Wang et al. 2011). AE has also proven to be successful tool in detecting the failure in different concrete types. For example, AE was used to characterize the crack propagation in fiber reinforced concrete (Abouhussien and Hassan 2019; Abouhussien and Hassan 2019), rubberized concrete (Abouhussien and Hassan 2020; Abouhussien et al. 2019), and strain hardening cement-based composites (Paul et al. 2015). AE parameters such as number of events and *b*-value analysis, and/or rise time/amplitude (RA) analysis were also used to understand the crack propagation with relation to the load and to categorize the failure mode in hybrid-composite beams (Selman et al. 2015; Verbruggen et al. 2015). In another study (Aggelis et al. 2019), AE parameters such as signal amplitude vs time was used to detect debonding in lightweight hybrid concrete beams.

Repair of deteriorated concrete beam is usually performed by adding a layer of fiber-reinforced cementitious composites (FRCC) to either the bottom side or the top side of the

beam. The new repair layer is normally made with higher strength/performance concrete compared to the concrete of existing beam in order to maximize the capacity of the whole composite. Steel fiber or polypropylene fibers are commonly added in the repair layer mixture to increase the flexural strength of such layer. The applications of AE in damage detection and classification of FRCC-repaired concrete beams in both compression and tension zones are very limited. In particular, the literature only includes experimental studies in utilizing AE analyses in detecting damage in carbon fiber reinforced polymers (FRP) strengthened reinforced concrete beams (Selman et al. 2015) and textile reinforced cements and FRP composite beams (Verbruggen et al. 2015 and Aggelis et al. 2019). The sensor location with respect to the FRCC repair layer is anticipated to have a significant impact on the AE results. Signal attenuation, a phenomenon where there is a change in the amplitude range, is expected to occur in repaired beams due to the presence of two different materials with two different densities/microstructures (FRCC repair layer and existing normal concrete beam). This is owing to the different AE wave propagation characteristics through these materials as a result of their different densities/microstructures and the interface (gap) between the two layers which contributes to wave attenuation when the AE signal path travels through the layers (Ervin et al. 2007; Schumacher et al. 2011). In addition, the variation in the type of fibers (PVA fiber or SFs, if present) in the repair material is anticipated to have an effect on AE parameters. Moreover, the difference in failure mode and crack propagation, particularly if the failure occurs in the bond between the new layer and existing beam, is expected to yield variations in terms of AE parameters. Therefore, more investigations are warranted to quantify the effect of wave attenuation in

repaired beams with two different concrete materials and to understand the impact of these factors on the AE parameters.

There is a gap in the literature involving the application of AE analysis on repaired concrete beams. Especially, the literature lacks information regarding the application of the RA and *b*-value analyses on large-scale repaired reinforced concrete beams. The purpose of this study was to investigate the effectiveness of the AE analysis including *b*-value and RA analyses in evaluating the cracking and failure behavior of repaired beams. This study also involved understanding the effect of sensor location with respect to the repair layer, using different fiber types, and changing the repair locations on the AE parameters. The results of the AE analyses were used to assess the development of the cracking till failure and to classify the failure mode (shear, flexural, or debonding failure) of large-scale repaired beams with the aid of AE analysis.

2.3. Research Significance

The addition of a new concrete layer in the repaired beam is expected to have some impact on AE readings. The presence of two different concrete layers with two different strengths and compositions may cause acoustic signal attenuation. Also, the presence of fibers in the repair concrete layer (if used) compared to no fibers in the existing beam may cause different wave propagation in the two concrete layers. Moreover, in addition to normal flexure and shear cracks, repaired beam may experience some crack activities at the interface between the existing beam and the new repair layer, and this will also affect the AE parameters. The available literature lacks information about the application of AE analysis in multi-layered repaired beams. Specifically, there is a gap in the literature regarding the effectiveness of using AE analysis for the evaluation of the crack propagation

in large-scale FRCC-repaired beams with two different concrete layers in both compression and tension zones. Therefore, this paper aims to cover this knowledge gap and to exploit traditional AE parameters as well as RA and b -value analyses to investigate the cracking behavior and development in large-scale reinforced concrete beams strengthened with FRCC layer. This study also aims to assess the impact of sensor location with respect to the repair layer, which is expected to have a significant effect on AE signal characteristics. In addition, this study exclusively characterizes the fracture modes in the repaired beams using RA analysis, which would be beneficial in understanding the structural behavior of composite reinforced concrete beams.

2.4. Overview of AE Analysis in Composite Concrete Structures

Different AE parameters were used to detect damage in concrete structures including energy, duration, counts, amplitude, and rise time (Abouhussien and Hassan 2015). Other AE parameters such as number of hits and signal strength can also be used in damage classification. Signal strength, one of the most crucial AE parameters, is described as the area under the amplitude-time envelope. Signal strength has units that are corresponding to V-s (a constant that is given by the AE instrument manufacturer). V-s incorporates the absolute values of the positive and negative areas of the amplitude-time envelopes (ElBatanouny et al. 2014). The collected raw AE parameters can be used to classify different types of damages and failures. For instance, RA (rise time/amplitude) vs. average frequency (counts/duration) is used to distinguish between flexural and shear failure (Ranjbar et al. 2016; Ohno and Ohtsu 2010; Prem and Murthy 2017) (Behnia et al. 2014). The values of cumulative signal strength (CSS), along with intensity analysis parameters namely historic index ($H(t)$) and severity (S_r) are used to detect early cracking in composite

structures subjected to four-point loading (ElBatanouny et al. 2014). *b*-value analysis is also another method to evaluate the cracking behavior of composite structures. *b*-value which is the amplitude number of hits can be used to represent the changes in the AE events to indicate the level of damage in a structure (Abouhussien and Hassan 2016; Abouhussien and Hassan 2019; Abouhussien et al. 2019).

2.5. Experimental Program

2.5.1. Material Properties

In this study, seven large-scale reinforced concrete beams were tested. The seven beams included one fully cast normal concrete (NC) beam, one fully cast FRCC beam with PVA fibers (ECC), one fully cast FRCC beam with steel fibers (SFRCC), and four repaired NC beams containing layers of either ECC or SFRCC. The mix design of the beams is presented in Table 2-1. The NC mixture was comprised of Type 1 Portland cement according to ASTM C150 (ASTM C150/C150M 2012), 10 mm crushed granite stone used as coarse aggregate, and crushed granite sand used as fine aggregate. The specific gravity of both aggregates was 2.6. The binder content in the ECC and SFRCC mixtures was a combination of Type 1 Portland cement and class F fly ash (FA) complying with ASTM C150 and ASTM C618 (ASTM C150/C150M 2012), respectively. Silica sand with a specific gravity of 2.65 as a fine aggregate was incorporated in both the ECC and SFRCC mixtures. ECC mixture consisted of 8 mm PVA fibers and the SFRCC design mix consisted of 13 mm steel fibers (Ismail and Hassan 2021). The properties of each fiber type used in this study are illustrated in Table 2-2.

Table 2- 1 Mix Design (Ismail and Hassan 2021).

Mixture	B	C/B	SCM Type	SCM/B	S/B	C.A./B	W/B	Fibers (%)	Fiber type	f_c	Ultimate STS (MPa)
NC	1	1	-	-	1.33	2	0.40	-	-	59.0	4.4
ECC	1	0.45	FA	0.55	0.36	-	0.27	2	PVA	62.6	8.7
SFRCC	1	0.45	FA	0.55	0.36	-	0.27	2	SF	76.5	10.1

Notes: B=binder content; C=cement; SCMs: supplementary cementing materials; FA=fly ash; S=sand; C.A. = coarse aggregate; W/B=water-to-binder (i.e., cement+ SCMs); PVA= polyvinyl alcohol fiber; SF= steel fiber, f_c =compressive strength; STS = splitting tensile strength.

Table 2- 2 Properties of Fibers (Ismail and Hassan 2021)

Fibers	Ultimate Tensile Strength (MPa)	Diameter (μm)	Length (mm)	Young's Modulus (GPa)	Density (kg/m^3)
PVA	1600	38	8	40	1300
SF	1900	200	13	203	7800

2.6. Details of Tested Beams

The dimensions, steel reinforcements, and geometry of all the tested repaired and unrepaired (control) beams are shown in **Figure 2-1**. As mentioned earlier, seven large-scale beams were tested. The first, second, and third beam were fully cast NC, ECC, and SFRCC, respectively. The fourth and fifth beams were referred to as ECC-C and SFRCC-C, respectively. In these beams, the repair layer was placed at the compression zone of the beam. The beam's compression zone was repaired with ECC and SFRCC aiming to boost its strength and strain capacity and then investigate the subsequent impacts of such improvements on the structural performance of beam in terms of load-carrying capacity, ductility, and energy absorption capacity. The sixth and seventh beams were referred to as ECC-T and SFRCC-T, respectively, and had their repair layers were placed in the tension

zone. The bond between the existing NC beam and the repair layer (ECC or SFRCC) was achieved through the shear stirrups which served to connect the two layers. To further enhance the bond between the NC and repair layer, the surface of the first casted layer was roughened before pouring of the second layer. Full details of the tested beam can be found elsewhere (Ismail and Hassan 2021).

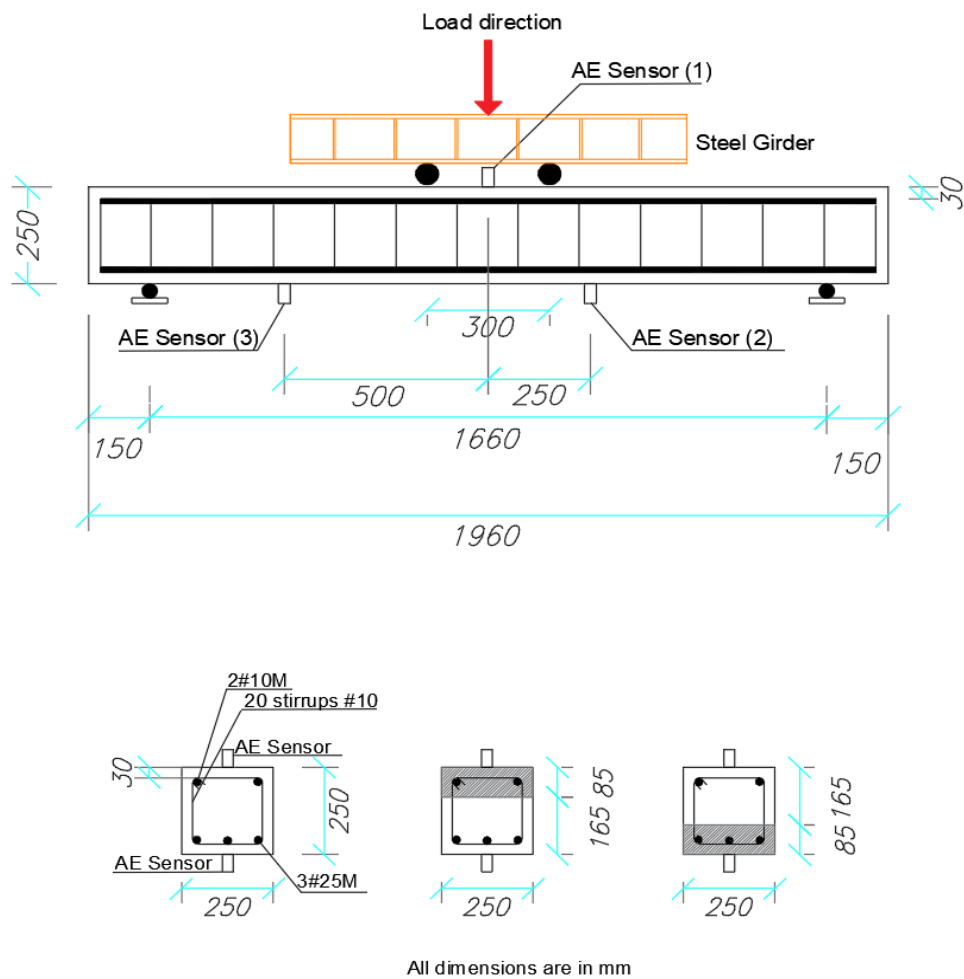


Figure 2- 1 Test Setup

2.7. Test Setup, Instrumentation, Loading Procedures, and AE Setup

The test set up for all beams is illustrated in **Figure 2-1**. The beams were tested by a four-point symmetrical vertical loading to analyze the flexural behavior. The load was monotonically applied until the first crack was visible and then was manually applied at constant increments of 45 kN until failure occurred. The loading was halted after each load step of 45 kN to identify and measure the cracks developed after each load step by a crack detection microscope. All beams were designed to fail in ductile flexural mode of failure. To avoid shear failure, 10 mm stirrups were spaced at a 100 mm distance along the length of the beam. Additionally, a single linear variable differential transformer (LVDT) was used to measure the vertical mid-span deflection. To observe the reinforcement bars yielding, strain gauges were placed at the mid-span of the longitudinal bars in the tension zone (Ismail and Hassan 2021). Test results of all beams are illustrated in **Table 2-3** (Ismail and Hassan 2021).

The AE signals were continuously acquired throughout the loading by using three AE sensors that were piezoelectric sensors having an integral preamplifier (R6I-AST). These sensors were selected for this research owing to their high sensitivity, low resonant frequency, and suitability for variety of applications including metal, FRP, and concrete structures (Physical Acoustics, 2005). This type of sensor was successfully used in preceding AE analysis performed by the authors in similar previous investigations (Abouhussien and Hassan 2015; Abouhussien and Hassan 2016; Abouhussien and Hassan 2019; Abouhussien and Hassan 2019). One sensor was placed at the surface of the beam and two were placed at the bottom of the beam, as illustrated in **Figure 2-1**. Sensor (1) was placed at the top mid-span of the beam while sensor (2) and sensor (3) were placed at the

bottom of the beam at distances 250 mm and 500 mm, respectively, measured from sensor (1). A two-part epoxy adhesive was used to attach the sensors to each beam prior to testing and allowed to dry for a few hours to achieve the full contact between the surface of the beam and the AE sensors. The AE data processed from the bending test was recorded using a four channel AE data acquisition system and AEWin signal processing software (Group 2007). An amplitude threshold of 40 dB was kept as a constant for all tests which was identified based on previous similar investigations (ElBatanouny et al. 2014; Abouhussien and Hassan 2015; Abouhussien and Hassan 2016; Abouhussien and Hassan 2019). Other acquisition system parameters are illustrated in **Table 2-4**. The values of the acquisition parameters are based on previous studies involving the application of AE monitoring in concrete structures (ElBatanouny et al. 2014; Abdelrahman et al. 2015; Abouhussien and Hassan 2015; Abouhussien and Hassan 2016; Abouhussien and Hassan 2019; Abouhussien et al. 2019). Several AE parameters were attained during the test. These parameters include signal amplitude, rise time, duration, counts, peak frequency, average frequency, signal strength, absolute energy, and energy. Definitions of the previously mentioned parameters can be found in ASTM E1316 (ASTM 2014).

Table 2- 3 Test Results of all Beams (Ismail and Hassan 2021)

Beam	Observed First Crack Load (kN)	Maximum Crack Width at Service Load		Failure stage				
		50%	75%	Failure Load (kN)	Number of Cracks	Maximum Crack Width (mm)	Crack Type	Failure Mode
NC	15.1	0.30	0.55	390.1	23	3.2	VL	Flexural
ECC	22.3	0.20	0.30	425.25	37	2.5	VL	Flexural
SFRCC	18.7	0.10	0.25	460.8	32	2.8	VL	Flexural
ECC-C	14.8	0.30	0.50	413.8	21	3.8	VL	Flexural
SFRCC-C	15.5	0.25	0.45	420.3	24	3.5	VL	Flexural
ECC-T	19.6	0.22	0.30	383.9	19	2.0	DL	Shear-interface debonding
SFRCC-T	17.9	0.15	0.28	321.6	27	3.0	DL	Shear-interface debonding

Notes: VL = vertical and DL= diagonal cracks.

Table 2- 4 AE System Configuration

AE Data Acquisition Setup	
Threshold	40 dB _{AE}
Sample rate	1 MSPS
Pre-trigger	256 μ s
Length	1 k points
Preamp gain	40 Db
Peak definition	200 μ s
Hit definition	800 μ s
Hit lockout time	1000 μ s
Maximum duration	1000 μ s

2.8. Processing and Analysis of AE data

2.8.1. AE Filtering

The raw data obtained from the four-point flexural tests was filtered in order to reduce any noise/unwanted signals, such as those generated due to the contact/friction between the loading points and the tested beam. The filtering of the data was carried out through an amplitude-duration-based-filter (Swansong II filter). The amplitude-based-filter was successfully implemented in previous related studies on AE analysis of reinforced concrete structures (Abouhussien and Hassan 2015; Abouhussien and Hassan 2016; Abouhussien and Hassan 2019; Abouhussien et al. 2019). The mechanism of the filter depends on the fact that actual AE signals with high signal amplitude are accompanied with large signal durations and vice versa (Abdelrahman et al. 2015). The values for the acceptance/rejection basis are presented in **Table 2-5**. The acceptance/rejection limits of this filter were determined based on an extensive analysis in the form of visual inspection of the AE signals obtained from all tested specimens. These ranges were also utilized in previous similar studies and proved their effectiveness in minimizing the unwanted noise resulting from the frictional or mechanical noise from the testing setups (Abouhussien and Hassan 2015; Abouhussien and Hassan 2016; Abouhussien and Hassan 2019; Abouhussien et al. 2019). The application of this filtering process resulted in a reduction of approximately 10–50% of the raw data between the tested beams. After carrying out the filtering procedure, all other AE signals are considered to be reliable and are a result of crack progression in the tested beams.

Table 2- 5 Rejection Limits for AE Data Filter

Amplitude (dB)	Duration (μ s)	
	Lower	Upper
$40 \leq A < 45$	0	400
$45 \leq A < 48$	0	500
$48 \leq A < 52$	0	600
$52 \leq A < 56$	0	700
$56 \leq A < 60$	100	800
$60 \leq A < 65$	300	1,000
$65 \leq A < 70$	500	2,000
$70 \leq A < 80$	1,000	4,000
$80 \leq A < 90$	2,000	7,000
$90 \leq A < 100$	3,000	10,000

2.8.2. *b*-value Analysis

A number of AE parameters have been investigated in this study. These parameters included the number of hits, cumulative signal strength (CSS), peak frequency, amplitude, and absolute energy. *b*-value analysis utilizes the AE signal amplitude and number of hits to create the *b*-value parameter. *b*-value is very sensitive to the crack development or progression and has been used successfully in several previous studies (Abouhussien and Hassan 2019; Abouhussien et al. 2019; Colombo et al. 2003; ElBatanouny et al. 2014) to characterize the level of damage in concrete structures. The *b*-value was calculated for all tested beams during the flexural tests using the following **Eq. (2-1)**:

$$\log N = a - b \log A \quad (2-1)$$

Where: *N* = number of hits having amplitudes larger than *A*; *A* = signal amplitude (dB); *a* = empirically derived constant (*a* = 4.7 for all specimens); *b* = *b*-value (Colombo et al. 2003; ElBatanouny et al. 2014; Vidya Sagar and Raghu Prasad 2013). The constant value “*a*” was acquired by plotting log *N* (y-axis) versus log *A* (x-axis) for all tested specimens.

The average “a” value was then calculated and applied in **Eq. (2-1)** in each beam to obtain the *b*-value.

2.8.3. RA Analysis

RA vs AF analysis is a useful tool in determining the failure mode. It has been used in former studies in the literature (Behnia et al. 2014; Ohno and Ohtsu 2010; Prem and Murthy 2017; Ranjbar et al. 2016) to differentiate between tension and shear cracking in different loading stages. RA and AF values are defined in **Eqs. (2-2) and (2-3)** as follows (Ohno and Ohtsu 2010):

$$\text{RA value} = \text{rise time}/\text{maximum amplitude} \quad (2-2)$$

$$\text{Average frequency} = \text{AF} = \text{counts}/\text{duration time} \quad (2-3)$$

Different types of acoustic emission signals (waveforms and frequency) are related to different types of failure modes. For instance, flexural failure that results in tensile cracks is usually in the form of brief volumetric change in the structure in which the released energy is transformed to longitudinal waves (P-waves). On the other hand, shear failure that results in shear cracks is usually represented by distortional waves (S-waves) (Ranjbar et al. 2016). It has been observed that at the beginning of the fracture process of any structure that the AF values is usually very high compared to the RA values whereas at the end of the process the RA value is usually very high compared with the AF values. This is due to the fact that tensile cracks tend to appear at the beginning of any testing process while shear cracks tend to appear towards the end. To further clarify, tensile cracks usually correspond to high AF values while shear cracks are usually accompanied by high RA values (Aggelis 2011; Grosse and Ohtsu 2008; Shahidan et al. 2013).

2.9. Results and Discussion

2.9.1. Structural Performance and Cracking Behavior of the Tested Beams

Figure 2-2 represents the mid-span deflection curves for all beams. **Tables 2-3** shows the values for first and failure crack loads, crack widths, failure crack types, and failure modes for all beams. Generally, the incorporation of fibers in the ECC beams resulted in enhanced load carrying capacity and cracking load as well as high deformability, ductility, and energy absorption, when compared to the NC beam (**Table 2-3**).

In the pre-cracking stage, all tested beams showed a linear relationship in the load vs displacement graph. No cracks were formed at the beginning of the loading as all beams had a high stiffness. At higher stages of loading, the first crack occurred at the maximum moment (at mid span) in the tension side of the beams. The first visible crack width for all beams was about 0.02 mm. During the post-cracking stage, the control beams (NC, ECC and SFRCC) started to experience vertical cracks with the increase of the loading. As the load increased, the width and length of the vertical cracks were also increased. Diagonal cracks were developed afterward at the shear span (distance between loading point and support). With the appearance of vertical and diagonal cracks, the stiffness of the beams was decreasing. The three control beams also exhibited large deflection before failure. The beams failed in flexural mode in which the longitudinal steel reinforcement at the tension side reached the yield stress and the concrete was crushed at the compression side of the beam. Compared to the NC beam, the ECC and SFRCC beams showed higher deformation/deflection and higher number of cracks with narrower widths. The higher number of cracks and narrow widths is due to the presence of fibers which prevents the cracks from opening wider (Ismail and Hassan 2021).

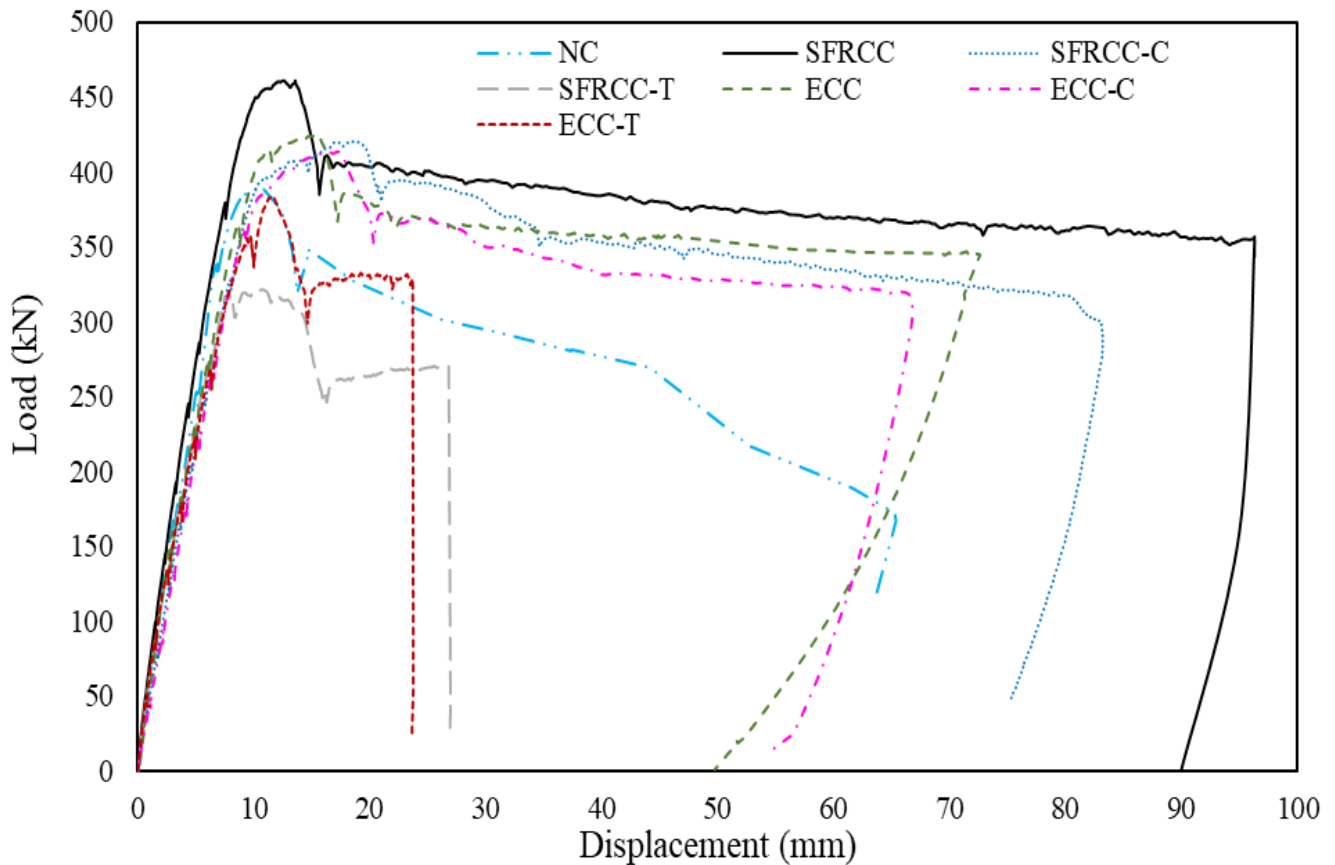


Figure 2- 2 Load vs. Displacement Curves for all Tested Beams

The repaired beams ECC-C and SFRCC-C both failed in flexure mode. Compared to the NC beam, the repaired beams experienced higher deformation prior to failure due to the high strain capacity of ECC and SFRCC. The deflection correlating to the peak load of the ECC-C and SFRCC-C beam was 16.3 mm and 18.4 mm, respectively which were 53.8% and 73.6%, higher than the deflection recorded by the NC beam (**Figure 2-2**). Both ECC-T and SFRCC-T beams failed in debonding in the NC-FRCC interface layer and as a result showed the lowest deflection. In the ECC-T and SFRCC-T, multiple thin cracks in the ECC or SFRCC layer followed the appearance of the first crack. As the loading increased, new cracks propagated at the NC-FRCC interface, spread to the NC layer (upward) afterward, and then moved back to the FRCC layer (downward). The width and rate of increase of the cracks was lower in the FRCC (ECC or SFRCC) than in the existing NC beam. The

longitudinal steel reinforcement at the tension side of ECC-T and SFRCC-T beams reached the yield stress but the concrete in the compression side did not crush. This is because of the debonding failure that occurred in those beams which was followed by shear diagonal cracks until failure (without crushing in the top compression zone). The angle of the shear cracks ranged from 35° to 45°. To get desirable results and to avoid such failure, it is recommended to use a higher strength FRCC, coarser interface and/or shear keys.

2.9.2. Evaluation of Damage Progression by AE analysis

This section discusses the effect of the crack progression on the AE parameters. AE parameters such as number of hits, cumulative signal strength (CSS), *b*-value, amplitude, peak amplitude, and absolute energy were considered. **Figure 2-3** represents the variations of the AE parameters collected during the testing process of the SFRCC-C beam (Sensor 3) in order to understand the changes in the cracking behavior of the beams. The purpose of this figure was to correlate between the time-dependent changes in AE parameters including number of hits, CSS, *b*-value, amplitude, peak frequency, and absolute energy to the crack initiation and propagation in the SFRCC-C beam. These parameters were recorded during the four-point testing as the loading was increasing until failure. SFRCC-C beam (sensor 3) was chosen to be a representative example (shown in **Figure 2-3**) as a typical sample of other sensors and beams. Other tested beams showed similar trends to those shown in **Figure 2-3** for all the studied AE parameters throughout the tests till failure. **Figures- 3(a)** and **3(b)** show an overall increase in both the number of hits and CSS which is a presentation of crack propagation over time. In general, the increase in AE activity is correlated to the progression of cracks until failure. The changes and fluctuations in the CSS chart are very similar to those of the number of hits. It can be inferred that the first

increase of number of hits (change in slope) is detected at about 80 s which is also similar to the first change in slope in the CSS curve which is also detected at about 80 s. This increase can be correlated to the occurrence of the first crack at the midspan of the beam which was confirmed by means of the visual inspection of the beam during the test similar to other previous studies (Abouhussien and Hassan 2019; Abouhussien et al. 2019).

Figure 2-3(c) represents the b -value which experienced a general decreasing trend as the crack propagation increased over time. As the load increased and AE activity increased, the b -value decreased. The fluctuation and jumps in the b -value also corresponded to the increases in the AE activity (slope changes in the number of hits and CSS curves). To further corroborate the time of the occurrence of the first crack, the lowest decreasing trend in the b -value was also spotted at about 80 s. b -value is an important tool that can be used to emphasize the location of high AE activities during the tests.

The amplitude, peak frequency, and absolute energy showed an overall fluctuation over time while CSS, number of hits, and b -value showed either increasing or decreasing trend over time. In **Figures 2-3(d), 3(e)** and **3(f)**, it is noticed that the areas of high fluctuations correspond to slope changes in **Figures 2-3(a)** and **3(b)**. The increase or fluctuations is due to the propagation of cracks which is a further corroboration along with the number of events, CSS, and b -value charts. The locations of the slope change and/or the sudden jumps of the aforementioned AE parameters have been found to be correlated to the occurrence of high AE activities (Colombo et al. 2003; ElBatanouny et al. 2014; Abouhussien and Hassan, 2019). These increased AE activities have been found to be associated with the fracture related properties of various types of FRCC (Thirumalaiselvi et al. 2020). The same parameters (number of hits, cumulative signal strength, b -value, amplitude, peak

amplitude, and absolute energy) were analyzed for all the tested beams similar to the example shown in **Figure 2-3**. The AE activity for all beams increased overtime until failure and this is due to the initiation of both micro and macro cracks. The values of the studied AE parameters for all tested beams at failure are summarized in **Table 2-6**. These results indicate that good correlation was found in both repaired and unrepaired beams between the AE parameters and progression of cracks beyond the first crack until failure.

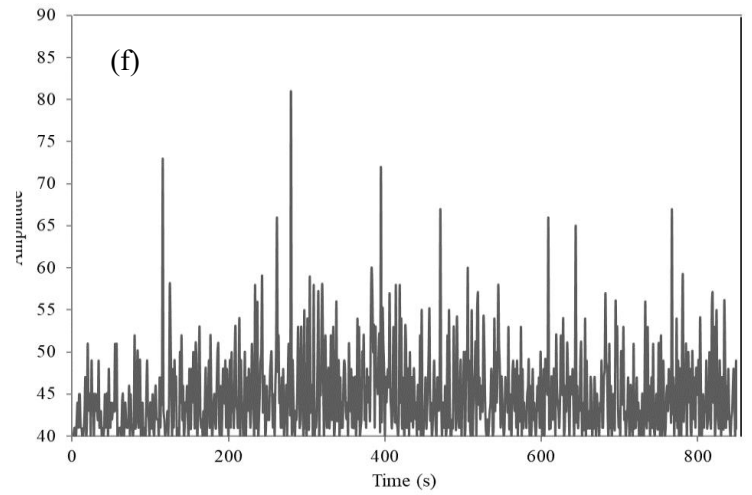
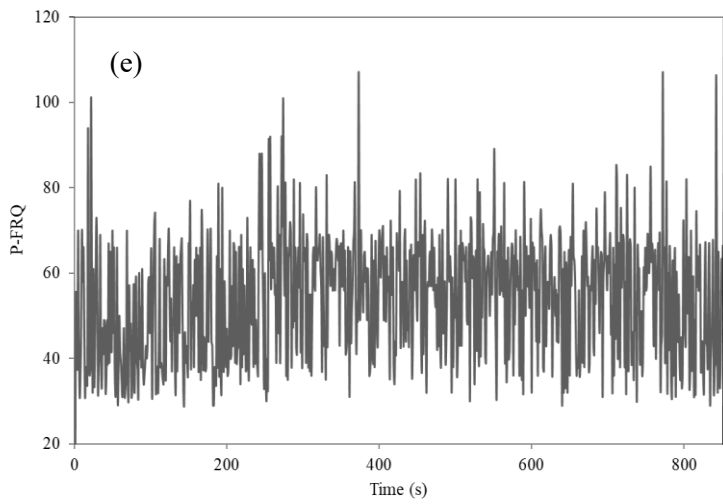
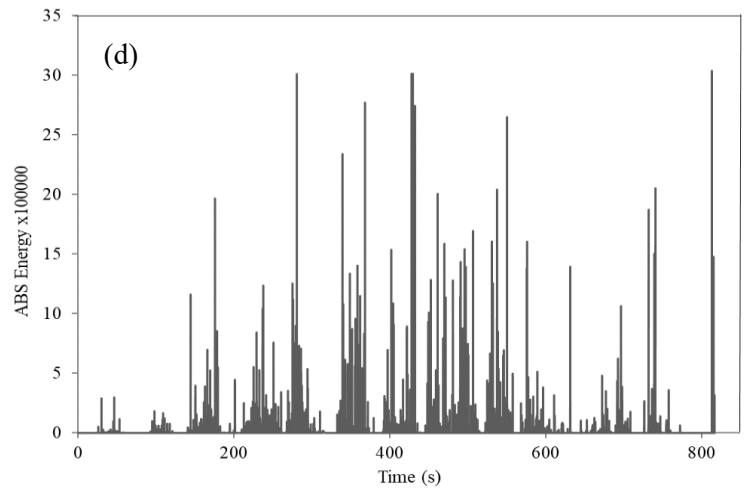
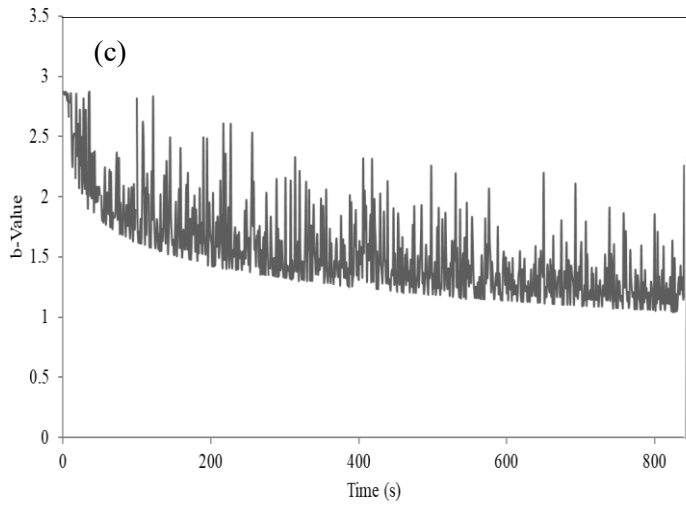
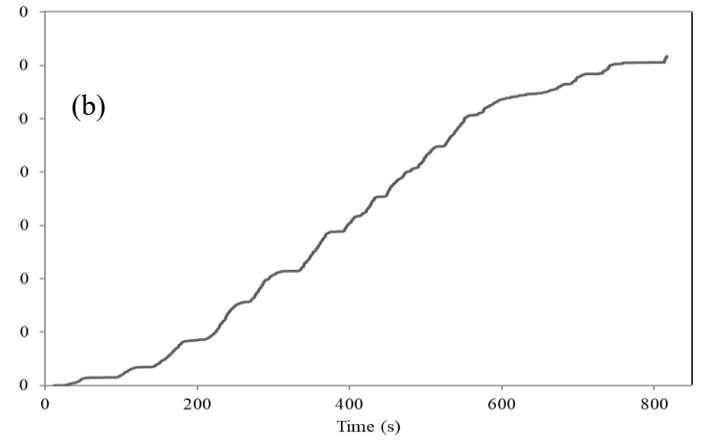
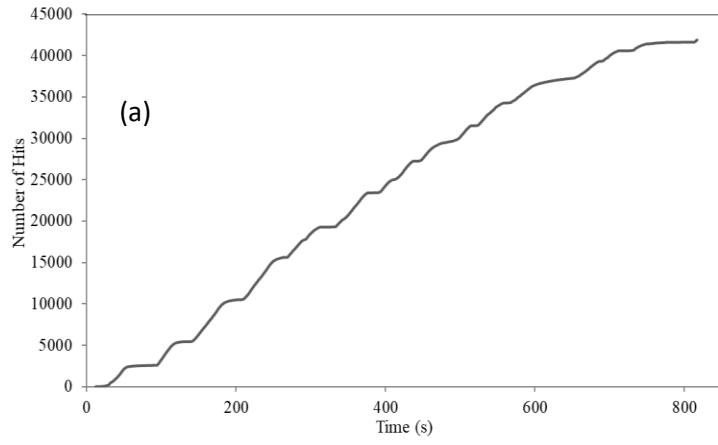


Figure 2- 3 Typical Variations in AE Parameters for SFRCC-C Beam (Sensor 3)

Table 2- 6 AE Parameters for all Beams at Failure

Mixture name	AE sensor	Average Amplitude (dB)	CSS x 10 ⁷ (pV.s)	b-value	Number of Hits
NC	AE 1	44	44.1	0.407	27686
	AE 2	44	65	0.263	29200
	AE 3	43	80.1	0.140	30500
SFRCC	AE 1	44	101	0.09	40000
	AE 2	44	67.1	0.12	36250
	AE 3	43	33.1	0.265	34150
SFRCC-C	AE 1	44	40.5	0.40	29225
	AE 2	45	121	0.27	41500
	AE 3	43	123	0.17	41615
SFRCC-T	AE 1	42	12.1	0.71	10900
	AE 2	44	22.7	0.41	15350
	AE 3	44	14	0.44	14011
ECC	AE 1	48	142	0.86	34020
	AE 2	49	140	0.88	33230
	AE 3	45	136	0.90	32560
ECC-C	AE 1	44	60.2	0.78	28345
	AE 2	45	94.6	0.48	33581
	AE 3	43	134	0.25	34866
ECC-T	AE 1	44	13.25	0.54	9930
	AE 2	46	17.4	0.09	12620
	AE 3	45	15.2	0.12	11732

2.9.3. Comparison of the First Crack Time between the Tested Beams

The time of the occurrence of the first crack for each beam based on evaluating the aforementioned AE parameters is summarized in **Figure 2-4**. In the NC tested beam, the first crack (slope change in both AE and CSS curves) was detected at about 80 s. The other fiber repaired beams (ECC and SFRCC) showed the first cracks at about 120 s and 100 s, respectively. The delayed occurrence of the first crack in the FRCC beams compared with

the NC beam was due to the presence of the fibers which tend to have crack arresting abilities that tend to delay the crack formation.

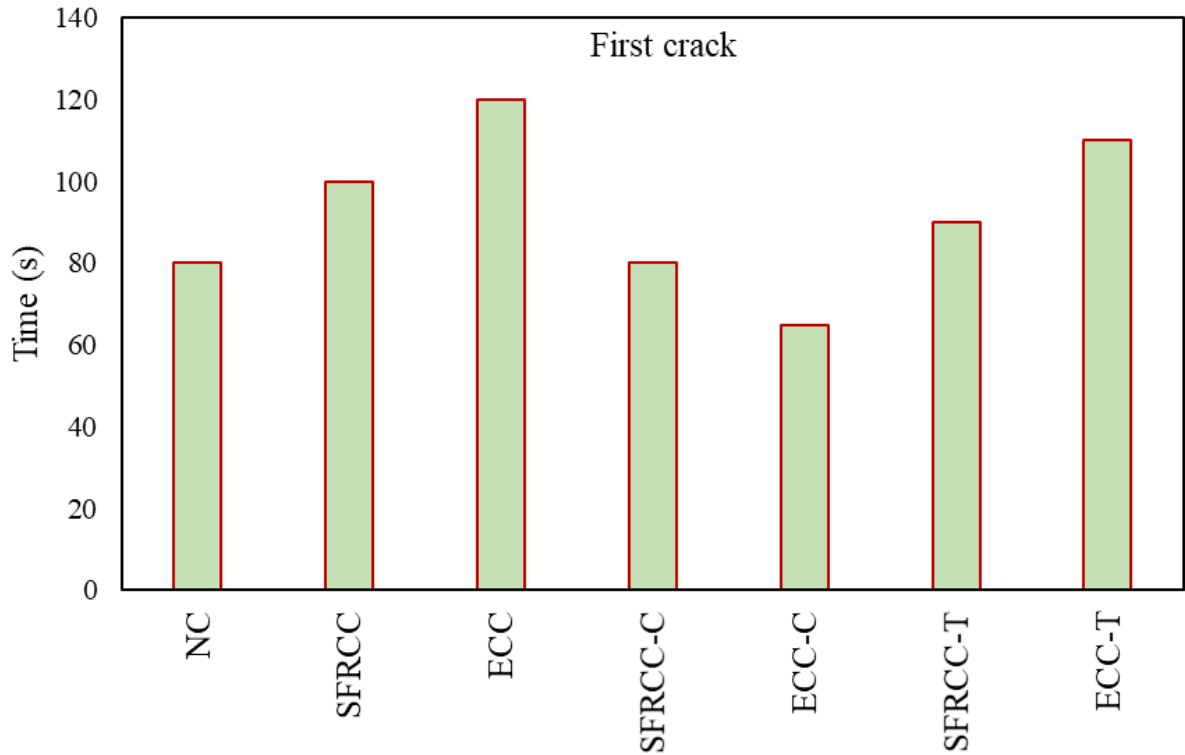


Figure 2- 4 Time for the First Crack for all Tested Beams

The ECC beam showed a more delayed crack initiation (at about 120 s) when compared to SFRCC beam (at about 100 s) due to the presence of the PVA fibers present in ECC that had lower density compared to the steel fibers present in SFRCC. Since both fibers were added at the same volume fraction in the mixture, there was a higher number of PVA fibers in ECC compared to steel fibers in SFRCC, resulting in a more delay of crack initiation. SFRCC-C and ECC-C beams (containing the repair layer in the compression side) showed a first crack at 80 s and 65 s, respectively, which were very comparable to the value recorded by NC. On the other hand, the recorded first cracks for beams repaired in the

tension side (ECC-T and SFRCC-T), were relatively higher than the control NC beam (110 s and 90 s in ECC-T and SFRCC-T, respectively). The higher first crack time for the ECC-T beam with the repair layer at the tension side was due to the ECC's higher energy absorbing ability, which resulted in higher deformability.

2.9.4. Classification of Damage Using AF and RA Analysis

As previously mentioned, AF values tend to be high at the beginning and RA values tend to be high at the end of any beam flexural testing (Aggelis 2011; Grosse and Ohtsu 2008; Shahidan et al. 2013). The reason for the previously explained phenomenon is that tensile cracks tend to appear at the beginning of testing (high AF) while shear cracks tend to appear at the end of testing (high RA when compared to AF) (Nejati et al. 2020). **Figure 2-5** shows the RA analysis from the beginning of the load application until failure for all tested beams. The average values of the rise time, max amplitude, and AF for all three sensors for each beam were first obtained and then RA and AF values were calculated based on 50 hits as defined in JCMS (B 2003). The proportion of the AF and RA value was set to be 1:100. The diagonal line separating the fracture modes was acquired by manually drawing a 45° line (Ohno and Ohtsu 2010; Prem and Murthy 2017). In **Figures 2-5(a), 5(b), 5(c), 5(d)** and **5(f)**, it is evident that the cracks are dominating the left side of the diagonal line even though there are also some cracks on the right side of the line. The majority of the cracks were tensile cracks and therefore it is considered as a flexural mode of failure. However, in **Figures 2-5(e)** and **5(g)**, it is shown that the cracks are dominating the right side of the diagonal line (even though some points lie on the left side of the line). The majority of cracks were shear cracks and therefore the mode of failure was depicted as shear (debonding). All beams except for SFRCC-T and ECC-T have failed in flexural after

the yielding of the longitudinal reinforcement and the crushing of the concrete at the compression zone. On the other hand, beams that were repaired in the tension zone (SFRCC-T and ECC-T) have failed in debonding which is the loss of the connection between the FRCC and NC interface. The cracking pattern of all tested beams at failure are shown in **Figure 2-6**. The debonding was characterized by diagonal (shear) cracks which is confirmed based on the RA vs AF analysis in **Figure 2-5(e)** and **5(g)**. Based on these

results, RA vs AF analysis proved to be a useful tool in differentiating the fracture mode for all tested beams.

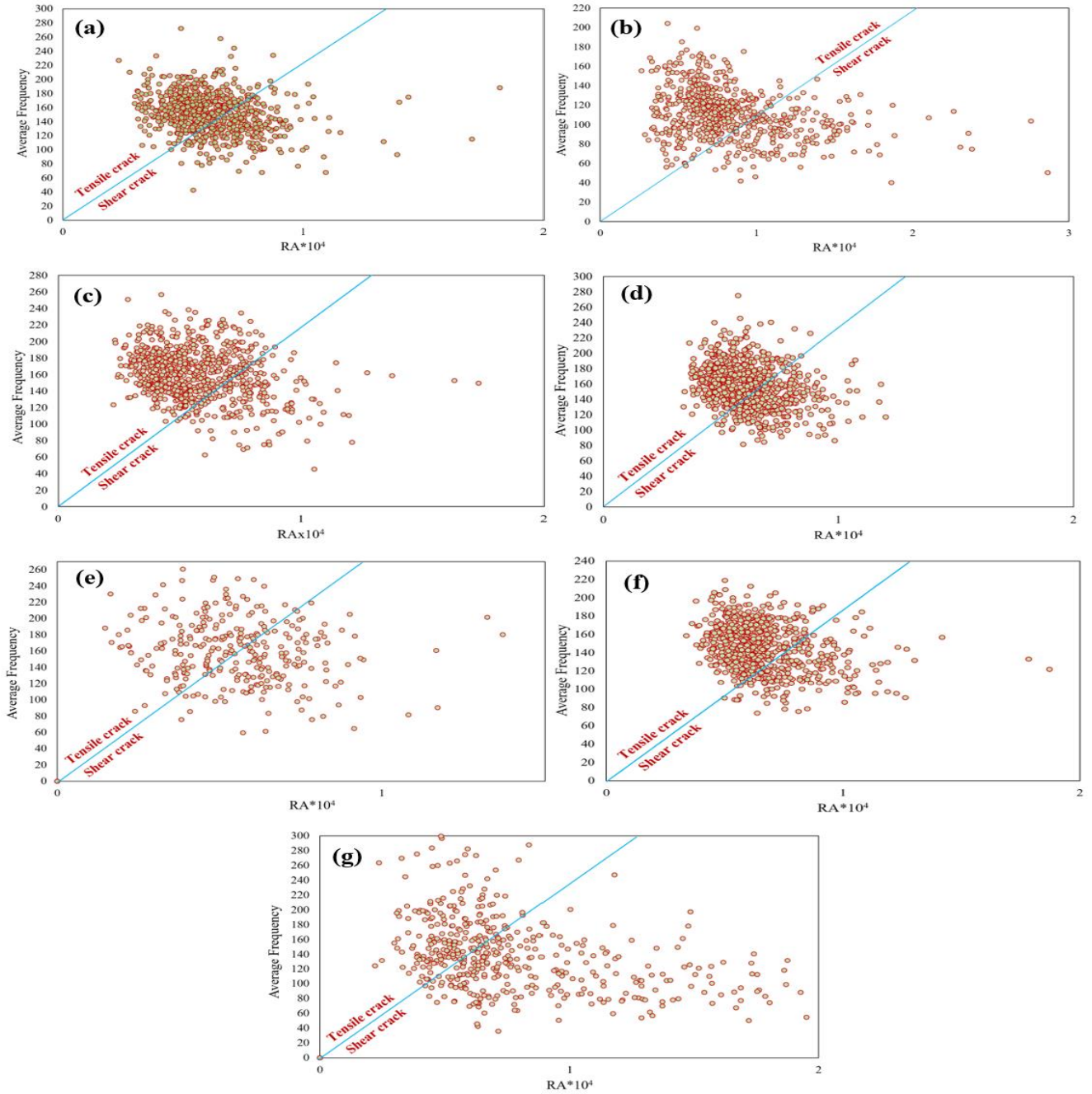


Figure 2- 5 Failure Mode Classification Based on AF vs RA for all Beams: (a) NC, (b)

ECC, (c) SFRCC, (d) SFRCC-C, (e) SFRCC-T, (f) ECC-C, and (g) ECC-T

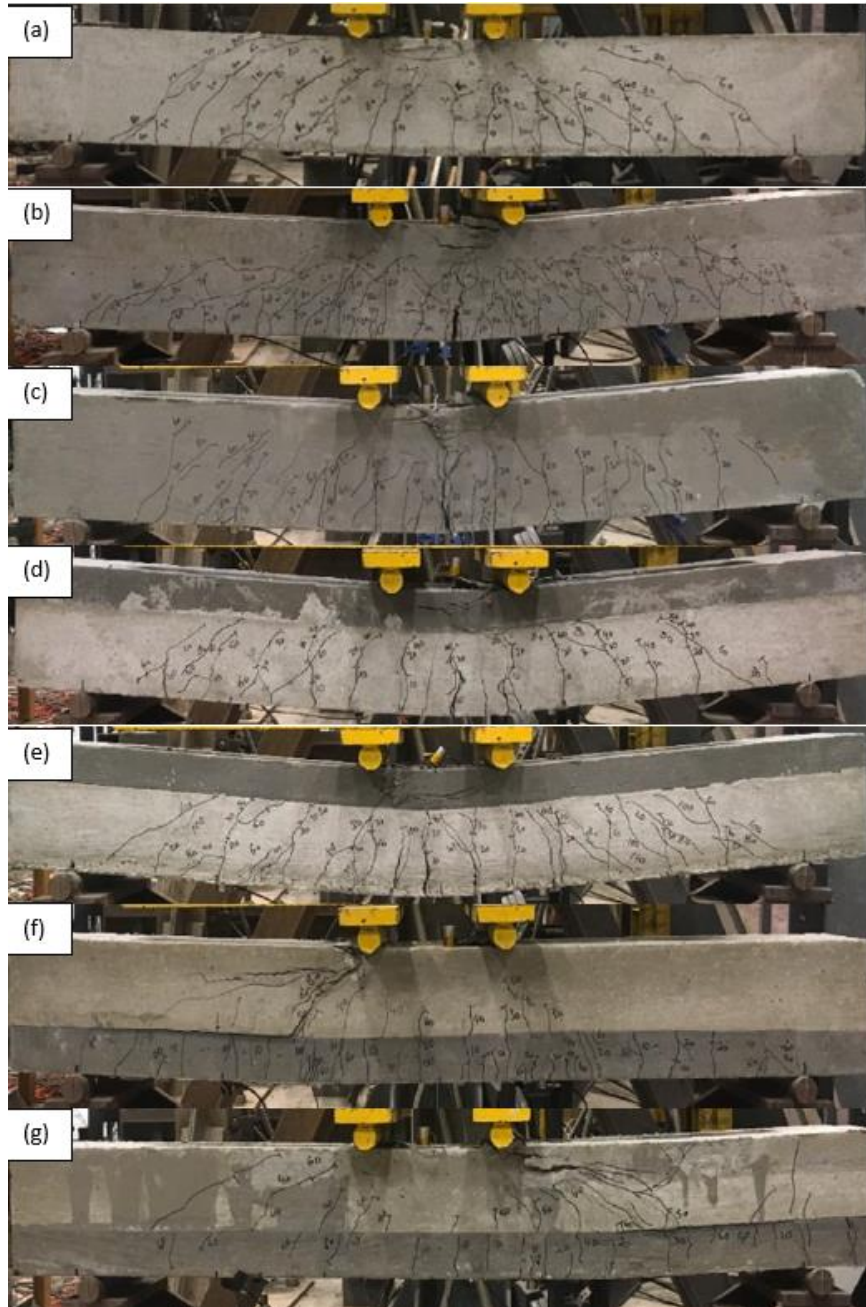


Figure 2- 6 Cracking pattern of the tested beams at failure: (a) NC, (b) ECC, (c) SFRCC, (d) ECC- C, (e) SFRCC-C. (f) ECC-T, and (g) SFRCC-T (Ismail and Hassan 2021).

Despite the use of shear reinforcement (stirrups) as well as surface roughening to connect the NC beam with the repair material (i.e., ECC or SFRCC), these two beams (SFRCC-T and ECC-T) suddenly failed in shear-interface debonding. It is worth noting that, the use of a FRCC layer in retrofitting the NC beam both in tension and compression was expected to result in a flexural (ductile) failure. The results of AF and RA analysis confirmed that both beams repaired on the compression side (SFRCC-C and ECC-C) failed by flexure as can be depicted from **Figures 2- 5(d)** and **5(f)**. However, a shear (brittle) failure was predominant in both SFRCC-T and ECC-T beams as can be seen in **Figures 2-5(e)** and **5(g)** as a result of shear-interface debonding. In particular, it can be observed that **Figures 2-5(e)** and **5(g)** that majority of the events are below the diagonal line for both SFRCC-T and ECC-T beams. This result could be attributable to the loss of bond between the FRCC repaired layer and the NC layer leading to the formation of a major diagonal crack starting from the interface upward to the loading point (**Figure 2-6**). This observation suggests that there is a need for further studies to enhance the FRCC-NC interface bonding strength when FRCC is placed at the tension side. Further improvements of the FRCC-NC interface bonding strength can be achieved by, for instance, using higher FRCC strength, coarser interface, and/or shear keys to avoid undesirable failure modes thereby amplifying the benefits of using FRCC in the repair of the tension side of beams (Ismail and Hassan 2021).

2.9.5. Effect of Sensor Location on Damage Detection

As illustrated in **Figure 2-1**, three sensors were attached to each beam during the test. Sensor 1 was placed at the top and sensors 2 and 3 were placed at the bottom of the beam. The position of the sensor with respect to the repair layer showed a noticeable change in the AE activity (number of hits, CSS, and *b*-value) especially in tension repaired beams

(SFRCC-T and ECC-T). For instance, a sensor placed in the NC zone is expected to show less AE activity due to the lack of presence of fibers; however, a sensor placed in the tension zone is expected to contribute to a higher number of AE activity due to the existence of fibers (steel or PVA) which are characterized by a higher number of cracking and a narrower width of cracks. For beams repaired in compression, sensor placed in the compression zone displayed a lower number of AE activity than the sensors placed in the tension zone, and this is due to the fact that beams repaired in the compression zone failed in flexural mode and therefore the tension part of the beam was characterized by a higher number of cracking activity.

Table 2-6 shows the number of hits for all repaired beams. It is evident that in ECC-T and SFRCC-T beams that sensor 1 displayed a lower number of hits compared to sensors 2 and 3. In ECC-C and SFRCC-C, sensor 1 displayed a lower number of AE activity when compared to sensors 2 and 3 in terms of number of hits. For instance, in ECC-T, sensor 1 displayed a number of hits of 9930 and a number of hits of 12620 and 11732 for sensors 2 and 3, respectively. In ECC-C, sensor 1 displayed a number of hits of 28345 and a number of hits of 33581 and 34866 for sensors 2 and 3, respectively. These results indicated that the AE activity displayed by the sensors depends on the location of the sensor (tension or compression) and the mode of failure of the beams.

Another parameter to be considered is the signal amplitude. **Figure 2-7** represents the signal amplitude (at the time of first crack detection) values for NC beam and SFRCC-T beam recorded using sensors 1, 2 and 3. It is evident that, in the NC beam values for signal amplitude are almost the same. Signal amplitude for sensor 3 is the lowest (47 dB) since it is the farthest sensor from the first crack occurrence (mid-span), however; signal amplitude

for sensor 1 and 2 (48 dB) are the same as they are the same distance from the mid-span. The value of the signal amplitude tends to be very close in homogenous materials (Abouhussien et al. 2019; Ervin et al. 2007; Schumacher et al. 2011). In contrast, signal amplitude for sensor 1 (50 dB) in SFRCC-T, is not close to the signal amplitude viewed by sensors 2 and 3 (59 and 58, respectively). These results could be due to the fact that one layer is NC and the other layer is SFRCC. The signal traveled between two layers that have different densities and therefore resulted in signal attenuation (Ervin et al. 2007; Schumacher et al. 2011).

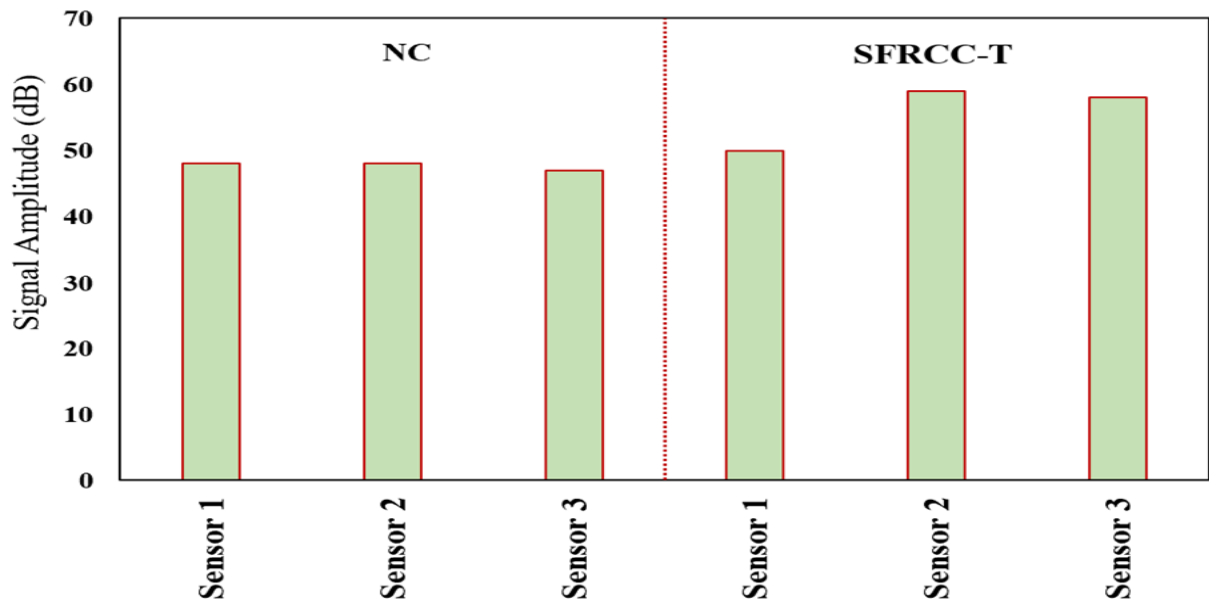


Figure 2- 7 Signal Amplitude at the First Crack for NC and SFRCC-T Beams

Table 2- 7 AE Parameters for all Beams at the First Crack

Mixture name	Channel	Average Amplitude (dB)	CSS x 10 ⁷ (pV.s)	<i>b</i> -value	Number of Hits
NC	AE 1	45	4.54	0.80	2506
	AE 2	45	5.63	0.79	3100
	AE 3	44	2.56	0.83	2278
SFRCC	AE 1	44	2.62	0.85	2856
	AE 2	45	3.00	0.77	3450
	AE 3	43	2.31	1.22	2490
SFRCC-C	AE 1	42	0.30	1.82	2557
	AE 2	45	0.49	0.77	3132
	AE 3	44	0.38	0.88	2820
SFRCC-T	AE1	45	0.12	0.97	1150
	AE 2	48	0.17	0.92	1761
	AE 3	47	0.19	0.72	1862
ECC	AE 1	45	3.47	0.97	2620
	AE 2	46	4.27	0.82	3230
	AE 3	45	3.12	0.90	2362
ECC-C	AE 1	43	4.09	1.33	2480
	AE 2	45	6.92	0.82	3086
	AE 3	45	4.18	1.15	2789
ECC-T	AE 1	46	34.8	1.90	1018
	AE 2	44	41.2	1.77	1210
	AE 3	43	45.9	1.60	1343

2.9.6. Effect of Fibers on AE Activity and Failure Mode of Beams

As mentioned earlier, this study included testing one fully cast NC beam, one fully cast SFRCC beam, one fully cast ECC beam, and four repaired FRCC beams (in either tension or compression). **Table 2-6** shows the parameters at the failure load. It can be noticed that the changes in the cracking behavior among the tested beams had a significant impact on the AE parameters. For instance, NC displayed an average of about 29129 hits at failure while SFRCC and ECC displayed an average of 36800 and 33270, respectively. For beams repaired in compression, the average number of hits for SFRCC-C and ECC-C were 37447

and 32264, respectively. SFRCC-T and ECC-T displayed the least average number of hits of 13420 and 11427, respectively. Varying the fiber type of the repaired beams had a noticeable effect on the AE parameters. This finding can be related to the effect of changing fiber types (steel versus PVA) on the characteristics of the fracture process zone of concrete (Bhowmik and Ray, 2019); on the fibers failure mechanisms including fiber pull-out and rupture (Thirumalaiselvi et al. 2020); on the crack bridging phenomenon/fiber-matrix interface properties due to the variable chemical and frictional bond strengths (Sindu and Sasmal, 2019); and on the splitting tensile strength of the cementitious composite materials (Georgiou and Pantazopoulou, 2019). The variations in fracture related properties of various types of FRCC showed to have a significant impact on the resulting AE activities (Thirumalaiselvi et al. 2020). It is also quite evident that beams that possess fibers displayed higher number of hits corresponding to the higher cracking when compared to the NC beam. Beams with fibers are known to have a higher cracking activity due to the bridging mechanism of the fibers which prevents cracks from expanding. All beams with fibers are characterized by an increased number of cracks when compared to the NC beam. These results may also be attributed to the effect of fibers in restricting the crack widening and transfer the stress across the cracked section, which enhance the load carrying capacity and accompanying large deflection. This large deflection resulted in initiating higher number of cracks instead of widening the existing cracks due to the fiber stitching mechanism. As a result, the initiation of cracks led to a higher number of AE events including number of hits and CSS and a lower number of b -value in both SFRCC and ECC beams when compared to NC beam (Thirumalaiselvi et al. 2020).

With regard to **Figure 2-2**, it is noteworthy that beams repaired with SFRCC in general possess higher deflection characteristics when compared to beams repaired with ECC. Concrete with SFs is characterized by higher load-bearing capacity when compared to concrete with PVA fibers (Ismail and Hassan 2021). The effect of fiber type in this investigation is evident in the higher AE activity (number of hits) acquired by beams containing SFRCC. All beams failed in flexural except for ECC-T and SFRCC-T. These beams displayed the least number of average hits as they both failed in debonding, as mentioned before. The low number of hits was a result of the low load bearing capacity which caused the beams to suddenly fail and hence displaying a low number of cracks. To further corroborate, **Figure 2-8** shows the signal amplitude vs time for NC (sensor 1) and ECC-T (sensor 2). In **Figure 2-8(a)**, the wavelengths appeared to be shorter and the highest amplitude is reached faster. However, in **Figure 2-8(b)** the major wavelengths seemed to be longer and the highest amplitude is reached slower which is an indication of debonding (Aggelis et al. 2019). Furthermore, the locations of high fluctuations of the signal amplitudes in **Figure 2-8** can be correlated to both crack propagation and new crack formation. Crack propagation was initiated at the beginning of the testing and as the load increased, crack widths expanded as well as new cracks formed. It can also be observed from **Figure 2-8** that these fluctuations are occupying a broad region (long time duration) and are narrower (occupying a short time duration) in the other regions. This observation may be due to the occurrence of both new cracks and opening of existing cracks in the long time duration instances while the short duration regions can be associated with either the onset of a new crack or opening of a fewer number of existing cracks. These observations

further confirm the sensitivity of the AE data to the process of crack initiation and propagation (Thirumalaiselvi et al. 2020).

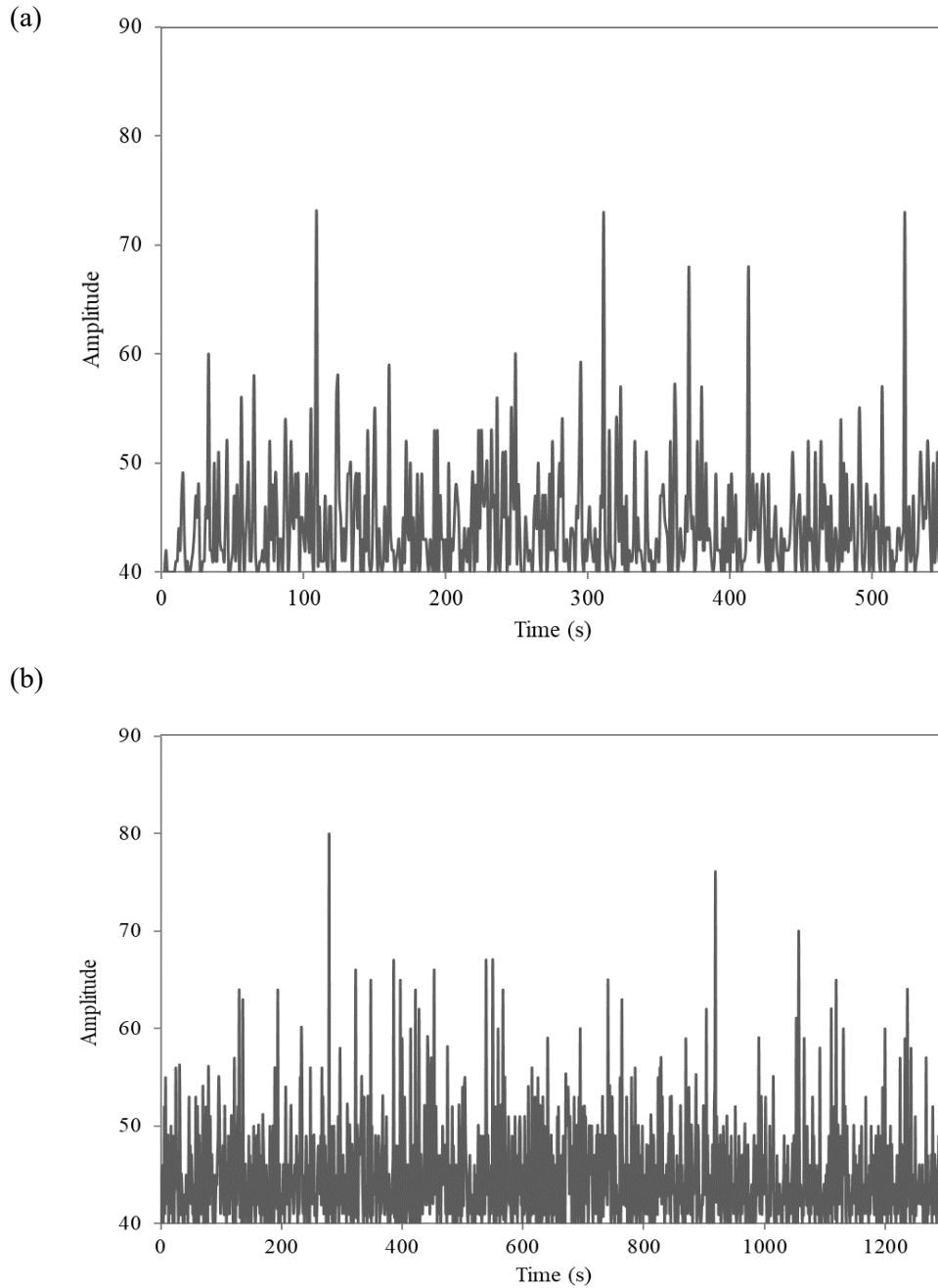


Figure 2- 8 Comparison of Amplitude vs Time between NC Beam and ECC-T Beam: (a) NC Beam (Sensor 1) and (b) ECC-T Beam (Sensor 2)

2.9.7. Effect of Strengthening Location/Failure Mode of Repaired Beams on AE

Parameters

In this study, two beams were strengthened in the compression zone (ECC-C and SFRCC-C) and two beams were strengthened in the tension zone (ECC-T and SFRCC-T). Changing the strengthening location had a significant effect on the cracking behavior and also yielded two failure modes in these four beams. Specifically, beams strengthened in the compression zone (ECC-C and SFRCC-C) failed in flexural mode after the longitudinal reinforcement in the tension zone reached yielding and the concrete in the compression zone crushed. On the other hand, beams repaired at the bottom (ECC-T and SFRCC-T) failed in sudden debonding which is the loss of bond between the NC and FRCC layer. Different modes of failure (flexural or debonding) also had a noticeable impact on the AE parameters in terms of number of hits, CSS, and b -value. Beams that failed in flexural mode showed higher AE events (higher number of hits and CSS and lower b -values) when compared to beams that failed in debonding (sudden failure). This observation was attributed to the higher number of cracks in the beams repaired in the compression side compared with those repaired in the tension side (**Table 2-6**). For instance, the AE events at failure for ECC-C (sensors 2 and 3 placed at the bottom) were 33581 and 34866 corresponding to b -values of 0.48 and 0.25, respectively (higher AE events result in lower b -values). The values were 12620 and 11732 with b -values of 0.09 and 0.12, respectively in ECC-T (sensors 2 and 3) (**Table 2-6**).

2.10. Conclusions

In this study, AE monitoring was utilized to assess the crack development and failure modes of large-scale repaired beams. Four-point load tests were performed on a control

beam (NC) along with six other repaired FRCC beams with different fibers and strengthening locations. The FRCC beams contained two types of fibers (PVA and SFs) to study the effect of the fiber type and strengthening locations on AE parameters. A series of AE analysis was carried out and the following results were obtained:

1. Several AE parameters including number of hits, CSS, b -value, absolute energy, amplitude, and peak frequency were found to be effective in analyzing the crack progression in unrepaired and repaired beams, regardless of the repair location and repair material type (either with steel fibers or polyvinyl fibers). During the loading period, there was a noticeable increase in both the number of hits and CSS and a decrease in b -value in all beams as a result of the progression of the crack formation.
2. AE recognized the first crack for all beams (whether they are repaired or unrepaired) by detecting the first change of slope in the number of hits and CSS as well as the lowest decrease in the first b -value fluctuation. In general, signal amplitude, peak frequency, and absolute energy displayed high fluctuating activities at the same time intervals where the change of slope in the number of hits, CSS, and b -value occurred.
3. RA vs. AF analysis proved to be a useful tool in the characterization of different failure modes for all beams. For example, RA vs. AF analysis showed that all beams that experimentally failed in flexure had majority of tensile/flexural cracks identified at the top zone of the AF vs RA chart.
4. The sensor location had a significant impact on AE parameters in terms of number of hits and signal amplitude. It was found in all beams that the location of the sensor closest to the highest cracks occurrence experienced the highest number of hits. It

was also observed that signal amplitude tends to be highest when the sensor is closest to the damage source. For control beams (unrepaired), for instance, the values of signal amplitudes for sensors 1 and 2 were very close in value while sensor 3 was the lowest in value. In repaired beams, there was a difference in the value of signal amplitudes between the three sensors due to the difference in the densities between NC and the repair materials.

5. In general, beams with fibers whether repaired or control, possessed higher AE events when compared to NC beam without fibers. In addition, beams with SFs showed higher cracking activity compared to beams with PVA fibers, which is attributed to the fact that SFs have a higher load-bearing capacity resulting in higher number of cracks.
6. AE detected very high AE activities for beams with flexural failure compared to beams with debonding failure. This was clear when comparing the AE activities for beams that were repaired in the top layer (which experienced high flexural cracking activities) compared to beams repaired in bottom layer (which experienced relatively less debonding cracking activities).

2.11. Chapter References

- Abdelrahman, M., ElBatanouny, M. K., Ziehl, P., Fasl, J., Larosche, C. J., and Fraczek, J. (2015). "Classification of alkali–silica reaction damage using acoustic emission: A proof-of-concept study." *Construction and Building Materials*, 95, 406-413.
- Abouhussien, A. A., and Hassan, A. A. (2019). "Crack Growth Monitoring in Fiber-Reinforced Self-Consolidating Concrete via Acoustic Emission." *ACI Materials Journal*, 116(5), 181-191.

- Abouhussien, A. A., and Hassan, A. A. (2020). "Classification of damage in self-consolidating rubberized concrete using acoustic emission intensity analysis." *Ultrasonics*, 100, 105999.
- Abouhussien, A. A., Hassan, A. A., and AbdelAleem, B. H. (2019). "Acoustic Emission Analysis of Self-Consolidating Rubberized Concrete Beam-Column Connections under Cyclic Loading." *ACI Structural Journal*, 116(6).
- Abouhussien, A. A., and Hassan, A. A. A. (2015). "Evaluation of damage progression in concrete structures due to reinforcing steel corrosion using acoustic emission monitoring." *Journal of civil structural health monitoring*, 5(5), 751-765.
- Abouhussien, A. A., and Hassan, A. A. A. (2016). "Detection of bond failure in the anchorage zone of reinforced concrete beams via acoustic emission monitoring." *Smart materials and structures*, 25(7), 75034-75046.
- Abouhussien, A. A., and Hassan, A. A. A. (2019). "Assessment of Crack Development in Engineered Cementitious Composites Based on Analysis of Acoustic Emissions." *Journal of materials in civil engineering*, 31(6), 4019078.
- Abouhussien, A. A., Hassan, A. A. A., Ismail, M. K., and AbdelAleem, B. H. (2019). "Evaluating the cracking behavior of ECC beam-column connections under cyclic loading by acoustic emission analysis." *Construction & building materials*, 215, 958-968.
- Physical Acoustics (2005). "R6I-AST sensor." Princeton Junction, NJ, USA.
- Aggelis, D., De Sutter, S., Verbruggen, S., Tsangouri, E., and Tysmans, T. (2019). "Acoustic emission characterization of damage sources of lightweight hybrid concrete beams." *Engineering Fracture Mechanics*, 210, 181-188.

- Aggelis, D. G. (2011). "Classification of cracking mode in concrete by acoustic emission parameters." *Mechanics Research Communications*, 38(3), 153-157.
- ASTM (2014). "Standard Terminology for Nondestructive Examinations (ASTM E1316)." ASTM International West Conshohocken, PA, USA.
- ASTM C150/C150M (2012). "Standard Specification for Portland Cement." *ASTM International* (West Conshohocken, PA, USA), 9 pp.
- B, J.-I. (2003). "Monitoring method for active cracks in concrete by acoustic emission." *Federation of Construction Material Industries, Japan*, 23-28.
- Behnia, A., Chai, H. K., and Shiotani, T. (2014). "Advanced structural health monitoring of concrete structures with the aid of acoustic emission." *Construction and Building Materials*, 65, 282-302.
- Bhowmik, S., and Ray, S. (2019). "An experimental approach for characterization of fracture process zone in concrete." *Engineering Fracture Mechanics*, 211, 401-419.
- Colombo, I. S., Main, I., and Forde, M. (2003). "Assessing damage of reinforced concrete beam using" b-value" analysis of acoustic emission signals." *Journal of materials in civil engineering*, 15(3), 280-286.
- ElBatanouny, M. K., Mangual, J., Ziehl, P. H., and Matta, F. (2014). "Early corrosion detection in prestressed concrete girders using acoustic emission." *J. Mater. Civ. Eng.*, 26(3), 504-511.
- ElBatanouny, M. K., Ziehl, P. H., Larosche, A., Mangual, J., Matta, F., and Nanni, A. (2014). "Acoustic emission monitoring for assessment of prestressed concrete beams." *Construction & building materials*, 58, 46-53.

- Ervin, B. L., Bernhard, J. T., Kuchma, D. A., and Reis, H. "Monitoring general corrosion of rebar embedded in mortar using high-frequency guided mechanical waves." *Proc., Sensors and Smart Structures Technologies for Civil, Mechanical, and Aerospace Systems 2007*, SPIE, 447-458.
- Farhidzadeh, A., Dehghan-Niri, E., Salamone, S., Luna, B., and Whittaker, A. (2013). "Monitoring crack propagation in reinforced concrete shear walls by acoustic emission." *J. Struct. Eng.*, 139(12), 04013010.
- Georgiou A. V., and Pantazopoulou, S. J. (2019). "Experimental and analytical investigation of the shear behavior of strain hardening cementitious composites." *Structural Engineering and Mechanics*, 72(1), 19-30.
- Golaski, L., Gebiski, P., and Ono, K. (2002). "Diagnostics of reinforced concrete bridges by acoustic emission." *Journal of acoustic emission*, 20(1), 83-98.
- Grosse, C. U., and Ohtsu, M. (2008). *Acoustic emission testing*, Springer Science & Business Media.
- Group, M. (2007). "PCI-2 based AE system 1 user's manual." *Physical Acoustics Corporation, Princeton Junction, NJ, USA*.
- Guo, B., and Li, Y. "Review of Research on Damage Identification of Reinforced Concrete Structures Based on Acoustic Emission Technology." *Proc., IOP Conference Series: Earth and Environmental Science*, IOP Publishing, 012039.
- Ismail, M. K., Abdelaleem, B. H., and Hassan, A. A. (2018). "Effect of fiber type on the behavior of cementitious composite beam-column joints under reversed cyclic loading." *Construction and Building Materials*, 186, 969-977.

- Ismail, M. K., Hassan, A. A., and Lachemi, M. (2018). "Effect of Fiber Type on Impact and Abrasion Resistance of Engineered Cementitious Composite." *ACI Materials Journal*, 115(6).
- Ismail, M. K., and Hassan, A. A. A. (2021). "Structural performance of large-scale concrete beams reinforced with cementitious composite containing different fibers." *Structures (Oxford)*, 31, 1207-1215.
- Jumaat, M. Z., Kabir, M., and Obaydullah, M. (2006). "A review of the repair of reinforced concrete beams." *Journal of Applied Science Research*, 2(6), 317-326.
- Kenai, S., and Bahar, R. (2003). "Evaluation and repair of Algiers new airport building." *Cement and concrete composites*, 25(6), 633-641.
- Kim, J.-H. J., Lim, Y. M., Won, J.-P., Park, H.-G., and Lee, K.-M. (2007). "Shear capacity and failure behavior of DFRCC repaired RC beams at tensile region." *Engineering structures*, 29(1), 121-131.
- Li, V. C. (1993). "From micromechanics to structural engineering the design of cementitious composites for civil engineering applications." *Doboku Gakkai Ronbunshu*, 1993(471), 1-12.
- Li, V. C. (1998). "Engineered cementitious composites (ECC)-tailored composites through micromechanical modeling." in *Fiber Reinforced Concrete: Present and the Future* edited by N. Banthia, A. Bentur, A. and A. Mufti, Canadian Society for Civil Engineering, Montreal, pp. 64-97, 1998. <<http://hdl.handle.net/2027.42/84667>>
- Li, V. C., Wu, C., Wang, S., Ogawa, A., and Saito, T. (2002). "Interface tailoring for strain-hardening polyvinyl alcohol-engineered cementitious composite (PVA-ECC)." *Materials Journal*, 99(5), 463-472.

- Mukherjeel, A., and Joshi, M. "Recent Advances in Repair and Rehabilitation of RCC Structures with Nonmetallic Fibers." Journal notes from Prof. A. Mukherjee, Dept. of Civil, IIT, Bombay, India.
- Nejati, H. R., Nazerigivi, A., Imani, M., and Karrech, A. (2020). "Monitoring of fracture propagation in brittle materials using acoustic emission techniques-A review." *Comput. Concr*, 25, 15-27.
- Ohno, K., and Ohtsu, M. (2010). "Crack classification in concrete based on acoustic emission." *Construction & building materials*, 24(12), 2339-2346.
- Paul, S., Pirskawetz, S., Van Zijl, G., and Schmidt, W. (2015). "Acoustic emission for characterising the crack propagation in strain-hardening cement-based composites (SHCC)." *Cement and concrete research*, 69, 19-24.
- Prem, P. R., and Murthy, A. R. (2017). "Acoustic emission monitoring of reinforced concrete beams subjected to four-point-bending." *Applied acoustics*, 117, 28-38.
- Ramachandra Murthy, A., Karihaloo, B. L., Vindhya Rani, P., and Shanmuga Priya, D. (2018). "Fatigue behaviour of damaged RC beams strengthened with ultra high performance fibre reinforced concrete." *International journal of fatigue*, 116, 659-668.
- Ranjbar, N., Behnia, A., Chai, H. K., Alengaram, U. J., and Jumaat, M. Z. (2016). "Fracture evaluation of multi-layered precast reinforced geopolymer-concrete composite beams by incorporating acoustic emission into mechanical analysis." *Construction & building materials*, 127, 274-283.
- Şahmaran, M., and Li, V. C. (2010). "Engineered Cementitious Composites: Can Composites Be Accepted as Crack-Free Concrete?" *Transportation research record*, 2164(1), 1-8.

- Saliba, J., Matallah, M., Loukili, A., Regoin, J.-P., Grégoire, D., Verdon, L., and Pijaudier-Cabot, G. (2016). "Experimental and numerical analysis of crack evolution in concrete through acoustic emission technique and mesoscale modelling." *Engineering Fracture Mechanics*, 167, 123-137.
- Schumacher, T., Higgins, C. C., and Lovejoy, S. C. (2011). "Estimating operating load conditions on reinforced concrete highway bridges with b-value analysis from acoustic emission monitoring." *Structural Health Monitoring*, 10(1), 17-32.
- Selman, E., Ghiami, A., and Alver, N. (2015). "Study of fracture evolution in FRP-strengthened reinforced concrete beam under cyclic load by acoustic emission technique: An integrated mechanical-acoustic energy approach." *Construction and Building Materials*, 95, 832-841.
- Shahidan, S., Pulin, R., Bunnori, N. M., and Holford, K. M. (2013). "Damage classification in reinforced concrete beam by acoustic emission signal analysis." *Construction and Building Materials*, 45, 78-86.
- Sindu, B.S., and Sasmal, S. (2019). "On the development and studies of nano- and micro-fiber hybridized strain hardened cementitious composite." *Archives of Civil and Mechanical Engineering*, 19, 348-359.
- Singh, M., Saini, B., and Chalak, H. D. (2019). "Performance and composition analysis of engineered cementitious composite (ECC) – A review." *Journal of Building Engineering*, 26, 100851.
- Thirumalaiselvi, A., Sindu, B. S., and Sasmal, S. (2020). "Crack propagation studies in strain hardened concrete using acoustic emission and digital image correlation

investigations." *European Journal of Environmental and Civil Engineering*, 26(20), 4346-4373, DOI: 10.1080/19648189.2020.1848640.

Verbruggen, S., De Sutter, S., Iliopoulos, S., Aggelis, D. G., and Tysmans, T. (2015). "Experimental Structural Analysis of Hybrid Composite-Concrete Beams by Digital Image Correlation (DIC) and Acoustic Emission (AE)." *Journal of nondestructive evaluation*, 35(1).

Vidya Sagar, R., and Raghu Prasad, B. (2013). "Laboratory investigations on cracking in reinforced concrete beams using on-line acoustic emission monitoring technique." *Journal of Civil Structural Health Monitoring*, 3(3), 169-186.

Wang, C., Zhang, Y., and Ma, A. (2011). "Investigation into the fatigue damage process of rubberized concrete and plain concrete by AE analysis." *Journal of materials in civil engineering*, 23(7), 953-960

3. Damage Characterization in Large-Scale Multi-Layered Reinforced Concrete Beams by Acoustic Emission Analysis

3.1. Abstract

In this study, acoustic emission (AE) analysis was carried out to evaluate and quantify the cracking behavior of large-scale multi-layered reinforced concrete beams under flexural tests. Four normal concrete beams were repaired by adding a layer of crumb rubberized engineered cementitious composites (CRECC) or powder rubberized engineered cementitious composites (PRECC), in either the tension or compression zone of the beam. Additional three unrepaired control beams, fully cast with either normal concrete, CRECC, or PRECC, were tested for comparison. Flexural tests were performed on all of the tested beams in conjunction with AE monitoring until failure. AE raw data obtained from the testing was filtered and then analyzed to detect and assess the cracking behavior of all the tested beams. A variety of AE parameters including number of hits and cumulative signal strength were utilized to study the crack propagation throughout the testing. Furthermore, b -value and intensity analyses were implemented and yielded additional parameters called b -value, historic index [$H(t)$], and severity (S_r). The analysis of the changes in the aforementioned parameters allowed the identification of the first crack in all tested beams. Moreover, varying the rubber particle size (crumb rubber or powder rubber), repair layer location, or AE sensor location, showed a significant impact on the number of hits and signal amplitude. Finally, by using the results of the study, it was possible to develop a damage quantification chart that can identify different damage stages (first crack and ultimate load), related to the intensity analysis parameters ($H(t)$ and S_r).

Keywords: rubberized engineered cementitious composites; acoustic emission analysis; first crack detection; damage quantification

3.2. Introduction

Concrete structures including bridges, parking garages, offshore structures, and other marine structures are exposed to external factors such as harsh environmental conditions, impact stresses, and high mechanical loading. Exposure to such factors eventually leads to deterioration of the concrete structures which immediately affects the intended service life (AbdelAleem and Hassan 2022). Repair or strengthening of those deteriorated structures is therefore inevitable to improve the functionality and performance of such structures (AbdelAleem and Hassan 2022; Safdar et al. 2016). Recently, engineered cementitious composites (ECC) were introduced for use in repairing concrete structures due to their high performance characteristics compared to the common cementitious repair materials (Siad et al. 2019). ECC exhibit very high ductility with strain-hardening and multi-cracking behavior.

ECC contribute to a tensile strain capacity that varies from 3% to 7% when compared to normal concrete, which exhibits a tensile strain capacity of 0.01% (Li 2002). Since ECC have strain-hardening characteristics, their cracks are characterized by fiber-bridging mechanisms and tight width (Huang et al. 2013; Şahmaran and Li 2010). ECC are generally comprised of relatively high volume of fibers such as Polyvinyl fibers (PVA) and high volume of fine silica sand (Siad et al. 2019). The volume of PVA fibers in ECC is normally 2% (Li et al. 2002). Recently, waste rubber started to be viewed as an economically recyclable material for use in the production of ECC (Rashad 2016). When rubber aggregates are placed in ECC, the strain rate and toughness tend to increase (Reda Taha et

al. 2008). Furthermore, rubberized concrete exhibits higher strain rates which allow for greater deformation and contributes to higher ductility compared to normal concrete (Ismail and Hassan 2016; Parveen and Sharma 2013; Thomas et al. 2016; Wang et al. 2013). Previous studies indicated that increasing the amount of rubber aggregates in concrete decreased the compressive and tensile strengths. This is due to the difference between the modulus of elasticity of rubber aggregate and cement paste (Ismail et al. 2018; Siad et al. 2019). However, the negative effect of rubber on the strength is alleviated in ECC mixtures because of the presence of high volume of fibers. The inclusion of PVA fibers in ECC does not only help to alleviate the reduction in mechanical strength, but also improve the ductility, energy absorption and impact resistance of concrete (AbdelAleem and Hassan 2022).

Acoustic Emission (AE) monitoring is a non-destructive method used to monitor the structural health of many existing concrete structures (Nair and Cai 2010; Pollock 1986; Ziehl et al. 2008). The AE technique has the ability to detect the strain energy in a structure by monitoring the released elastic waves. The strain energy is recorded by AE sensors and related to different types of damage that is occurring in the monitored structure (Guo and Li 2020). AE analysis also has the ability to categorize different types of failures and to quantify the severity of damage (Behnia et al. 2014).

AE analyses have shown their effectiveness in evaluating the cracking and damage behavior of self-compacting rubberized concrete (Abouhussien and Hassan 2020; Abouhussien et al. 2019), fiber-reinforced concrete (Abouhussien and Hassan 2019; Gostautas et al. 2005; Xargay et al. 2021), and strain-hardening cement-based composites (Paul et al. 2015). In particular, *b*-value analysis (amplitude/number of hits) and intensity

analysis (historic index $H(t)$ and severity S_r) were found to be very useful tools in assessing the cracking behavior (micro-cracking and macro-cracking) of composite structures (Li et al. 2021). Besides, RA (Rise time/amplitude) vs. average frequency (AF) analysis was also utilized as good crack classification tool to differentiate between different types of failure modes (shear, tensile, or debonding). Ranjbar et al. used RA and AF analysis to categorize the types of failure of multi-layered composite beams consisting of geopolymer and normal concrete (Ranjbar et al. 2016). Also, Verbruggen et al. used the analysis of AE events vs time to represent the crack propagation over time in multi-layered textile reinforced concrete-carbon FRP hollow beams.

To date, the implementation of AE analyses for evaluating/quantifying the cracking behavior of multi-layered beams is limited. There is a need to study the change in the AE parameters in multi-layered composite beams due to the variation in the wave propagation characteristics through the two layers, especially when rubberized engineering cementitious composites (RECC) is used. Furthermore, the location of the sensor with respect to the two different layers is anticipated to be a factor owing to the contribution of rubber particles to sound absorption and the properties of interfacial bond between the two layers. In addition, the impact of using multi-layered RECC on the effectiveness of b -value and intensity analyses for the purpose of detection/quantification of the cracking and severity of damage requires further investigation. This study aims to assess the effectiveness of b -value and intensity analysis for characterizing the crack propagation in RECC beams with different strengthening locations and different rubber particle sizes. This study also attempts to quantify the cracking behavior of multi-layered RECC beams by developing a damage classification tool for different cracking stages (first crack and

ultimate load) with the aid of intensity analysis parameters. The effect of using different strengthening locations in multi-layered RECC beams on AE parameters is also examined in this study.

3.3. Research Significance

The implementation of AE monitoring and analyses has proven its efficacy in damage classification including detection of crack propagation in several concrete and composite structures. However, there is a gap in the literature regarding the application of AE analyses in multi-layered RECC beams, especially with rubber particle. The integrity of AE analyses in evaluating the structural performance of RECC composite beams requires further investigation as rubber particles have sound-absorbing properties which may have a significant impact on the AE parameters. Alternating the RECC layer along with the strengthening/sensor location is anticipated to show prominent changes on the AE signal parameters. Moreover, AE wave propagation is expected to be different in repaired beams when compared to the normal concrete beam due to signal attenuation. The literature also lacks information regarding the implementation of b -value and intensity analyses in the crack quantification of multi-layered RECC beams. The AE analyses presented in this paper will aid in categorizing the different damage stages and will help to better understand the structural performance of multi-layered RECC beams (in terms of crack initiation and crack propagation).

3.4. Experimental program

3.4.1. Material properties

Table 3-1 represents the three mixtures used in this study (one normal concrete mixture and two rubberized engineering cementitious composites mixtures). The normal concrete

mixture (NC) was comprised of type GU Portland cement complying with ASTM C150 Type 1 (ASTM C150/C150M 2012). The NC mixture also consisted of coarse aggregate (natural crushed stone) with a maximum aggregate size of 10 mm and fine aggregate (natural sand). The coarse and fine aggregate had a specific gravity of 2.6 and an absorption ratio of 1%. RECC mixtures consisted of type GU Portland cement complying with ASTM C150 Type 1] (ASTM C150/C150M 2012) and fly ash (FA) complying with ASTM C618 Type F (ASTM International 2012). The fine aggregate used for RECC mixtures is silica sand with a maximum grain size of 0.4 mm and a specific gravity of 2.65. Crumb rubber (CR) and powder rubber (PR) were used to partially replace the silica sand. Both CR and PR had a specific gravity of 0.95 and 0.86, respectively with negligible water absorption. The replacement level for both types of rubber was 20% (by volume). This replacement was determined based on a previous study (Ismail et al. 2018) focused on optimizing the content of CR and PR in RECC. PVA fibers were used in all RECC mixtures. The PVA fibers had a length of 8 mm, tensile strength of 1600 MPa, modulus of elasticity of 40 GPa, and a specific gravity of 1.3 (**Figure 3-1**). More details of the tested beams can be found elsewhere (AbdelAleem and Hassan 2022).

Table 3- 1 Mix design for all tested beams

Mixture no.	Mixture ID	BC	C/BC	SCM (type)	SCM/BC	S/BC	C.A./BC	W/BC	PVA (volume %)	CR/SS (volume%)	PR/SS	f _c (MPa)	STS (MPa)	Modulus of elasticity (GPa)
1	NC	1	1	-	-	1.52	1.82	0.4	-	-	-	59	4.4	22
2	CRECC	1	0.45	FA	0.55	0.29	-	0.27	2	0.2	-	59.6	6.5	17
3	PRECC	1	0.45	FA	0.55	0.29	-	0.27	2	-	0.2	64.2	8.6	18.2

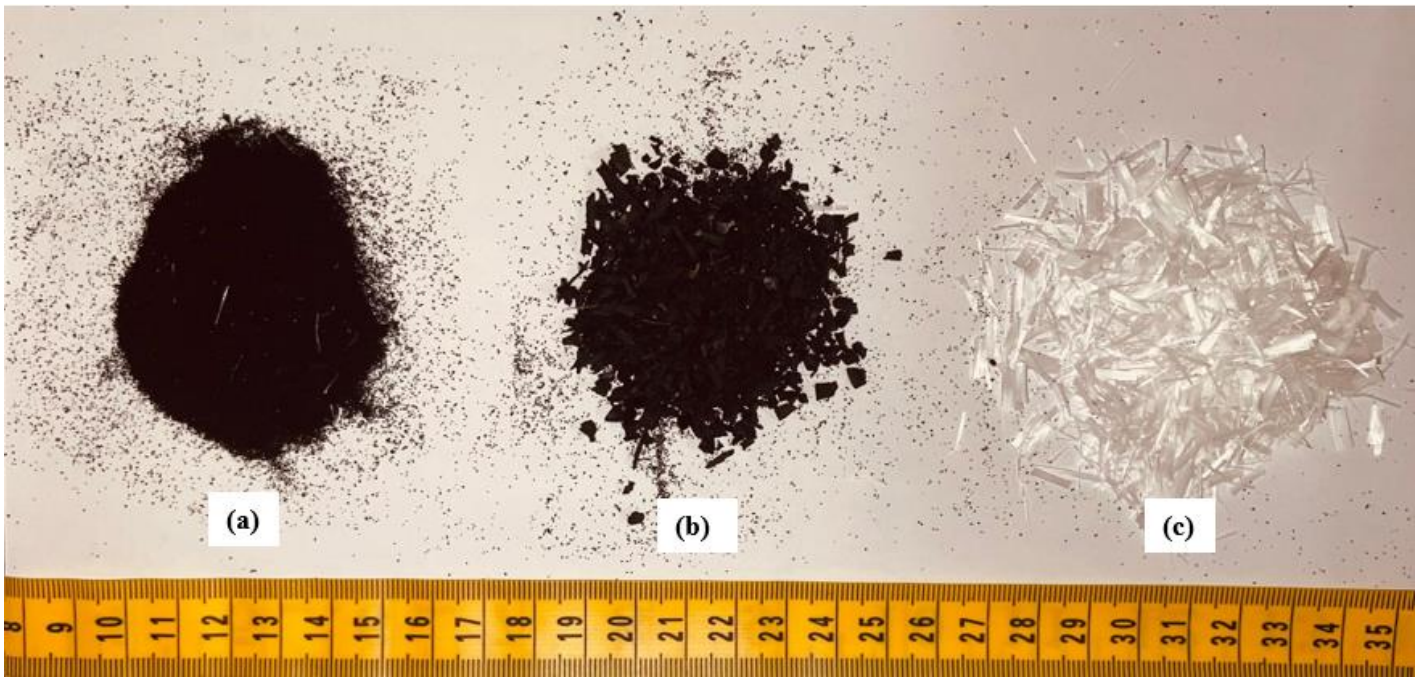


Figure 3- 1 (a) Powder rubber; (b) Crumb rubber; (c) PVA fibers

3.4.2. Selection of beam specimens

The seven tested beams were selected and as follows:

- One NC beam was fully cast with a normal concrete mixture and was used as a control beam/mixture for comparison (denoted as B1).
- Two RECC beams were fully cast with ECC containing different rubber sizes (CR or PR). B2 consisted of CR while B3 consisted of PR. These beams were referred to as CRECC and PRECC, respectively.
- Two beams repaired in the compression zone (B4 and B5) contained different sizes of rubber (CR or PR). B4 contained RECC layer of CR while B5 contained RECC layer of PR. These beams had NC layer with a depth of 165 mm in the tension zone and RECC layers (either with CR or PR) with a depth of 85 mm in the compression zone. Both beams were denoted as CRECC-C and PRECC-C, respectively.
- Two beams repaired in the tension zone (B6 and B7) contained different sizes of rubber (CR or PR). B6 contained a RECC layer of CR while B7 contained a RECC

layer of PR. These beams had RECC layer with a depth of 85 mm in the tension zone and NC layer with a depth of 165 mm in the compression zone and were designated as CRECC-T and PRECC-T, respectively.

3.4.3. Four-point loading test setup and loading procedure

Dimensions, steel reinforcement, and test setup for all beams are illustrated in **Figure 3-2**. The cross-sectional dimensions for all tested beams were 250 mm x 250 mm. All beams had a total length of 1960 mm and an effective load span of 1660 mm. Three 25M bars were used in the tension zone while two 20M bars were used in the compression zone. All beams were designed to fail in flexural, and to avoid shear failure, shear reinforcement in the form of 10 mm diameter stirrups with a spacing of 100 mm were used. The concrete cover for the tested beams was 30 mm. All beams were tested under four-point loading and simply supported with a span of 1660 mm (**Figure 3-2**). The single-point load on a steel beam was applied using an actuator with a load capacity of 500 kN. The load was distributed on two points spaced at 300 mm. The load was first applied until the first crack occurred and then applied gradually using a displacement control rate in increments until failure. After each load increment, the cracks were measured using a crack microscope. **Table 3-2** illustrates the results of the flexural testing of all beams.

Table 3- 2 Flexural test results for all tested beams

Beam #	Beam ID	Load capacity (kN)			Failure mode	Cracking at failure stage	
		First crack	Ultimate	Yield		Number	Maximum width (mm)
B1	NC	25.2	390.5	6.8	Flexure	23	3.2
B2	CRECC	29.9	414.9	6.4	Flexure	39	2
B3	PRECC	35.6	425.4	5.1	Flexure	36	2.2
B4	NC-CRECC-C	25.5	404.1	8.5	Flexure	32	3.6
B5	NC-PRECC-C	26.8	410.4	8.2	Flexure	28	4.2
B6	NC-CRECC-T	32.8	411.9	6.5	Flexure	30	1.5
B7	NC-PRECC-T	36.9	368.3	-	Debonding	21	0.9

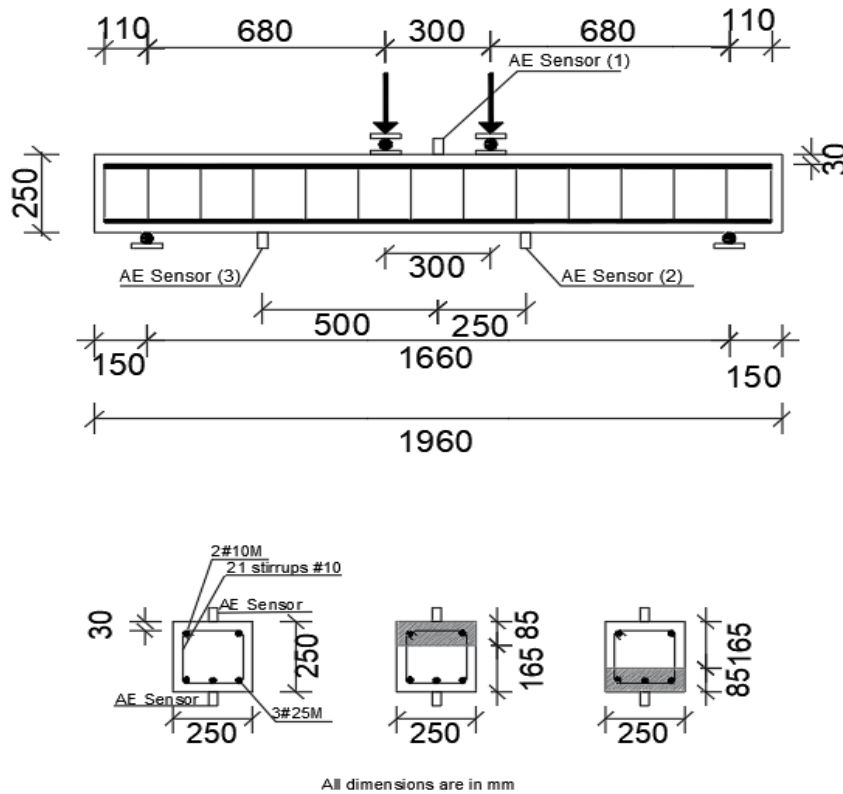


Figure 3- 2 Test setup for all tested beams

3.5. AE monitoring procedure

3.5.1. AE setup

Three sensors at different locations were attached to each beam to record the released AE during the testing. As shown in **Figure 3-2**, sensor 1 was placed in the mid-span of the beam, sensor 2 was placed at a distance of 250 mm measured from sensor 1, and sensor 3 was placed at a distance of 500 mm measured from sensor 1. All AE sensors were attached to the surface of the beam using a two-part epoxy adhesive prior to the flexural tests. The AE sensors used in this study were piezoelectric sensors with an integral preamplifier having a model number of R61-AST (Acoustics 2005). The recording and processing of the signals released during the testing were carried out by an AE system and an AE signal processing software (AEwin) from Mistras Group (Group 2007). An amplitude threshold of 40 dB was kept constant during the testing. Other data acquisition parameters used to set up the hardware are illustrated in **Table 3-3**. Parameters such as amplitude, signal strength, duration, energy, absolute energy, counts, rise time, average frequency, and peak frequency were obtained. The definitions of the previously mentioned AE terms are found in ASTM E1316 (ASTM 2014).

Table 3- 3 Pre-testing AE data built-in filter ranges

AE Data Setup	
Threshold	40 dB
Sample rate	1 MSPS
Pre-trigger	256 μ s
Length	1 k points
Preamp gain	40 dB
Peak definition	200 μ s
Hit definition	800 μ s
Hit lockout time	1000 μ s
Maximum duration	1000 μ s

3.5.2. Post-testing AE Data filtering

An amplitude-duration-based filter (Swansong II filter) was used to filter all the raw data extracted from the four-point load tests. The filtering process is carried out in order to minimize noise/unwanted wave reflections that may occur in the beams (FOWLER et al. 1989). This amplitude-duration filter was successfully used in several previous investigations in AE monitoring in the concrete industry (Abdelrahman et al. 2014; ElBatanouny et al. 2014; Vélez et al. 2015). The filter works by assuming that the real AE events with high values of amplitude are characterized by long magnitudes of duration and vice versa (Abdelrahman et al. 2015). The rejection limits for the AE signals are presented in **Table 3-4**. After completing the filtering process, the remaining the AE signals are

considered to be real AE sources resulting from the crack propagation from the four-point load tests.

Table 3- 4 Post-testing AE data amplitude-duration filter ranges

Amplitude (dB)	Duration (μ s)	
	Lower	Upper
$40 \leq A < 45$	0	400
$45 \leq A < 48$	0	500
$48 \leq A < 52$	0	600
$52 \leq A < 56$	0	700
$56 \leq A < 60$	100	800
$60 \leq A < 65$	300	1,000
$65 \leq A < 70$	500	2,000
$70 \leq A < 80$	1,000	4,000
$80 \leq A < 90$	2,000	7,000
$90 \leq A < 100$	3,000	10,000

3.6. AE Analysis and Processing

3.6.1. *b*-value analysis

A variety of parameters were analyzed in this paper to classify the damage in all beams. Firstly, traditional parameters that were directly extracted from the AE monitoring such as signal amplitude, number of hits, cumulative signal strength (CSS) were evaluated. Secondly, *b*-value analysis was performed by calculating the *b*-value from the

amplitude and number of hits. The b -value is then used to indicate the severity of damage (crack development) in the tested beams. This analysis was originally used in the seismic analysis and was then further applied in AE analysis (ElBatanouny et al. 2014). b -value analysis was successfully employed in several previous investigations in concrete materials and structures (Colombo et al. 2003) (ElBatanouny et al. 2014; Ohtsu 2008; Vidya Sagar and Raghu Prasad 2013). The b -value was calculated using **Eq. (3-1)** for all tested beams.

$$\log N = a - b \log A \quad (3-1)$$

Where:

N = number of hits with an amplitude larger than A ; A =signal amplitude (dB); a = empirically derived constant; and $b = b$ -value (Colombo et al. 2003; Ohtsu 2008; Vidya Sagar and Raghu Prasad 2013); the value ‘ a ’ was obtained by plotting $\log N$ (y-axis) versus $\log A$ (x-axis) for the seven beams. The average magnitude of ‘ a ’ for all beams was then obtained and applied in **Eq (3-1)**.

3.5.2. Intensity analysis

In addition to the b -value analysis, intensity analysis was also carried out for the tested beams. The intensity analysis was performed on the strength of the acquired AE signals and generated two additional parameters: historic index [$H(t)$] and severity [S_r]. The aforementioned parameters were utilized in several previous investigations to detect and quantify damage in concrete structures (Abdelrahman et al. 2015; Li et al. 2015; Ridgley et al. 2019; Vélez et al. 2015) The historic index spots the locations where there are sudden changes in the CSS curve. $H(t)$ was calculated for all the beams using the following **Eq. (3-2)**:

$$H(t) = \frac{N}{N-K} \frac{\sum_{i=K+1}^N S_{oi}}{\sum_{i=1}^N S_{oi}} \quad (3-2)$$

Where:

N = cumulative number of hits up to a certain time (t) while S_{oi} is the signal strength of the i^{th} signal.

The severity indicates the average value of signal strength of J number of hits and was calculated by **Eq (3-3)**.

$$S_r = \sum_{i=1}^J \frac{S_{oi}}{J} \quad (3-3)$$

The values of K and J in **Eqs. (3-2)** and **(3-3)** were kept as constants for all the seven beams. The values for the previously mentioned variables depend on the damage mechanism and the material being analyzed. For this study, the magnitudes for K and J were acquired from intensity analysis successfully implemented from similar previous studies (Abdelrahman et al. 2015; Abdelrahman et al. 2014).

The K in Eq. **(3-2)** was calculated based on the cumulative number of hits (N) as follows:

3. a) $K = 0$: if $N \leq 50$, b) $K = N - 30$: if $51 \leq N \leq 200$, c) $K = 0.85 N$: if $201 \leq N \leq 500$,
and
- d) $K = N - 75$: if $N \geq 501$.

However, the value for J was kept at a constant of 50 for all tested beams based on the analysis conducted in similar previous studies (Abdelrahman et al. 2015; Abdelrahman et al. 2014).

3.7. Results and discussion

The test results including the modes of failure, mid-span deflections, and number/width of cracks are illustrated in **Table 3-2**. **Figure 3-3** demonstrates the cracking patterns for

all tested beams at failure. All the control beams (PRECC, CRECC, and NC) failed in flexural mode in which the longitudinal reinforcement in the tension zone yielded and the concrete crushed in the compression zone of the beam. RECC control beams incorporating PR or CR exhibited higher deformation when compared to the NC beam (**Table 3-2**). The improvement in the deformation characteristics of the RECC beams when compared to NC was attributed to the nature of the rubber particles which are characterized by large elastic deformations before failure (Ganesan et al. 2013). RECC beams also showed a large number of cracks with tight widths compared to NC beam. RECC beam with CR (CRECC) displayed 39 cracks with a maximum width of 2 mm, whilst RECC beam with powder rubber (PRECC) displayed 36 cracks with a maximum width of 2.2 mm (**Table 3-2**). The increase of the number of cracking in the RECC beams when compared to the NC beam was due to the presence of fibers which tends to control cracks from expanding.

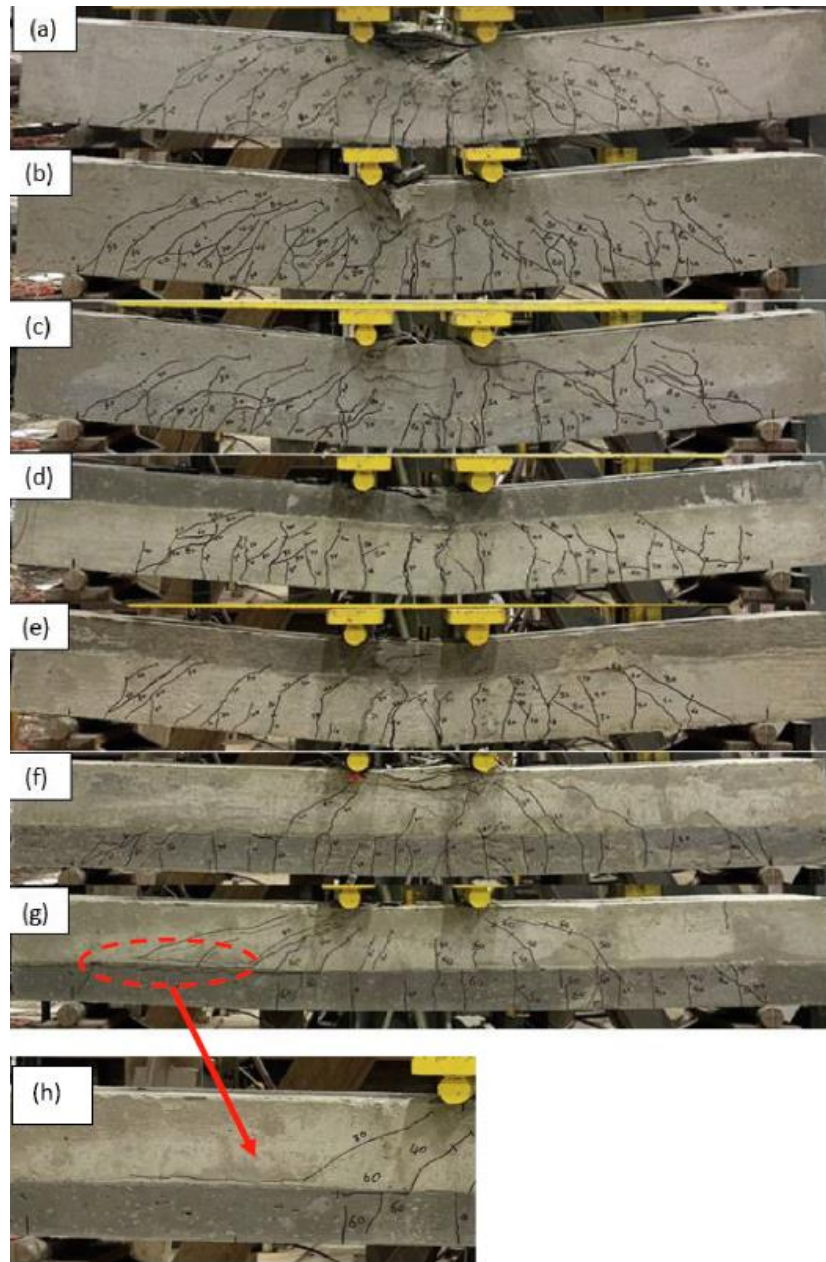
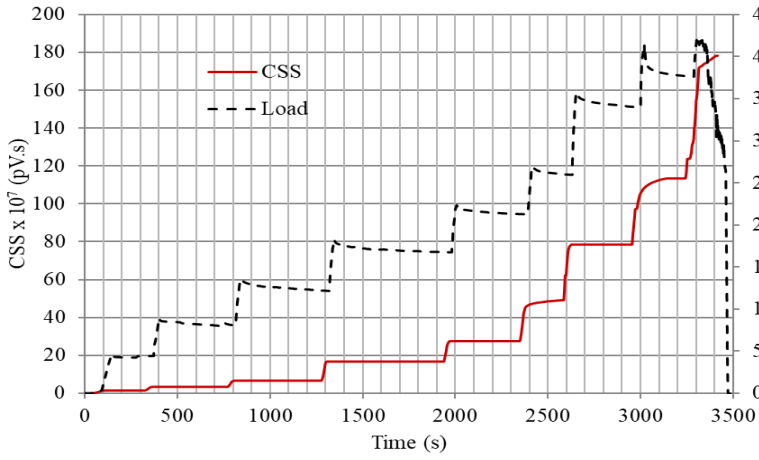


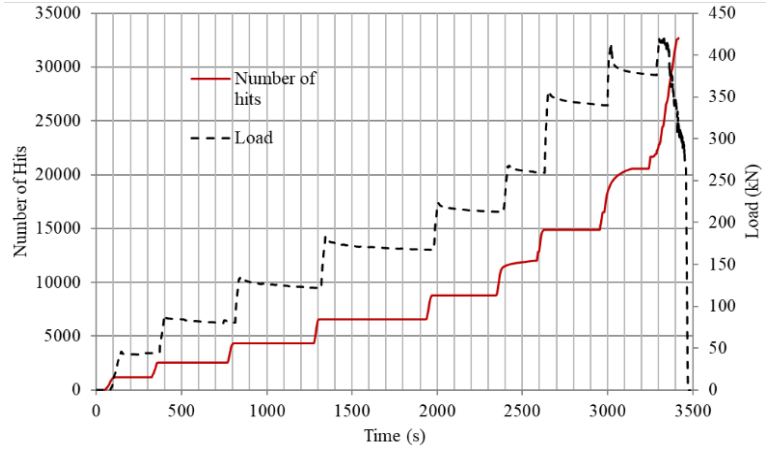
Figure 3- 3 Cracking behavior for all tested beams: (a) NC; (b) CRECC; (c) PRECC; (d) NC-CRECC-C; (e) NC-PRECC-C; (f) NC-CRECC-T; (g) NC-PRECC-T; (h) Debonding of NC-PRECC-T (AbdelAleem and Hassan 2022)

3.7.1. Crack detection using AE analysis

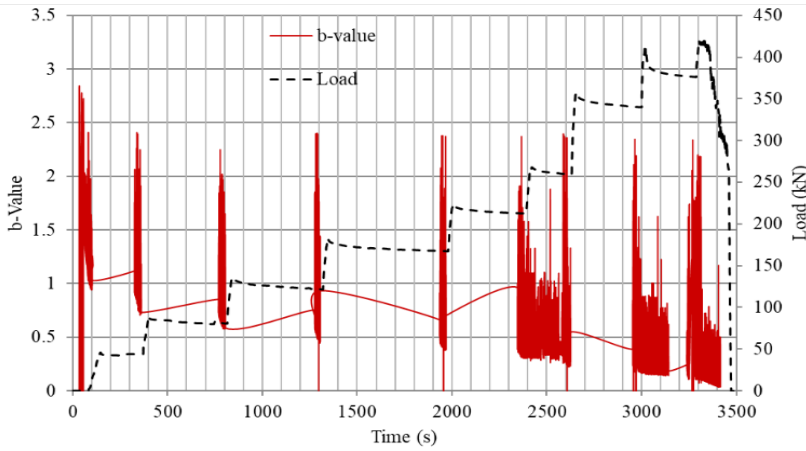
In this section, the effect of the cracking behavior of the seven beams on the AE signals and parameters during the testing process was studied. **Figure 3-4** illustrates a number of AE parameters from the PRECC beam (sensor 2) that was chosen to be an example and representative of other beams and sensors. Several AE parameters such as cumulative signal strength (CSS), number of hits, amplitude, b -value, $H(t)$ and S_r were analyzed over time for the PRECC beam in **Figure 3-4**. All the previously mentioned parameters were analyzed throughout the testing procedure until failure. In **Figures 3-4(a)** and **3-4(c)**, both the CSS and number of hits showed very similar trends and experienced an overall increase overtime. The increase in the AE activity is an indication of crack occurrence and propagation in the tested beam till failure. In particular, the first significant activity which can be correlated to the appearance of the first crack was detected at about 70 s (**Figure 3-4**). To further elaborate, the first change in slope in the CSS curve (**Figure 3-4(a)**), number of hits curve (**Figure 3-4(b)**), and S_r (**Figure 3-4(e)**) were displayed at about 70 s. b -value (**Figure 3-4(c)**) experienced a general decrease (increase in crack activity) and an increase in variations that also correlated to increase in activities in CSS, number of hits, S_r , and $H(t)$. The first decreasing activity (first crack) detected in the b -value also occurred at about 70 s. To further corroborate the occurrence of the first crack, **Figure 3-4(d)** shows the AE activity of $H(t)$. The first sudden increase in the $H(t)$ curve (**Figure 3-4(d)**) also occurred at about 70 s.



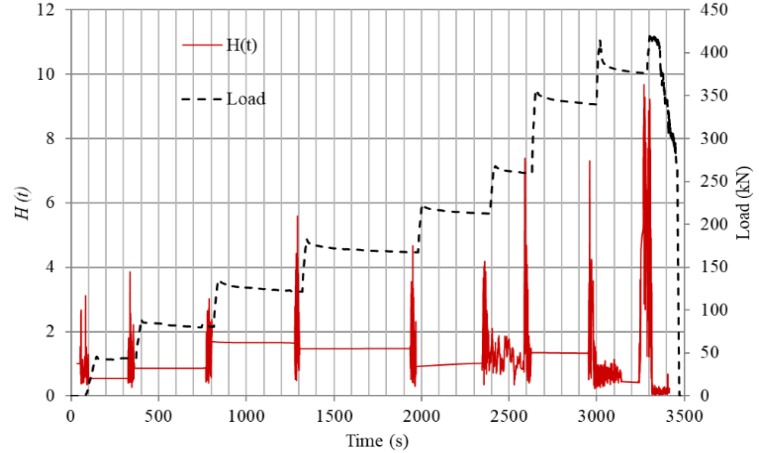
a) CSS



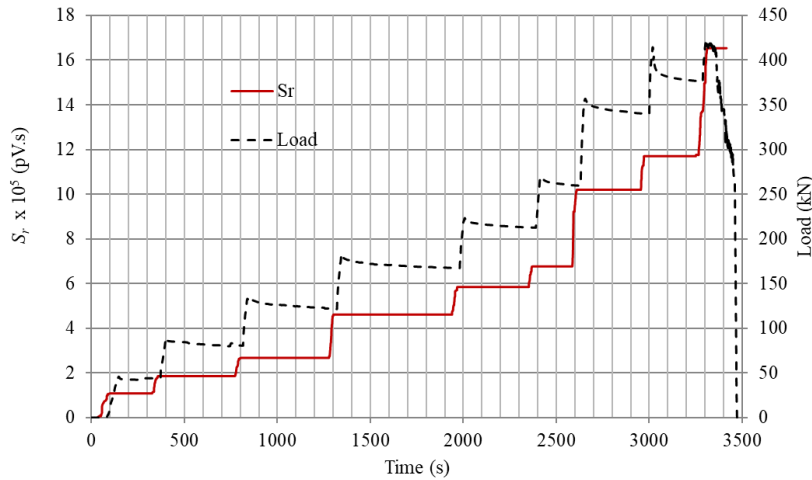
b) Number of hits



c) b -value



d) $H(t)$



e) S_r

Figure 3- 4 AE parameters and load vs time curves for PRECC beam sensor 2: a) CSS;

b) number of hits; c) b -value; d) $H(t)$; e) S_r

3.7.2. Time to first crack detection comparison among the tested beams

Figure 3-5 shows the time for the first crack for all tested beams. For the control beams (NC, CRECC and PRECC), it is evident that RECC beams showed a delayed first crack when compared to the NC beam (45 s). CRECC beam displayed the first crack at about 60 s while PRECC beam showed the first crack at about 70 s. This could be due to the higher tensile strength of RECC beams (**Table 3-2**). In terms of AE parameters, both CRECC and PRECC beams resulted in average number of hits of 302 and 344 hits, average CSS values of 0.42 and 0.48 pV.s, and average b -values of 1.19 and 1.59, respectively, at the first crack (**Table 3-5**). On the other hand, NC beam showed an average number of hits of 171.3, an average CSS value of 0.15 pV.s, and an average b -value of 2 (at the first crack). Referring to beams repaired in the compression zone (CRECC-C and PRECC-C), the time of the first crack in those beams was very comparable to the NC beam. CRECC-C and PRECC-C beams exhibited the first crack at 50 s and 55 s, respectively. The comparable time of the initiation of the first crack in beams repaired in the compression zone and NC beam is related to the fact that the first crack occurred in the tension zone of the beam (bottom part), which is made with NC mixture in both fully cast NC beam or beams repaired in the compression zone. The slight increase in the time of the first crack in CRECC-C and PRECC-C beams compared to NC beam (55 s compared to 50 s) is maybe due to the higher compression strain of CRECC-C and PRECC-C compared to NC (AbdelAleem and Hassan 2022). With regard to beams repaired in the tension zone, both CRECC-T and PRECC-T showed a more delayed first crack (65 s and 80s, respectively) due to the higher tensile strength (when compared to NC beam) (AbdelAleem and Hassan 2022). CRECC-C beam was accompanied by an average number of hits of 251.3 hits, an average CSS value of 1.79

pV.s, and an average b -value of 1.53 while PRECC-C was accompanied by an average number of hits of 273.6 hits, an average CSS value of 3.3 pV.s, and an average b -value of 1.15 at the time of first crack (**Table 3-5**). In addition, both CREEC-T and PRECC-T were followed by average of number of hits of 321.3 and 395.3 hits, average CSS values of 0.85 and 3.47 pV.s, and average b -values of 1.4 and 2.71, respectively at the time of first crack (**Table 3-5**). AE analysis, therefore, has shown efficacy in obtaining the time for the first crack (first change in slope in AE parameter curves) for all tested beams.

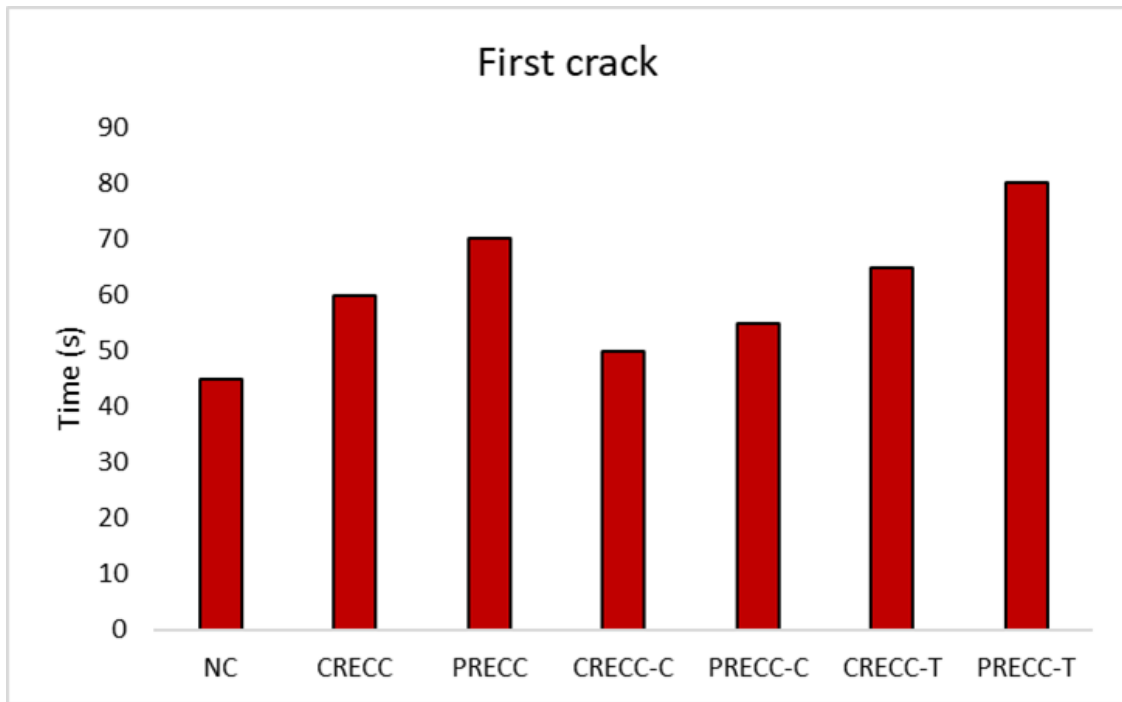


Figure 3- 5 Time of the first crack load for all beams

Table 3- 5 AE parameters obtained at the first crack and ultimate load

Beam #	AE Sensor	Amplitude		CSS x10 ⁷		<i>b-value</i>		Number of hits		<i>S_v</i> x10 ⁴		<i>H (t)</i>	
		First crack	Ultimate load	First crack	Ultimate load	First crack	Ultimate load	First crack	Ultimate load	First crack	Ultimate load	First crack	Ultimate load
NC	AE-1	48	45	0.12	57.2	2.11	0.58	113	15454	2.66	123.5	0.23	2.3
	AE-2	46	44	0.19	87.8	1.83	0.35	244	20910	4.65	155.6	0.45	2.1
	AE-3	47	46	0.14	65.4	2.08	0.49	157	17733	4.09	134	0.26	2.15
CRECC	AE-1	42	43	0.36	22.5	1.70	0.82	260	16424	4.69	131.5	0.36	3.08
	AE-2	40	43	0.48	32.4	0.80	0.42	343	22220	6.35	140	0.51	2.21
	AE-3	40	42	0.42	31.4	1.07	0.68	303	18845	5.21	122.4	0.47	2.01
PRECC	AE-1	42	42	0.41	76.8	1.95	0.92	295	16820	5.73	120	0.45	3.68
	AE-2	41	40	0.55	154	1.29	0.68	391	22755	7.32	150	0.57	2.87
	AE-3	41	40	0.47	95.6	1.55	0.86	345	19300	6.29	132	0.53	3.15
CRECC-C	AE-1	40	42	0.97	6.79	1.92	0.72	216	16030	3.89	132.3	0.35	2.75
	AE-2	44	44	2.80	24.5	1.01	0.59	290	21685	5.33	139.6	0.42	2.16
	AE-3	43	44	1.61	14.1	1.68	0.66	248	18391	4.36	138.5	0.39	2.41
PRECC-C	AE-1	40	41	2.05	51.8	1.76	0.62	236	16305	6.79	132.3	0.30	2.82
	AE-2	43	42	4.04	72.7	0.83	0.24	309	22060	8.33	125.5	0.44	3.60
	AE-3	44	43	3.81	62.4	0.85	0.34	276	18709	7.46	129.5	0.38	2.06
CRECC-T	AE-1	44	44	0.78	45.5	1.66	0.1	275	16384	6.34	161	0.23	3.53
	AE-2	40	42	0.92	81	1.26	0.06	367	22166	8.21	155	0.75	2.82
	AE-3	41	41	0.84	50.9	1.29	0.08	322	18800	7.15	134	0.33	2.98
PRECC-T	AE-1	45	46	3.02	43.9	2.72	0.45	340	14445	6.83	143	0.54	2.40
	AE-2	40	44	3.87	81.5	2.80	0.31	450	19542	8.87	174	0.68	3.12
	AE-3	40	45	3.52	59.7	2.60	0.40	396	16575	7.71	163	0.60	1.95

3.7.3. Impact of rubber particle size on the AE parameters

As previously illustrated, this study included two different rubber particle sizes incorporated in ECC: crumb rubber (CRECC) and powder rubber (PRECC). Two beams were fully cast in RECC and four other beams were repaired using RECC in either the tension side or compression side of the beam. **Table 3-5** shows the AE parameters at the

first crack and ultimate load. It can be concluded that the rubber particle size utilized had a noticeable effect on the AE parameters. For instance, the NC beam displayed an average number of hits of 18032 hits, average number of CSS of 70.13 pV.s, and an average b -value of 0.47 at the ultimate load while CRECC and PRECC displayed an average number of hits of 19163 and 19625, an average number of CSS of 28.7, 108.8 pV.s, and an average b -value of 0.64 and 0.82, respectively. In addition, beams repaired using powder rubber (PR) seemed to have a higher number of AE activities/parameters when compared to beams repaired in crumb rubber (CR).

The different types of rubber particles (CR or PR) used in the strengthening seemed to also have a distinguished effect on the AE parameters. For example, with reference to beams repaired in compression, CRECC-C displayed an average number of hits (at the ultimate load) of 18702, an average number of CSS of 15.13 and, and an average b -value of 0.66, respectively while PRECC-C exhibited an average number of hits of 19025, an average CSS value of 62.3, and an average b -value of 0.4 at the ultimate load, respectively. For beams repaired in tension, CRECC-T displayed an average number of hits at the ultimate load of 19117, a CSS average number of 59.13 pV.s, and average b -value of 0.08 while PRECC-T displayed an average number of hits of 16854, average number of CSS of 61.7, and an average b -value of 0.38. It is noticeable that beams with CR in general displayed a lower number of hits and CSS s (lower number of hits and CSS) than beams with PR (except PRECC-T). To further elaborate, the reasoning behind the lower strength accompanied by CR could be due to the larger particle size of the crumb rubber that reduced the strength of the rubber-mortar interface, which resulted in the propagation of micro-cracks contributing to a weaker strength that limited the continuation of deformation

beyond the yield point (AbdelAleem and Hassan 2022). PR, on the other hand, is smaller in particle size and exhibits a stronger rubber- mortar interfacial strength.

Moreover, beams with CR or PR generally displayed higher ductility and strain capacity (higher number of hits) than that of the NC beam due to the presence of fibers which are known to transfer the stress over the cracked section, resulting in a higher tensile strain capacity. Other reasons include the presence of rubber particles which enhance the strain capacity and deformability of the RECC beams. It should be noted that, PRECC-T beam displayed the least average of number of hits (when compared to all beams). This is attributed to the fact that all beams failed in flexural failure while PRECC-T beams experienced a failure between the NC-RECC interface (debonding).

3.7.4. Impact of layer/sensor location on AE parameters

As shown in **Figure 3-2**, all tested beams included three attached sensors. One sensor (sensor 1) was attached at the top of the beams (compression zone) and two sensors (sensors 2 and 3) were attached at the bottom (tension zone) of the beams. Sensor 1 (placed in the compression zone) in beams repaired in the tension zone showed a lower number of AE activity (CSS, number of hits and *b-value*) when compared to sensors 2 and 3 (placed in the tension zone) due to the lack of fibers and rubber in these beams (top part is made with NC mixture). The higher number of AE activities resulting from sensors 2 and 3 was due to the presence of fibers and rubber particles that both allow for higher deformation and therefore higher cracking and AE activities. For instance, in Table 5, CRECC-T displayed 16384 number of hits in sensor 1, 22166 in sensor 2, and 18800 in sensor 3. PRECC-T also showed 14445 number of hits in sensor 1, 19542 in sensor 2 and 16575 in sensor 3.

Furthermore, in beams repaired in compression, sensor 1 (compression zone) showed a lower number of activity than that of sensors 2 and 3 (tension zone) even though the repaired layer was in the compression zone. The lower number of AE activities displayed by sensor 1 is attributed to the fact that beams repaired in compression failed in flexural and therefore the highest number of cracks (highest number of activities) existed in the tension zone of the beam. For instance, CRECC-C showed 16030, 21685, and 18391 number of hits for sensors 1, 2 and 3, respectively. Also, PRECC-C displayed 16305, 22060, and 18709 number of hits for sensors 1, 2 and 3, respectively. Repair layer location (tension or compression side of the beam) resulted in a significant effect on the other studied AE parameters (similar to the above trends of the number of hits) and was further accentuated through the position of the sensor placement.

To highlight the effect of multi layers on AE parameters, the values of the amplitude of the three sensors were evaluated. Referring to **Figure 3-6**, it is evident that there are variations in the values of amplitude (ultimate load) in the three sensors. In fully cast beams (NC, PRECC and CRECC), the values of the amplitude were very close in the three sensors. For the NC beam, sensor 1, 2 and 3 at the ultimate load displayed amplitude values of 45, 44, and 46 dB, respectively. CRECC beam showed amplitude values of 43, 43, and 42 dB for sensor 1, 2 and 3, respectively. For sensor 1 at the ultimate load in the PRECC beam an amplitude value of 42 dB was displayed while sensors 2 and 3 at the ultimate load displayed amplitudes of 40 and 40 dB, respectively. The closeness of the amplitude values is due to the homogeneousness of the materials, thus yielding similar wave propagation characteristics. On the other hand, repaired beams either in compression or tension showed noticeable variations in the three sensors. For instance, in PRECC-T beam, the value of the

amplitude at the ultimate load for sensor 1 was 46 while the values for the amplitudes at the ultimate load for sensors 2 and 3 (tension zone) were 44 and 45, respectively.

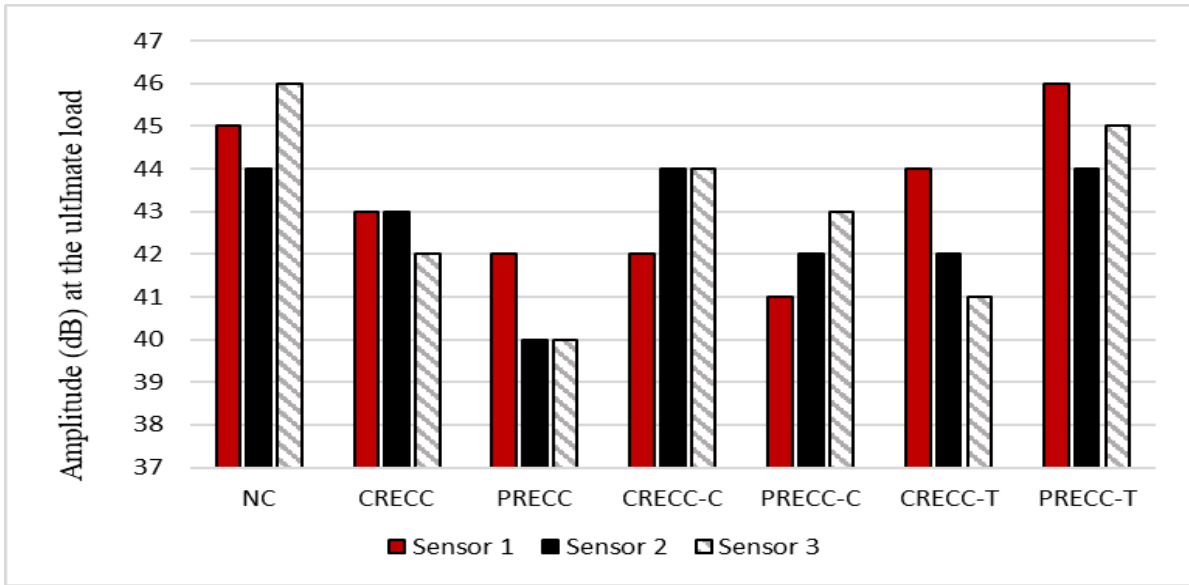


Figure 3- 6 Variations in the Amplitude (ultimate load) of the three sensors

The variations in the values of the amplitudes is due to the difference in the materials. This phenomenon is known as signal attenuation which tends to occur when there is difference in densities between two materials as well as lack of homogeneousness which in this study occurred in repaired beams (Ervin et al. 2007; Schumacher et al. 2011). The type of concrete used in the repair layers also proved to be another factor that affected the values of the amplitude. Rubber is known to have sound absorbing characteristics which tends to lower the value of the amplitude (Abouhussien and Hassan 2020). It is evident that in all repaired beams the NC layer displayed a higher amplitude whether it was placed in the compression or tension zone of the beam. For instance, in the CRECC-C beam, an amplitude value of 42 dB was shown in sensor 1 while amplitude values of 44 and 44 dB were shown in sensors 2 and 3, respectively.

3.7.5. Damage classification by AE intensity analysis

As shown in the previous sections, AE analysis proved to be useful in detecting different damage stages and also was beneficial in understanding the effect of the repair material used. To categorize the type of damage that occurred, intensity analysis parameters ($H(t)$ and S_r) were correlated to two stages of cracking (first crack and ultimate load). The values of $H(t)$ and S_r acquired from all the three sensors are illustrated in **Table 3-5**. The average values of the three sensors of $H(t)$ and S_r (for the seven tested beams) were calculated and then placed in **Table 3-6** to create the chart shown in **Figure 3-7**. This chart is used to represent the progression of cracking stages at both the first crack and ultimate load for all the tested beams. This chart included two ranges for $H(t)$ as well as S_r . For $H(t)$, the values ranged from 0.32 to 0.61 at the first crack and 2.2 to 3.23 for cracks at the ultimate load, respectively. Furthermore, for S_r , the magnitudes varied from 3.8 to 7.8×10^4 pV.s at the first crack and 129.1 to 160×10^4 pV.s correlating to the progression of cracks at the ultimate load, respectively. Both the values of $H(t)$ and S_r can be employed to represent the stages of cracking. For instance, a $H(t)$ value of 2.82 and a S_r value of 129.1 represent the stage of cracking at the ultimate load (as shown in **Figure 3-7**). This chart can possibly be used as a damage diagnosis tool for composite beams incorporating RECC. Similar charts have been executed successfully in different investigations and were utilized in damage quantification of reinforced concrete structures (Abouhussien and Hassan 2017; Abouhussien and Hassan 2015; Abouhussien and Hassan 2016).

Table 3- 6 Severity analysis parameters obtained at two different cracking stages

Beam ID	Avg S_r (pV.s) x10⁴		Avg H (t)	
	First-crack	Ultimate load	First-crack	Ultimate load
NC	3.8	137.7	0.32	2.2
CRECC	5.42	131.3	0.45	2.4
PRECC	6.45	134	0.52	3.23
CRECC-C	4.52	136.8	0.39	2.46
PRECC-C	7.53	129.1	0.37	2.82
CRECC-T	7.23	134.6	0.44	3.11
PRECC-T	7.80	160	0.61	2.49

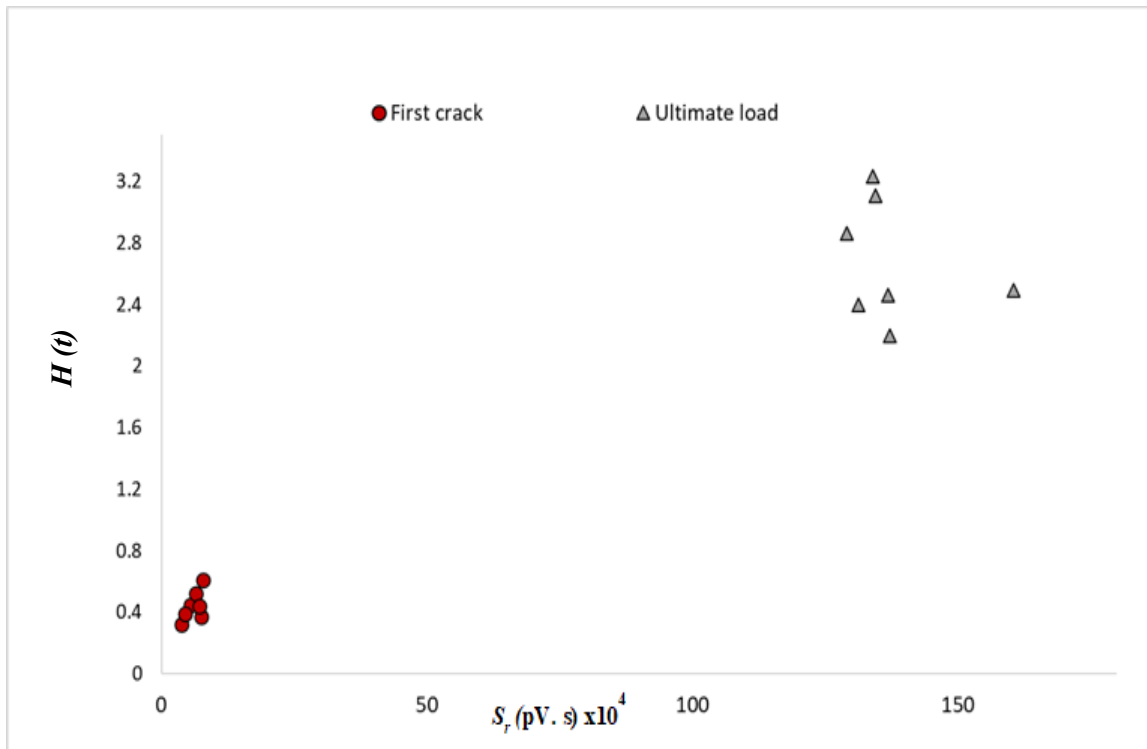


Figure 3- 7 Crack classification chart for all tested beams

3.8. Conclusions

This study utilized AE to analyze the crack initiation and propagation process of seven large-scale beams. Flexural tests were performed on three control beams (NC, CRECC and PRECC) and four other RECC beams that were either repaired in the compression or tension zone of the beam. The RECC beams contained PVA and two types of recycled rubber with different particle sizes (4.75 and 0.4 mm). Several AE analyses were performed and the following conclusions were drawn:

- All beams with rubberized ECC (RECC) that failed in flexural mode showed a higher load-carrying capacity, higher cracking activity, and smaller crack widths when compared to the NC beam.
- AE parameters such as number of hits, CSS, b -value, $H(t)$ and S_r were found to be useful in understanding the cracking behavior of the tested beams. The number of hits,

CSS, and S_r during the loading period, displayed an overall increase until the ultimate load. The overall increase was an indication of the crack initiation and propagation until failure. b -value, in contrast, experienced an overall decrease until the ultimate load. $H(t)$ showed jumps and fluctuations that correlated to AE changes in slopes displayed in the number of hits, CSS, b -value and S_r curves.

- The time for the first crack of the beam was experimentally detected and successfully confirmed through the analysis of the number of hits, CSS, b -value, $H(t)$ and S_r . The first crack was spotted at the first change of slope in the CSS, number of hits and S_r curves. For the b -value, the first crack was noticed at the first significant decreasing activity. $H(t)$ curve also showed the first crack at the first sudden activity.
- The inclusion of rubber in concrete mixtures seemed to have an impact on AE parameters such as number of hits. It was found that beams with rubber particles (RECC beams) showed higher AE activities compared to beam without rubber (NC beam). In addition, the use of smaller rubber size (PR) showed higher number of hits when compared to beams with larger rubber size (CR).
- The region with the highest cracking activity in the beam was found to have the highest impact on AE activities, regardless of the repair layer location. For example, when the repair layer was placed the tension zone (NC layer at the top and RECC layer at the bottom), sensors 2 and 3, which were placed in the tension zone (highest cracking activities) displayed the highest number of AE events (compared to sensor 1, placed on the top layer). Also, when the repair layer was placed in the compression zone (NC layer at the bottom and RECC layer at the top), sensors 2 and 3 (placed at the bottom) still displayed

the highest number of AE events due to the highest cracking activities at the bottom side of the beam.

- Analyzing the amplitude values revealed a wave attenuation in beams with multi layers compared to the single layer beams (fully cast beams). It was found that in fully cast beams (NC, CRECC or PRECC), the values of the amplitude from the three sensors were very close, while in repaired beams (either in compression or tension) the amplitude experienced attenuation. This is owing to a) the presence of rubber in the repair material (due to its sound absorbing capacity) and b) due to the presence of two non-homogenous materials with two different densities (NC and RECC).
- Intensity analysis was utilized to develop a damage quantification chart. The two intensity analysis parameters, $H(t)$ and S_r , were utilized to represent two cracking stages: first crack and ultimate load. For each parameter, there was a range of numbers representing a crack quantification stage. The chart can be used as a tool to categorize and quantify damage severity in terms of crack growth in composite beams

3.9. Chapter References

- AbdelAleem, B. H., and Hassan, A. A. (2022). "Use of rubberized engineered cementitious composite in strengthening flexural concrete beams." *Engineering Structures*, 262, 114304.
- Abdelrahman, M., ElBatanouny, M. K., Ziehl, P., Fasl, J., Larosche, C. J., and Fraczek, J. (2015). "Classification of alkali-silica reaction damage using acoustic emission: A proof-of-concept study." *Construction and Building Materials*, 95, 406-413.

- Abdelrahman, M., ElBatanouny, M. K., and Ziehl, P. H. (2014). "Acoustic emission based damage assessment method for prestressed concrete structures: Modified index of damage." *Engineering Structures*, 60, 258-264.
- Abouhussien, A. A., and Hassan, A. A. (2017). "Acoustic emission monitoring for bond integrity evaluation of reinforced concrete under pull-out tests." *Advances in Structural Engineering*, 20(9), 1390-1405.
- Abouhussien, A. A., and Hassan, A. A. (2019). "Crack Growth Monitoring in Fiber-Reinforced Self-Consolidating Concrete via Acoustic Emission." *ACI Materials Journal*, 116(5), 181-191.
- Abouhussien, A. A., and Hassan, A. A. (2020). "Classification of damage in self-consolidating rubberized concrete using acoustic emission intensity analysis." *Ultrasonics*, 100, 105999.
- Abouhussien, A. A., Hassan, A. A., and AbdelAleem, B. H. (2019). "Acoustic Emission Analysis of Self-Consolidating Rubberized Concrete Beam-Column Connections under Cyclic Loading." *ACI Structural Journal*, 116(6).
- Abouhussien, A. A., and Hassan, A. A. A. (2015). "Evaluation of damage progression in concrete structures due to reinforcing steel corrosion using acoustic emission monitoring." *Journal of civil structural health monitoring*, 5(5), 751-765.
- Abouhussien, A. A., and Hassan, A. A. A. (2016). "Detection of bond failure in the anchorage zone of reinforced concrete beams via acoustic emission monitoring." *Smart materials and structures*, 25(7), 75034-75046.
- Acoustics, P. (2005). "R6I-AST sensor." *Princeton Junction, NJ, USA*.

- ASTM (2014). "Standard Terminology for Nondestructive Examinations (ASTM E1316)." ASTM International West Conshohocken, PA, USA.
- ASTM C150/C150M (2012). "Standard Specification for Portland Cement." *ASTM International* (West Conshohocken, PA, USA), 9 pp.
- ASTM International, W. C., PA, USA (2012). "Standard Specification for Coal Fly ash and Raw or Calcined Natural Pozzolan for Use in Concrete " *ASTM C618*, 5, 2012.
- Batran, T. Z., Ismail, M. K., and Hassan, A. A. (2021). "Flexural behavior of lightweight self-consolidating concrete beams strengthened with engineered cementitious composite." *ACI Materials Journal*, 118(4), 39-50.
- Behnia, A., Chai, H. K., and Shiotani, T. (2014). "Advanced structural health monitoring of concrete structures with the aid of acoustic emission." *Construction and Building Materials*, 65, 282-302.
- Colombo, I. S., Main, I., and Forde, M. (2003). "Assessing damage of reinforced concrete beam using" b-value" analysis of acoustic emission signals." *Journal of materials in civil engineering*, 15(3), 280-286.
- Di Benedetti, M. (2012). *Acoustic emission in structural health monitoring of reinforced concrete structures*, University of Miami.
- ElBatanouny, M. K., Larosche, A., Mazzoleni, P., Ziehl, P., Matta, F., and Zappa, E. (2014). "Identification of cracking mechanisms in scaled FRP reinforced concrete beams using acoustic emission." *Experimental Mechanics*, 54(1), 69-82.

- ElBatanouny, M. K., Ziehl, P. H., Larosche, A., Mangual, J., Matta, F., and Nanni, A. (2014). "Acoustic emission monitoring for assessment of prestressed concrete beams." *Construction & building materials*, 58, 46-53.
- Engindeniz, M., Kahn, L. F., and Abdul-Hamid, Z. (2005). "Repair and strengthening of reinforced concrete beam-column joints: State of the art." *ACI structural journal*, 102(2), 1.
- Ervin, B. L., Bernhard, J. T., Kuchma, D. A., and Reis, H. "Monitoring general corrosion of rebar embedded in mortar using high-frequency guided mechanical waves." *Proc., Sensors and Smart Structures Technologies for Civil, Mechanical, and Aerospace Systems 2007*, SPIE, 447-458.
- Farrar, C. R., and Worden, K. (2007). "An introduction to structural health monitoring." *Philosophical Transactions of the Royal Society A: Mathematical, Physical and Engineering Sciences*, 365(1851), 303-315.
- FOWLER, T., BLESSING, J., and CONLISK, P. "New directions in testing." *Proc., AECM-3: International Symposium on Acoustic Emission from Composite Materials, 3 rd, Paris, France*, 16-27.
- Ganesan, N., Raj, B., and Shashikala, A. (2013). "Behavior of self-consolidating rubberized concrete beam-column joints." *ACI Materials Journal*, 110(6), 697.
- Gostautas, R. S., Ramirez, G., Peterman, R. J., and Meggers, D. (2005). "Acoustic emission monitoring and analysis of glass fiber-reinforced composites bridge decks." *Journal of bridge engineering*, 10(6), 713-721.
- Group, M. (2007). "PCI-2 based AE system 1 user's manual." *Physical Acoustics Corporation*.(Princeton Junction, NJ).

- Guo, B., and Li, Y. "Review of Research on Damage Identification of Reinforced Concrete Structures Based on Acoustic Emission Technology." *Proc., IOP Conference Series: Earth and Environmental Science*, IOP Publishing, 012039.
- Huang, X., Ranade, R., Ni, W., and Li, V. C. (2013). "Development of green engineered cementitious composites using iron ore tailings as aggregates." *Construction and Building Materials*, 44, 757-764.
- Ismail, M. K., and Hassan, A. A. (2016). "Impact Resistance and Acoustic Absorption Capacity of Self-Consolidating Rubberized Concrete." *ACI Materials Journal*, 113(6).
- Ismail, M. K., and Hassan, A. A. A. (2016). "Impact resistance and acoustic absorption capacity of self-consolidating rubberized concrete." *ACI materials journal*, 113(6), 725-736.
- Ismail, M. K., Sherir, M. A., Siad, H., Hassan, A. A., and Lachemi, M. (2018). "Properties of self-consolidating engineered cementitious composite modified with rubber." *Journal of materials in civil Engineering*, 30(4), 04018031.
- Li, D., Chen, Z., Feng, Q., and Wang, Y. (2015). "Damage analysis of CFRP-confined circular concrete-filled steel tubular columns by acoustic emission techniques." *Smart materials and structures*, 24(8), 85017-85011.
- Li, S., Zhang, L., Guo, P., Zhang, P., Wang, C., Sun, W., and Han, S. (2021). "Characteristic analysis of acoustic emission monitoring parameters for crack propagation in UHPC-NC composite beam under bending test." *Construction & building materials*, 278, 122401.

- Li, V. C. (1993). "From micromechanics to structural engineering the design of cementitious composites for civil engineering applications." *Doboku Gakkai Ronbunshu*, 1993(471), 1-12.
- Li, V. C. (1998). "Engineered cementitious composites (ECC)-tailored composites through micromechanical modeling."
- Li, V. C. (2002). "Advances in ECC research." *ACI Special Publications*, 206, 373-400.
- Li, V. C. (2012). "Tailoring ECC for special attributes: A review." *International Journal of Concrete Structures and Materials*, 6, 135-144.
- Li, V. C., Wu, C., Wang, S., Ogawa, A., and Saito, T. (2002). "Interface tailoring for strain-hardening polyvinyl alcohol-engineered cementitious composite (PVA-ECC)." *Materials Journal*, 99(5), 463-472.
- Mechtcherine, V. (2013). "Novel cement-based composites for the strengthening and repair of concrete structures." *Construction & building materials*, 41, 365-373.
- Nair, A., and Cai, C. (2010). "Acoustic emission monitoring of bridges: Review and case studies." *Engineering structures*, 32(6), 1704-1714.
- Ohtsu, M., and Y. Tomoda. (2008). "Phenomenological model of corrosion process in reinforced concrete identified by acoustic emission." *ACI Mater. J.*, 105 (2), 194-199.
- Parveen, S. D., and Sharma, A. (2013). "Rubberized concrete: Needs of good environment (overview)." *Int. J. Emerg. Technol. Adv. Eng*, 3, 192-196.
- Paul, S., Pirskawetz, S., Van Zijl, G., and Schmidt, W. (2015). "Acoustic emission for characterising the crack propagation in strain-hardening cement-based composites (SHCC)." *Cement and concrete research*, 69, 19-24.

- Pollock, A. A. (1986). "Classical wave theory in practical AE testing." *Progress in acoustic emission III-JAP society of non-destructive testing*, 708-721.
- Ramachandra Murthy, A., Karihaloo, B. L., Vindhya Rani, P., and Shanmuga Priya, D. (2018). "Fatigue behaviour of damaged RC beams strengthened with ultra high performance fibre reinforced concrete." *International journal of fatigue*, 116, 659-668.
- Ranjbar, N., Behnia, A., Chai, H. K., Alengaram, U. J., and Jumaat, M. Z. (2016). "Fracture evaluation of multi-layered precast reinforced geopolymer-concrete composite beams by incorporating acoustic emission into mechanical analysis." *Construction and Building Materials*, 127, 274-283.
- Ranjbar, N., Behnia, A., Chai, H. K., Alengaram, U. J., and Jumaat, M. Z. (2016). "Fracture evaluation of multi-layered precast reinforced geopolymer-concrete composite beams by incorporating acoustic emission into mechanical analysis." *Construction & building materials*, 127, 274-283.
- Rashad, A. M. (2016). "A comprehensive overview about recycling rubber as fine aggregate replacement in traditional cementitious materials." *International Journal of Sustainable Built Environment*, 5(1), 46-82.
- Reda Taha, M. M., El-Dieb, A. S., Abd El-Wahab, M., and Abdel-Hameed, M. (2008). "Mechanical, fracture, and microstructural investigations of rubber concrete." *Journal of materials in civil engineering*, 20(10), 640-649.
- Ridgley, K. E., Abouhussien, A. A., Hassan, A. A., and Colbourne, B. (2019). "Characterisation of damage due to abrasion in SCC by acoustic emission analysis." *Magazine of Concrete Research*, 71(2), 85-94.

- Safdar, M., Matsumoto, T., and Kakuma, K. (2016). "Flexural behavior of reinforced concrete beams repaired with ultra-high performance fiber reinforced concrete (UHPFRC)." *Composite structures*, 157, 448-460.
- Şahmaran, M., and Li, V. C. (2010). "Engineered cementitious composites: Can composites be accepted as crack-free concrete?" *Transportation Research Record*, 2164(1), 1-8.
- Schumacher, T., Higgins, C. C., and Lovejoy, S. C. (2011). "Estimating operating load conditions on reinforced concrete highway bridges with b-value analysis from acoustic emission monitoring." *Structural Health Monitoring*, 10(1), 17-32.
- Selman, E., Ghiami, A., and Alver, N. (2015). "Study of fracture evolution in FRP-strengthened reinforced concrete beam under cyclic load by acoustic emission technique: An integrated mechanical-acoustic energy approach." *Construction and Building Materials*, 95, 832-841.
- Siad, H., Lachemi, M., Ismail, M. K., Sherir, M. A., Sahmaran, M., and Hassan, A. A. (2019). "Effect of rubber aggregate and binary mineral admixtures on long-term properties of structural engineered cementitious composites." *Journal of Materials in Civil Engineering*, 31(11), 04019253.
- Thomas, B. S., Gupta, R. C., and Panicker, V. J. (2016). "Recycling of waste tire rubber as aggregate in concrete: durability-related performance." *Journal of Cleaner Production*, 112, 504-513.
- Vélez, W., Matta, F., and Ziehl, P. (2015). "Acoustic emission monitoring of early corrosion in prestressed concrete piles." *Structural Control and Health Monitoring*, 22(5), 873-887.

- Verbruggen, S., De Sutter, S., Iliopoulos, S., Aggelis, D., and Tysmans, T. (2016). "Experimental structural analysis of hybrid composite-concrete beams by digital image correlation (DIC) and acoustic emission (AE)." *Journal of Nondestructive Evaluation*, 35, 1-10.
- Vidya Sagar, R., and Raghu Prasad, B. (2013). "Laboratory investigations on cracking in reinforced concrete beams using on-line acoustic emission monitoring technique." *Journal of Civil Structural Health Monitoring*, 3(3), 169-186.
- Volovski, M. (2015). "FUNDING FOR HIGHWAY ASSET CONSTRUCTION AND MAINTENANCE: SUSTAINABLE ALTERNATIVES TO THE TRADITIONAL GAS TAX." *IRF*, 6.
- Wang, H.-Y., Chen, B.-T., and Wu, Y.-W. (2013). "A study of the fresh properties of controlled low-strength rubber lightweight aggregate concrete (CLSRLC)." *Construction and Building Materials*, 41, 526-531.
- Xargay, H., Ripani, M., Folino, P., Núñez, N., and Caggiano, A. (2021). "Acoustic emission and damage evolution in steel fiber-reinforced concrete beams under cyclic loading." *Construction and Building Materials*, 274, 121831.
- Ziehl, P. H., Galati, N., Nanni, A., and Tumialan, J. G. (2008). "In-situ evaluation of two concrete slab systems. II: evaluation criteria and outcomes." *Journal of Performance of Constructed Facilities*, 22(4), 217-227.

4. Summary and recommendations

4.1. Summary

This research consisted of two experimental studies presented in chapters 2, and 3. The primary goal of each study was to evaluate and analyze the changes of different AE parameters as a result of adding a repair layer to an existing concrete layer under flexural loading conditions. A variety of ECC mixtures were used as repair materials of reinforced concrete beams while alternating the sensor/repair location. All of the AE sensors in the studies were placed prior to testing and all the raw data was then recorded throughout the flexural loading tests. The AE activities were then collected and analyzed post testing. The following conclusions were drawn based on the results obtained from both studies:

1) AE parameters such as number of hits, CSS, b -value, absolute energy, amplitude, peak frequency, $H(t)$, and S_r were found to be successful in evaluating the crack propagation in all tested beams. Number of hits, CSS, and S_r experienced a gradual increase while b -value experienced a gradual decrease as a result of crack development. $H(t)$ showed jumps and fluctuations that were related with changes in slopes in the AE events displayed by CSS, number of hits, b -value, and S_r .

2) The first crack detection using AE parameters such as CSS, number of hits, b -value, $H(t)$, and S_r successfully validated the time of the crack obtained experimentally. For AE parameters including CSS, number of hits, and S_r , the time of the crack was detected at the first change of slope in the AE activity. For the b -value, the time of the first crack was detected at the first decreasing activity. Moreover, $H(t)$ showed the time of the first crack at the first increasing AE activity.

3) RA vs. AF proved to be an effective tool in classifying the failure modes (flexural, shear, or debonding) for all beams. It was found out that in beams that failed in flexure, the majority of the points were dominating the top side of the chart while in beams that failed in debonding, majority of the points were domineering the bottom side of the chart.

4) Varying the fiber type (PVA or SF) was found to have an effect on the number of hits. Generally, repaired beams displayed a higher number of hits when compared to unrepaired beams. Beams repaired with SF showed the highest number of hits (when compared to beams repaired by PVA fibers) due to the high load-bearing capacity accompanied by the SFs.

5) The effect of using different rubber particle size seemed to show an impact on AE parameters such as number of hits. It was discerned that beams incorporating rubber particles resulted in number of activities that were high than that of beams without rubber. In addition, the use of powder rubber (PR) in the repaired beams showed a higher number of hits when compared to the use of crumb rubber (CR) due to the smaller particle size of the PR when compared to the larger particle size of CR.

6) Evaluating the signal amplitude variations showed a wave attenuation as a result of adding a new concrete layer to an old concrete layer. It was observed that in fully cast beams (NC, CRECC, PRECC, ECC, and SFRCC), the signal amplitude values displayed by the three sensors were very close in magnitude. However, in repaired beams, the signal amplitude values accompanied by the sensors experienced attenuation. This is owing to a) the presence of two materials with different densities and mechanical properties b) sound absorbing properties accompanied by rubber particles.

7) Intensity analysis was proven effective in creating a damage quantification chart pertaining to two different cracking stages: first crack and ultimate load. Different ranges were accompanied by $H(t)$, and S_r and were directly correlated to different cracking stages. The chart showed to be effective in quantifying the severity of the cracking activities in all beams.

8) Beams that failed in flexural seemed to display higher AE activities when compared to beams that failed in debonding. This was clearly highlighted when the AE activities of beams repaired in compression were compared to the AE activities of beams repaired in tension.

9) The regions in the beams with the most cracking activities were found to display the highest number of hits, regardless of the repair layer. For instance, in beams repaired in the tension zone, sensors 2 and 3 displayed the highest number of hits when compared to sensor 1. Moreover, in beams repaired in the compression zone, sensors 2 and 3 (when compared to sensor 1) also displayed the highest number of hits due to the high cracking activity accompanied by the tension zone.

4.2. Recommendations for Future Research and Potential Applications/Limitations of the Current Study

The main objective of this thesis was to examine the variations in the AE parameters as a result of adding an ECC repair layer to an old concrete layer as well as using different ECC materials in the repair layer. Two studies included testing large-scale normal concrete beams of repaired with ECC incorporating fibers (PVA and SF) and ECC incorporating rubber particles (PR and CR).

- It is recommended for future research to consider alternative concrete types (such as lightweight concrete) with a different composition and mixture design instead of normal concrete to verify the ability of AE monitoring to distinguish the presence of two different materials via wave propagation characteristics. All tests were performed on large-scale beams that were repaired for either tension or compression. For a potential application, it is suggested to perform flexural loading testing on beam-column connections (see figure X below) repaired in the critical zone using either ECC with fiber or rubber to simulate earthquake loads and validate the ability of AE technique to distinguish the change in AE waveforms emitted in different locations and propagating in either one or two materials.

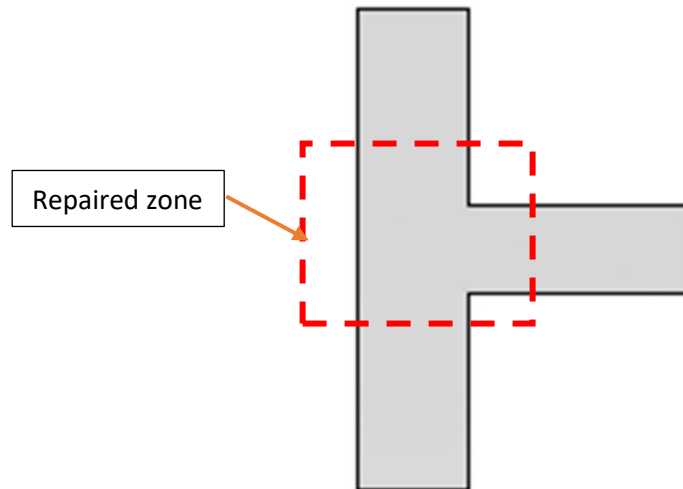


Figure X

- The generated charts from the intensity and RA analyses can be utilized to pertain to and categorize different damage levels in large-scale structures repaired with ECC. Furthermore, AE parameters such as b -value, number of hits, CSS, S_r , and H

(i) can potentially be used to indicate early damage occurrence as well as crack propagation in several repaired concrete structures.

- All the resulting AE analyses, damage quantification charts, and failure classification charts are only valid for large-scale ECC repaired in either tension or compression beams tested under flexural loading. Furthermore, the AE wave propagation characteristics resulting from the material's non homogeneousness are only relevant to the use of fibers such as PVA and SF as well as rubber particles such as PR and CR.
- The obtained AE analyses results and charts based on the testing and evaluation of thirteen beams under flexural testing. To further validate the AE's accuracy in identifying damage of multi-layered structures and to determine whether the variations obtained are statistically significant, it is advised that future research include testing a greater number of multi-layered beams along with additional control beams.

Bibliography

- AbdelAleem, B. H., and Hassan, A. A. (2022). "Use of rubberized engineered cementitious composite in strengthening flexural concrete beams." *Engineering Structures*, 262, 114304.
- Abdelrahman, M., ElBatanouny, M. K., and Ziehl, P. H. (2014). "Acoustic emission based damage assessment method for prestressed concrete structures: Modified index of damage." *Engineering Structures*, 60, 258-264.
- Abdelrahman, M., ElBatanouny, M. K., Ziehl, P., Fasl, J., Larosche, C. J., and Fraczek, J. (2015). "Classification of alkali–silica reaction damage using acoustic emission: A proof-of-concept study." *Construction and Building Materials*, 95, 406-413.
- Abouhussien, A. A., and Hassan, A. A. (2017). "Acoustic emission monitoring for bond integrity evaluation of reinforced concrete under pull-out tests." *Advances in Structural Engineering*, 20(9), 1390-1405.
- Abouhussien, A. A., and Hassan, A. A. (2017). "Application of acoustic emission monitoring for assessment of bond performance of corroded reinforced concrete beams." *Structural Health Monitoring*, 16(6), 732-744.
- Abouhussien, A. A., and Hassan, A. A. (2019). "Crack Growth Monitoring in Fiber-Reinforced Self-Consolidating Concrete via Acoustic Emission." *ACI Materials Journal*, 116(5), 181-191.
- Abouhussien, A. A., and Hassan, A. A. A. (2015). "Evaluation of damage progression in concrete structures due to reinforcing steel corrosion using acoustic emission monitoring." *Journal of civil structural health monitoring*, 5(5), 751-765.

- Abouhussien, A. A., and Hassan, A. A. A. (2016). "Detection of bond failure in the anchorage zone of reinforced concrete beams via acoustic emission monitoring." *Smart materials and structures*, 25(7), 75034-75046.
- Abouhussien, A. A., and Hassan, A. A. A. (2019). "Assessment of Crack Development in Engineered Cementitious Composites Based on Analysis of Acoustic Emissions." *Journal of materials in civil engineering*, 31(6).
- Abouhussien, A. A., and Hassan, A. A. A. (2020). "Classification of damage in self-consolidating rubberized concrete using acoustic emission intensity analysis." *Ultrasonics*, 100, 105999-105999.
- Abouhussien, A. A., Hassan, A. A. A., Ismail, M. K., and AbdelAleem, B. H. (2019). "Evaluating the cracking behavior of ECC beam-column connections under cyclic loading by acoustic emission analysis." *Construction & building materials*, 215, 958-968.
- Abouhussien, A. A., Hassan, A. A., and AbdelAleem, B. H. (2019). "Acoustic Emission Analysis of Self-Consolidating Rubberized Concrete Beam-Column Connections under Cyclic Loading." *ACI Structural Journal*, 116(6).
- Aggelis, D. G. (2011). "Classification of cracking mode in concrete by acoustic emission parameters." *Mechanics Research Communications*, 38(3), 153-157.
- Aggelis, D., De Sutter, S., Verbruggen, S., Tsangouri, E., and Tysmans, T. (2019). "Acoustic emission characterization of damage sources of lightweight hybrid concrete beams." *Engineering Fracture Mechanics*, 210, 181-188.
- ASCE [Report card for America's infrastructure,] American Society of Civil Engineers, Reston, VA, 73-81 (2009)

- ASTM (2014). "Standard Terminology for Nondestructive Examinations (ASTM E1316)." ASTM International West Conshohocken, PA, USA.
- ASTM C150/C150M (2012). "Standard Specification for Portland Cement." *ASTM International* (West Conshohocken, PA, USA), 9 pp.
- ASTM International, W. C., PA, USA (2012). "Standard Specification for Coal Fly ash and Raw or Calcined Natural Pozzolan for Use in Concrete " *ASTM C618*, 5, 2012.
- B, J.-I. (2003). "Monitoring method for active cracks in concrete by acoustic emission." *Federation of Construction Material Industries, Japan*, 23-28.
- Batran, T. Z., Ismail, M. K., and Hassan, A. A. (2021). "Flexural behavior of lightweight self-consolidating concrete beams strengthened with engineered cementitious composite." *ACI Materials Journal*, 118(4), 39-50.
- Behnia, A., Chai, H. K., and Shiotani, T. (2014). "Advanced structural health monitoring of concrete structures with the aid of acoustic emission." *Construction and Building Materials*, 65, 282-302.
- Bhowmik, S., and Ray, S. (2019). "An experimental approach for characterization of fracture process zone in concrete." *Engineering Fracture Mechanics*, 211, 401-419.
- Colombo, I. S., Main, I., and Forde, M. (2003). "Assessing damage of reinforced concrete beam using" b-value" analysis of acoustic emission signals." *Journal of materials in civil engineering*, 15(3), 280-286.
- Di Benedetti, M. (2012). *Acoustic emission in structural health monitoring of reinforced concrete structures*, University of Miami.

- ElBatanouny, M. K., Larosche, A., Mazzoleni, P., Ziehl, P., Matta, F., and Zappa, E. (2014). "Identification of cracking mechanisms in scaled FRP reinforced concrete beams using acoustic emission." *Experimental Mechanics*, 54(1), 69-82.
- ElBatanouny, M. K., Mangual, J., Ziehl, P. H., and Matta, F. (2014). "Early corrosion detection in prestressed concrete girders using acoustic emission." *J. Mater. Civ. Eng.*, 26(3), 504-511.
- ElBatanouny, M. K., Ziehl, P. H., Larosche, A., Mangual, J., Matta, F., and Nanni, A. (2014). "Acoustic emission monitoring for assessment of prestressed concrete beams." *Construction & building materials*, 58, 46-53.
- Engindeniz, M., Kahn, L. F., and Abdul-Hamid, Z. (2005). "Repair and strengthening of reinforced concrete beam-column joints: State of the art." *ACI structural journal*, 102(2), 1.
- Ervin, B. L., Bernhard, J. T., Kuchma, D. A., and Reis, H. "Monitoring general corrosion of rebar embedded in mortar using high-frequency guided mechanical waves." *Proc., Sensors and Smart Structures Technologies for Civil, Mechanical, and Aerospace Systems 2007*, SPIE, 447-458.
- Farhidzadeh, A., Dehghan-Niri, E., Salamone, S., Luna, B., and Whittaker, A. (2013). "Monitoring crack propagation in reinforced concrete shear walls by acoustic emission." *J. Struct. Eng.*, 139(12), 04013010.
- Farhidzadeh, A., Salamone, S., Luna, B., and Whittaker, A. (2013). "Acoustic emission monitoring of a reinforced concrete shear wall by b-value-based outlier analysis." *Structural health monitoring*, 12(1), 3-13.

- Farrar, C. R., and Worden, K. (2007). "An introduction to structural health monitoring." *Philosophical Transactions of the Royal Society A: Mathematical, Physical and Engineering Sciences*, 365(1851), 303-315.
- FOWLER, T., BLESSING, J., and CONLISK, P. "New directions in testing." *Proc., AECM-3: International Symposium on Acoustic Emission from Composite Materials, 3 rd, Paris, France*, 16-27.
- Ganesan, N., Raj, B., and Shashikala, A. (2013). "Behavior of self-consolidating rubberized concrete beam-column joints." *ACI Materials Journal*, 110(6), 697.
- Georgiou A. V., and Pantazopoulou, S. J. (2019). "Experimental and analytical investigation of the shear behavior of strain hardening cementitious composites." *Structural Engineering and Mechanics*, 72(1), 19-30.
- Golaski, L., Gebiski, P., and Ono, K. (2002). "Diagnostics of reinforced concrete bridges by acoustic emission." *Journal of acoustic emission*, 20(1), 83-98.
- Gostautas, R. S., Ramirez, G., Peterman, R. J., and Meggers, D. (2005). "Acoustic emission monitoring and analysis of glass fiber-reinforced composites bridge decks." *Journal of bridge engineering*, 10(6), 713-721.
- Grosse, C. U., and Ohtsu, M. (2008). *Acoustic emission testing*, Springer Science & Business Media.
- Grosse, C. U., Reinhardt, H. W., and Finck, F. (2003). "Signal-based acoustic emission techniques in civil engineering." *Journal of materials in civil engineering*, 15(3), 274-279.
- Group, M. (2007). "PCI-2 based AE system 1 user's manual." *Physical Acoustics Corporation, Princeton Junction, NJ, USA*.

- Guo, B., and Li, Y. "Review of Research on Damage Identification of Reinforced Concrete Structures Based on Acoustic Emission Technology." *Proc., IOP Conference Series: Earth and Environmental Science*, IOP Publishing, 012039.
- Huang, X., Ranade, R., Ni, W., and Li, V. C. (2013). "Development of green engineered cementitious composites using iron ore tailings as aggregates." *Construction and Building Materials*, 44, 757-764.
- Ismail, M. K., Abdelaleem, B. H., and Hassan, A. A. (2018). "Effect of fiber type on the behavior of cementitious composite beam-column joints under reversed cyclic loading." *Construction and Building Materials*, 186, 969-977.
- Ismail, M. K., and Hassan, A. A. A. (2016). "Impact resistance and acoustic absorption capacity of self-consolidating rubberized concrete." *ACI materials journal*, 113(6), 725-736.
- Ismail, M. K., and Hassan, A. A. A. (2021). "Structural performance of large-scale concrete beams reinforced with cementitious composite containing different fibers." *Structures (Oxford)*, 31, 1207-1215.
- Ismail, M. K., Hassan, A. A., and Lachemi, M. (2018). "Effect of Fiber Type on Impact and Abrasion Resistance of Engineered Cementitious Composite." *ACI Materials Journal*, 115(6).
- Ismail, M. K., Sherir, M. A., Siad, H., Hassan, A. A., and Lachemi, M. (2018). "Properties of self-consolidating engineered cementitious composite modified with rubber." *Journal of materials in civil Engineering*, 30(4), 04018031.
- Jumaat, M. Z., Kabir, M., and Obaydullah, M. (2006). "A review of the repair of reinforced concrete beams." *Journal of Applied Science Research*, 2(6), 317-326.

- Kenai, S., and Bahar, R. (2003). "Evaluation and repair of Algiers new airport building." *Cement and concrete composites*, 25(6), 633-641.
- Kim, J.-H. J., Lim, Y. M., Won, J.-P., Park, H.-G., and Lee, K.-M. (2007). "Shear capacity and failure behavior of DFRCC repaired RC beams at tensile region." *Engineering structures*, 29(1), 121-131.
- Kong, H.-J., Bike, S. G., and Li, V. C. (2003). "Development of a self-consolidating engineered cementitious composite employing electrosteric dispersion/stabilization." *Cement and Concrete Composites*, 25(3), 301-309.
- Li, D., Chen, Z., Feng, Q., and Wang, Y. (2015). "Damage analysis of CFRP-confined circular concrete-filled steel tubular columns by acoustic emission techniques." *Smart materials and structures*, 24(8), 85017-85011.
- Li, S., Zhang, L., Guo, P., Zhang, P., Wang, C., Sun, W., and Han, S. (2021). "Characteristic analysis of acoustic emission monitoring parameters for crack propagation in UHPC-NC composite beam under bending test." *Construction & building materials*, 278, 122401.
- Li, V. C. (1993). "From micromechanics to structural engineering the design of cementitious composites for civil engineering applications." *Doboku Gakkai Ronbunshu*, 1993(471), 1-12.
- Li, V. C. (1998). "Engineered cementitious composites (ECC)-tailored composites through micromechanical modeling."
- Li, V. C. (2002). "Advances in ECC research." *ACI Special Publications*, 206, 373-400.
- Li, V. C. (2012). "Tailoring ECC for special attributes: A review." *International Journal of Concrete Structures and Materials*, 6, 135-144.

- Li, V. C., Wu, C., Wang, S., Ogawa, A., and Saito, T. (2002). "Interface tailoring for strain-hardening polyvinyl alcohol-engineered cementitious composite (PVA-ECC)." *Materials Journal*, 99(5), 463-472.
- Masuelli, M. A. (2013). "Introduction of fibre-reinforced polymers– polymers and composites: concepts, properties and processes." *Fiber reinforced polymers-the technology applied for concrete repair*, IntechOpen.
- Mechtcherine, V. (2013). "Novel cement-based composites for the strengthening and repair of concrete structures." *Construction & building materials*, 41, 365-373.
- Mukherjeel, A., and Joshi, M. "Recent Advances in Repair and Rehabilitation of RCC Structures with Nonmetallic Fibers." Journal notes from Prof. A. Mukherjee, Dept. of Civil, IIT, Bombay, India.
- Nair, A., and Cai, C. (2010). "Acoustic emission monitoring of bridges: Review and case studies." *Engineering structures*, 32(6), 1704-1714.
- Nejati, H. R., Nazerigivi, A., Imani, M., and Karrech, A. (2020). "Monitoring of fracture propagation in brittle materials using acoustic emission techniques-A review." *Comput. Concr*, 25, 15-27.
- Ohno, K., and Ohtsu, M. (2010). "Crack classification in concrete based on acoustic emission." *Construction and Building Materials*, 24(12), 2339-2346
- Ohtsu, M., and Y. Tomoda. (2008). "Phenomenological model of corrosion process in reinforced concrete identified by acoustic emission." *ACI Mater. J.*, 105 (2), 194–199.
- Parveen, S. D., and Sharma, A. (2013). "Rubberized concrete: Needs of good environment (overview)." *Int. J. Emerg. Technol. Adv. Eng*, 3, 192-196.

- Paul, S., Pirskawetz, S., Van Zijl, G., and Schmidt, W. (2015). "Acoustic emission for characterising the crack propagation in strain-hardening cement-based composites (SHCC)." *Cement and concrete research*, 69, 19-24.
- Physical Acoustics (2005). "R6I-AST sensor." Princeton Junction, NJ, USA.
- Pollock, A. A. (1986). "Classical wave theory in practical AE testing." *Progress in acoustic emission III-JAP society of non-destructive testing*, 708-721.
- Prem, P. R., and Murthy, A. R. (2017). "Acoustic emission monitoring of reinforced concrete beams subjected to four-point-bending." *Applied acoustics*, 117, 28-38.
- Ramachandra Murthy, A., Karihaloo, B. L., Vindhya Rani, P., and Shanmuga Priya, D. (2018). "Fatigue behaviour of damaged RC beams strengthened with ultra high performance fibre reinforced concrete." *International journal of fatigue*, 116, 659-668.
- Ranjbar, N., Behnia, A., Chai, H. K., Alengaram, U. J., and Jumaat, M. Z. (2016). "Fracture evaluation of multi-layered precast reinforced geopolymer-concrete composite beams by incorporating acoustic emission into mechanical analysis." *Construction & building materials*, 127, 274-283.
- Rashad, A. M. (2016). "A comprehensive overview about recycling rubber as fine aggregate replacement in traditional cementitious materials." *International Journal of Sustainable Built Environment*, 5(1), 46-82.
- Reda Taha, M. M., El-Dieb, A. S., Abd El-Wahab, M., and Abdel-Hameed, M. (2008). "Mechanical, fracture, and microstructural investigations of rubber concrete." *Journal of materials in civil engineering*, 20(10), 640-649.

- Ridgley, K. E., Abouhussien, A. A., Hassan, A. A., and Colbourne, B. (2019). "Characterisation of damage due to abrasion in SCC by acoustic emission analysis." *Magazine of Concrete Research*, 71(2), 85-94.
- Safdar, M., Matsumoto, T., and Kakuma, K. (2016). "Flexural behavior of reinforced concrete beams repaired with ultra-high performance fiber reinforced concrete (UHPRFC)." *Composite structures*, 157, 448-460.
- Şahmaran, M., and Li, V. C. (2010). "Engineered cementitious composites: Can composites be accepted as crack-free concrete?" *Transportation Research Record*, 2164(1), 1-8.
- Said, S. H., and Razak, H. A. (2015). "The effect of synthetic polyethylene fiber on the strain hardening behavior of engineered cementitious composite (ECC)." *Materials & Design*, 86, 447-457.
- Saliba, J., Matallah, M., Loukili, A., Regoin, J.-P., Grégoire, D., Verdon, L., and Pijaudier-Cabot, G. (2016). "Experimental and numerical analysis of crack evolution in concrete through acoustic emission technique and mesoscale modelling." *Engineering Fracture Mechanics*, 167, 123-137.
- Schumacher, T., Higgins, C. C., and Lovejoy, S. C. (2011). "Estimating operating load conditions on reinforced concrete highway bridges with b-value analysis from acoustic emission monitoring." *Structural Health Monitoring*, 10(1), 17-32.
- Selman, E., Ghiami, A., and Alver, N. (2015). "Study of fracture evolution in FRP-strengthened reinforced concrete beam under cyclic load by acoustic emission technique: An integrated mechanical-acoustic energy approach." *Construction and Building Materials*, 95, 832-841.

- Shahidan, S., Pulin, R., Bunnori, N. M., and Holford, K. M. (2013). "Damage classification in reinforced concrete beam by acoustic emission signal analysis." *Construction and Building Materials*, 45, 78-86.
- Siad, H., Lachemi, M., Ismail, M. K., Sherir, M. A., Sahmaran, M., and Hassan, A. A. (2019). "Effect of rubber aggregate and binary mineral admixtures on long-term properties of structural engineered cementitious composites." *Journal of Materials in Civil Engineering*, 31(11), 04019253.
- Sindu, B.S., and Sasmal, S. (2019). "On the development and studies of nano- and micro-fiber hybridized strain hardened cementitious composite." *Archives of Civil and Mechanical Engineering*, 19, 348-359.
- Singh, M., Saini, B., and Chalak, H. D. (2019). "Performance and composition analysis of engineered cementitious composite (ECC) – A review." *Journal of Building Engineering*, 26, 100851.
- Thirumalaiselvi, A., Sindu, B. S., and Sasmal, S. (2020). "Crack propagation studies in strain hardened concrete using acoustic emission and digital image correlation investigations." *European Journal of Environmental and Civil Engineering*, 26(20), 4346-4373, DOI: 10.1080/19648189.2020.1848640.
- Thomas, B. S., Gupta, R. C., and Panicker, V. J. (2016). "Recycling of waste tire rubber as aggregate in concrete: durability-related performance." *Journal of Cleaner Production*, 112, 504-513.
- Vélez, W., Matta, F., and Ziehl, P. (2015). "Acoustic emission monitoring of early corrosion in prestressed concrete piles." *Structural Control and Health Monitoring*, 22(5), 873-887.

- Verbruggen, S., De Sutter, S., Iliopoulos, S., Aggelis, D., and Tysmans, T. (2016). "Experimental structural analysis of hybrid composite-concrete beams by digital image correlation (DIC) and acoustic emission (AE)." *Journal of Nondestructive Evaluation*, 35, 1-1.
- Vidya Sagar, R., and Raghu Prasad, B. (2013). "Laboratory investigations on cracking in reinforced concrete beams using on-line acoustic emission monitoring technique." *Journal of Civil Structural Health Monitoring*, 3(3), 169-186.
- Volovski, M. (2015). "FUNDING FOR HIGHWAY ASSET CONSTRUCTION AND MAINTENANCE: SUSTAINABLE ALTERNATIVES TO THE TRADITIONAL GAS TAX." *IRF*, 6.
- Wang, C., Zhang, Y., and Ma, A. (2011). "Investigation into the fatigue damage process of rubberized concrete and plain concrete by AE analysis." *Journal of materials in civil engineering*, 23(7), 953-960
- Wang, H.-Y., Chen, B.-T., and Wu, Y.-W. (2013). "A study of the fresh properties of controlled low-strength rubber lightweight aggregate concrete (CLSRLC)." *Construction and Building Materials*, 41, 526-531.
- Xargay, H., Ripani, M., Folino, P., Núñez, N., and Caggiano, A. (2021). "Acoustic emission and damage evolution in steel fiber-reinforced concrete beams under cyclic loading." *Construction and Building Materials*, 274, 121831.
- Ziehl, P. H., Galati, N., Nanni, A., and Tumialan, J. G. (2008). "In-situ evaluation of two concrete slab systems. II: evaluation criteria and outcomes." *Journal of Performance of Constructed Facilities*, 22(4), 217-227.